3-D seismic and structural investigation of a suspected hydrothermal dolomite reservoir in the Trenton-Black River, Saybrook, Ohio

By

Justine A. SAGAN

Department of Earth and Planetary Sciences
McGill University, Montréal, Canada

April 2004

**A thesis submitted to McGill University in partial fulfillment
of the degree of Master of Science.**

Library and
Archives Canada

Bibliothèque et
Archives Canada

Published Heritage
Branch

Direction du
Patrimoine de l'édition

395 Wellington Street
Ottawa ON K1A 0N4
Canada

395, rue Wellington
Ottawa ON K1A 0N4
Canada

Canada

Abstract

Trenton-Black River reservoirs in the Appalachian Basin are typically associated with fault-related hydrothermal dolomites that are sealed by unaltered host rocks. However the details of fault geometry and where porosity develops around faults remains poorly documented. Integration of 3-D seismic, wireline and production data from Saybrook Field in northeastern Ohio has shown that the productive trend is controlled by a 3.4mi (5.5 km) long, NW-SE oriented basement fault that was probably reactivated during the Taconic Orogeny in the Mid- to Late Ordovician. The far-field stresses of this compressional activity caused strike-slip movement of the pre-existing fault to create en echelon synthetic shear faults that branch 1350ft (411.5m) upward into the Trenton-Black River interval. Circular collapse structures between overlapping shear faults are the primary drilling targets. Faults were mapped using amplitude and coherency versions of the seismic data. Curvature analysis of horizons mapped in the seismic data allowed us to further constrain the location and orientation of subtle structures. Fault morphology provides insights into the path of the dolomitizing fluids. The distribution of porosity, and thus the location of the reservoir, has been mapped in 3-D using a seismic attribute study that integrated wireline log-based measurements of porosity with seismic attributes. Our results show that the best porosity is developed in areas between overlapping synthetic shear faults. These locations likely represent areas where antithetic shear faults formed, and when combined with minor dip-slip movement created conduits for subsequent porosity generating fluids. The results of this study and the methodology presented here have application in analog settings elsewhere.

Résumé

Les réservoirs Trenton-Black River du bassin appalachien sont typiquement associés à des dolomies hydrothermales reliées à des failles; ces dolomies sont scellées par des roches encaissantes non altérées. Toutefois, les détails de l'interaction entre les failles et l'écoulement des fluides sont mal compris. L'intégration de données sismiques 3-D, de travail au câble et de production provenant de Saybrook Field au nord-est de l'Ohio a démontré que la zone productive est contrôlée par une faille dans le socle de 5,5 km de longueur, orientée nord-ouest sud-est et probablement réactivée pendant l'orogénie taconienne au cours de l'Ordovicien moyen à tardif. Les contraintes distales associées à cette activité de compression ont causé du mouvement directionnel sur une faille pré-existante qui a résulté en la création de failles de cisaillement synthétiques en échelon qui s'embranchent vers le haut sur une distance de 411,5 m pour pénétrer dans l'intervalle Trenton-Black River. Des structures d'effondrement circulaires entre des failles de cisaillement superposées sont les cibles de forage primaires. Les failles ont été cartographiées en utilisant les amplitudes et la concordance des données sismiques. L'analyse de la courbure d'horizons cartographiés à l'aide des données sismiques nous a permis de contraindre la localisation et l'orientation de structures subtiles. La morphologie des failles fournit des indications du cheminement des fluides responsables de la dolomitisation. La distribution de la porosité, et donc la localisation du réservoir, a été cartographiée en 3-D en utilisant une approche d'étude des attributs sismiques qui a intégré les données de porosité mesurées par le travail au câble avec les attributs sismiques. Nos résultats démontrent que la meilleure porosité est développée entre les failles de cisaillement synthétiques. Ces endroits représentent probablement des zones où se sont formées des failles de cisaillement antithétiques. La combinaison de celles-ci avec un léger mouvement en direction du pendage aurait créé des conduits canalisant des fluides qui ont par après produit la porosité. Les résultats de cette étude et la méthodologie présentée ici ont des applications dans des contextes analogues ailleurs.

Preface

This thesis consists of three chapters. The second chapter is intended for submission to a refereed journal, but has been formatted to be consistent with the general layout of the thesis.

The following is an excerpt from the Guidelines for Thesis Preparation as distributed by the Faculty of Graduate Research, McGill University:

"Candidates have the option of including, as part of the thesis, the text of one or more papers submitted, or to be submitted, for publication, or the clearly-duplicated text (not the reprints) of one or more published papers. These texts must conform to the "Guidelines for Thesis Preparation" with respect to font size, line spacing and margin sizes and must be bound together as an integral part of the thesis.

The thesis must be more than a collection of manuscripts. All components must be integrated into a cohesive unit with a logical progression from one chapter to the next. In order to ensure that the thesis has continuity, connecting texts that provide logical bridges preceding and following each manuscript are mandatory.

The thesis must conform to all other requirements of the "Guidelines for Thesis Preparation" in addition to the manuscripts. The thesis must include: a table of contents; a brief abstract in both English and French; an introduction which clearly states the rational and objectives of the research; a comprehensive review of the literature (in addition to that covered in the introduction to each paper); a final conclusion and summary; a thorough bibliography.

As manuscripts for publication are frequently very concise documents, where appropriate, additional material must be provided (e.g., in appendices) in sufficient detail to allow a clear and precise judgment to be made of the importance and originality of the research reported in the thesis.

In general, when co-authored papers are included in a thesis the candidate must have made a substantial contribution to all papers included in the thesis. In addition, the candidate is required to make an explicit statement in the thesis as to who contributed to such work and to what extent. This statement should appear in a single section entitled "Contributions of Authors" as a preface to the thesis. The supervisor must

attest to the accuracy of this statement at the doctoral oral defense. Since the task of the examiners is made more difficult in these cases, it is in the candidate's interest to clearly specify the responsibilities of all the authors of the co-authored papers"

Contribution of Authors

I hereby declare that all practical and analytical aspects of the studies described in this thesis were carried out by me. Dr. Bruce Hart supervised the investigational work and advised me during critical evaluation of the data and ensured that a logical and coherent scientific approach was maintained throughout the study.

Acknowledgements

Table of Contents

List of Figures

List of Tables

List of Appendices

Thesis Outline

This study is organized in three parts. Chapter 1 consists of a summary of the previous work done on the Trenton-Black River both at the Saybrook Field and elsewhere. The second chapter consists of the main body of work completed including an overview of the regional geology, the database that was made available and the methodology employed in order to complete the stated objectives. In addition, it also covers results and the interpretation of the fault mapping and the attribute-based porosity prediction. Finally, the last chapter examines some of the conclusions that were drawn from this analysis and the possible implications this study may have for future exploration and development of fault-related hydrothermal dolomite.

Chapter 1 - Introduction

1.1 General Introduction

In the Appalachian and Michigan Basins of eastern North America, the Middle Ordovician Trenton-Black River Limestone has been successfully explored for hydrocarbons for over a century. In Ohio, where this study is based, production is typically from linear, dolomitized bodies that are attributed to fault-related fluid flow at depth (Keith, 1989). The heterogeneous nature of these reservoirs is such that less than one hundred feet (~30m) may separate productive from non-productive wells (Prouty, 1989). Despite this heterogeneity, exploration continues to be carried out primarily with two-dimensional (2-D) seismic data. On 2-D lines these targets are characterized by dimming of reflection amplitude combined with structural sags along the Trenton horizon. These sags have been primarily ascribed to collapse structures forming due to the brecciated, vuggy nature of the dolomite reservoirs and associated negative flower structures (Hurley and Budros, 1990). Very little three-dimensional (3-D) seismic data has been made available for study, and consequently the 3-D controls on reservoir formation and morphology remain poorly understood.

To date, most studies of the Trenton-Black River have involved understanding the depositional history and determining the diagenetic conditions responsible for creating the dolomite reservoirs in the Appalachian and Michigan Basins (Keith, 1989; Budai and Wilson, 1991; Hurley and Budros, 1990; Coniglio and Williams-Jones, 1992; Middleton et al., 1993; Yoo et al., 2000). In general

there have been four types of dolomite found in the Trenton-Black River interval, cap dolomite at the top of the Trenton, fracture-related dolomite, regional dolomite, and fracture-filling saddle dolomite (Wickstrom and Gray, 1989). Most reservoirs are associated with the fracture-related dolomite (Keith, 1989) and given the lack of evidence supporting regional dolomite throughout Ohio, a fracture-related origin seems likely in this study area.

This study focused on Saybrook Field in the northeast corner of Ohio. A 3-D seismic survey was shot over the field, which is currently producing from a linear trend of seven wells in the Trenton-Black River interval. In cross section the productive areas exhibit the typical 2-D seismic signatures of Trenton-Black River plays. These synclinal structures were initially thought to have formed from karst-related collapse due to subaerial exposure in the Ordovician combined with more recent fracturing (MacKenzie and Grubaugh, 2000). However, there has been some debate over whether or not the Trenton in general was subaerially exposed before the overlying Utica Shale was deposited, as initially suggested by Rooney (1966). More recent facies analysis combined with paleobathymetry and subsidence modeling has supported the presence of a marine hardground at the Trenton-Utica contact and an overall deepening upward trend (Keith, 1985; Wickstrom and Gray, 1989; Howell and Budai, 1989). For these reasons this study sought a primarily structural explanation to account for the reservoir distribution at Saybrook.

The prevalence of faulting in relation to Trenton-Black River hydrocarbon reservoirs has been well documented (Keith, 1989; Prouty, 1989; Versical, 1991;

Middleton et al., 1993; Carter et al., 1996). The most famous examples of this type of reservoir include the Albion-Scipio and Lima–Indiana Trends. Prouty (1989) measured lineament (fault) patterns and outcrop fractures in the Michigan Basin and used well data to support a wrenching (or strike-slip) model for various Trenton-Black River fields (including Albion-Scipio). He found that some kind of wrenching model, either left or right lateral, could generally be used to account for the dolomite distribution at many of these fields. Studies in southwestern Ontario have also indicated a relationship between deep-seated faults and Trenton-Black River reservoirs. The majority of fields in the area are oriented NW-SE to E-W in linear trends (Carter et al., 1996). In some cases Ordovician oil and gas pools directly overlay aeromagnetic highs that have been interpreted as plutons, as at the Dover and Romney Fields (Carter et al., 1996). These relationships reinforce the importance of understanding basement structures when pursuing these targets.

Previous work on the Saybrook 3-D survey was completed by Minken (2002) who used a purely geophysical approach to characterizing the reservoir. He attempted three analyses, amplitude versus offset (AVO), seismic inversion, and a probabilistic neural network using the photoelectric log as the target (PNN). Of the three, only the PNN showed promise, but with an overall correlation of 64% between measured and predicted values, also showed room for improvement. In addition, the results were not combined with a structural interpretation examining controls on dolomite distribution.

This study attempts to build upon this previous work using probabilistic neural networks to better constrain the distribution of porosity and thus the dolomite reservoir. This approach has proven successful in a previous study involving a dolomitic reservoir in the Red River Formation of the Williston Basin by Pearson and Hart (2004). They used a horizon-based approach was used to estimate the porosity thickness and when combined with structural interpretations, provided insight into the controls on dolomite formation in the area. This study uses a volume-based approach as proposed by Hampson et al. (2001) in order to create a porosity volume of the Trenton-Black River interval. This porosity volume will be combined with an interpretation of the structural setting to help elucidate the 3-D controls on dolomite distribution.

1.2 Thesis Objectives

The main objectives of this study are to:

i)   Establish the structural setting of Saybrook by mapping the faults in the 3-D seismic data and relating their formation to the local and regional tectonic settings.

ii) Create a porosity volume of the entire Trenton-Black River interval by first estimating the porosity using a volume based 3-D seismic attribute study.

iii) Validate the porosity prediction through the integration of the structural model and the porosity volume.

References

Budai, J.M., and Wilson, J.L., 1991. Diagenetic history of the Trenton and Black
River Formations. *In:* Early sedimentary evolution of the Michigan Basin.
P. A. Catacosinos and P.A. Daniels Jr. (eds.). Geological Society of
America Special Paper 256, p. 73-88.

Carter, T., Trevail, R., Easton, R., 1996. Basement controls on some
hydrocarbon traps in southern Ontario, Canada. *In:* Basement and Basins
of Eastern North America. B.A. van der Pluijm and P.A. Catacosinos
(eds.). Geological Society of America Special Paper 308, p.95-107.

Coniglio, M., and Williams-Jones, A.E., 1992. Diagenesis of Ordovician
carbonates from the northeast Michigan Basin, Manitoulin Island area,
Ontario: evidence from petrography, stable isotopes and fluid inclusions.
Sedimentology, p. 813-836.

Hampson, D., Schuelke, J., and Quirein, 2001. Use of multi-attribute transforms
to predict log properties from seismic data. Geophysics, v. 66, p. 220-236.

Howell, P.D., and Budai, J.M., 1989. Quantitative paleobathymetric analysis
from subsidence data: Example from Middle Ordovician of Michigan
Basin. AAPG Bulletin (abstract) p. 365.

Hurley, N. and Budros, R., 1990. Albion-Scipio and Stoney Point fields, USA,
Michigan Basin. *In:* Stratigraphic Traps I: Treatise of Petroleum Geology
Atlas of Oil and Gas Fields. E.A. Beaumont and N.H. Forster (eds.).
American Association of Petroleum Geologists, p. 1-37.

Keith, B.D., 1989. Reservoirs resulting from facies-independent dolomitization:

Case histories from the Trenton and Black River carbonate rocks of the Great Lakes Area. *In:* The Trenton Group (Upper Ordovician Series) of Eastern North America. B.D. Keith (ed.). American Association of Petroleum Geologists, Studies in Geology No. 29, p. 267-276.

Keith, B.D., 1985. Top of the Trenton Limestone in Indiana – subaerial unconformity or submarine discontinuity? SEPM Annual Meeting (abstract), v.2, p. 48.

MacKenzie, P., and Grubaugh, W., 2000. Discovery of a new field in the Trenton-Black River Interval, Northeastern Ohio: AAPG Bulletin, v. 84, p. 1388.

Middleton, K., Coniglio, M., Sherlock, R., Frape, S., 1993. Dolomitization of Middle Ordovician carbonate reservoirs, southwestern Ontario. Bulletin of Canadian Petroleum Geology, v. 41, p. 150-163.

Minken, D.A., 2002. A 3-D seismic case study investigating AVO, acoustic inversion, and probabilistic neural networks in the Trenton-Black River interval, NE Ohio. (M.Sc. thesis): University of Oklahoma, 147p.

Rooney, L.F., 1966. Evidence of unconformity at the top of Trenton Limestone in Indiana and adjacent states. AAPG Bulletin, p. 533-545.

Pearson, R.A., and Hart, B.S., 2004. 3-D seismic attributes help define controls on reservoir development: Case study from the Red River Formation, Williston Basin. *In:* Seismic Imaging of Carbonate Reservoirs and Systems. G.P. Eberli, J.L. Masaferro, and J.F. Sarg (eds.). American Association of Petroleum Geologists Memoir.

Prouty, C., 1989. Trenton exploration and wrenching tectonics – Michigan Basin

and environs. *In:* The Trenton Group (Upper Ordovician Series) of Eastern North America. B.D. Keith (ed.). American Association of Petroleum Geologists, Studies in Geology No. 29, p. 207-236.

Versical, R.T., 1991. Basement control on the development of selected Michigan Basin oil and gas fields as constrained by fabric elements in Paleozoic limestones. (MSc Thesis): Western Michigan University, 104p.

Wickstrom, L.H., and Gray, J.D., 1989. Geology of the Trenton Limestone in northwestern Ohio. *In:* The Trenton Group (Upper Ordovician Series) of Eastern North America. B.D. Keith (ed.). American Association of Petroleum Geologists, Studies in Geology No. 29, p. 159-167.

Yoo, C.M., Gregg, J.M., and Shelton, K.L., 2000. Dolomitization and dolomite neomorphism: Trenton and Black River Limestones (Middle Ordovician) Northern Indiana, U.S.A. Journal of Sedimentary Research, p. 265-274.

Chapter 2 – 3-D Seismic and Structural Investigation of a Suspected Hydrothermal Dolomite Reservoir in the Trenton-Black River, Saybrook, Ohio

2.1 Introduction

This paper integrates 3-dimensional (3-D) seismic-based structural interpretations and a 3-D seismic attribute study to examine the relationships between faulting and porosity development in a fault-related hydrothermal dolomite gas reservoir in the Appalachian Basin. Interest in hydrothermal dolomite reservoirs has been piqued by the recent discoveries of highly productive fields such as Ladyfern in northeast British Columbia (Boreen and Colquhoun, 2003), as well as continued success in the Trenton-Black River play in the eastern United States and Canada (Smith et al., 2003; Jacobi et al., 2004). This has spurred debates over issues ranging from possible emplacement mechanisms to the definition of a hydrothermal dolomite (Berger and Davies, 1999; Machel and Lonnee, 2002).

Currently there exists very little work related to the 3-D seismic imaging of hydrothermal dolomite (HTD) reservoirs. Most previous studies of such reservoirs, for example Qing and Mountjoy's (1994) study of Pres'quile Slave Point field in the Northwest Territories, have focused on the diagenetic aspects, including the timing and depth of burial in relation to fluid flow events. In the Trenton-Black River, the prolific Albion-Scipio field in the Michigan Basin has been well studied (Hurley and Budros, 1990; Prouty, 1989, etc.), as have several

Trenton-Black River fields in southern Ontario (Middleton et al, 1993; Carter et al., 1996). However, most exploration and development of these areas has been completed using two-dimensional (2-D) seismic lines, which may fail to capture the true structural complexity of these plays. In 2-D seismic profiles, hydrothermal targets have been associated with a combination of characteristics including structural sag along the horizon and dimming of reflection amplitudes in the area. These features have been interpreted as a response to faulting at depth and the resulting brecciation, dissolution collapse, and low velocity pull-down from the ensuing dolomitization. The importance of structural controls on the development of hydrothermal dolomite plays, including their relationship to strike-slip faulting, has been recognized in the Western Canada Sedimentary Basin (WCSB) and the Appalachian and Michigan Basins, (Prouty, 1989; Berger and Davies, 1999; Smith et al., 2003). However, to our knowledge there are no papers that specifically examine the structural setting of these systems using 3-D seismic data.

Seismic attributes have been used successfully to predict the 3-D distribution of physical properties such as porosity (Russell et al., 1997; Scheulke and Quirein, 1998; Hart and Balch, 2000; Hampson et al., 2001; Leiphart and Hart, 2001). Porosity in hydrothermal dolomite reservoirs is thought to be associated with dolomitization, therefore, by using seismic attributes to image porosity, we sought to delineate the extent of the dolomitized reservoir (c.f., Pearson and Hart, 2004). By integrating the results of our structural mapping

with our porosity prediction, we can further constrain the location and structural setting of the dolomite reservoir.

2.2 Geological Setting and Field History

The Trenton-Black River interval has produced hydrocarbons in the Michigan and Appalachian Basins since 1884. The most productive fields include the 500 million barrel Lima-Indiana and the 290 million barrel Albion-Scipio Trends. While some Trenton-Black River reservoirs in the Appalachian Basin are associated with facies-related or fractured-enhanced limestone porosity, the most prolific fields produce from dolomites (Keith, 1989). Dolomite reservoirs occur in two forms, regional dolomite or localized fault-related dolomite. In Ohio, there has been no conclusive evidence of the regional dolomitization that has been observed in the adjacent Michigan Basin (Wickstrom and Gray, 1989). Thus exploration has focused on linear, fault-related trends as exemplified by the Albion-Scipio Field.

Saybrook Field is located in northeastern Ohio, on the northwestern edge of the Appalachian Foreland Basin that covers much of the northeastern United States and parts of eastern Canada (Figure 1a). There are a number of complex basement structures in the Ohio area, for example, the Cambridge Arch that runs approximately north-south and is about 80mi (129km) to the southwest of Saybrook Field (Root, 1996). Another important feature is the Bowling Green Fault Zone which marks the western limit of the Grenville Province (Wickstrom

Figure 1: a) Location of the study area and the Saybrook 3-D survey in Ashtabula County, northeast Ohio. b) Base map of the Saybrook 3-D survey with the locations of Figures 5 (A-A'), 10 (B-B'), and 18a (B-B') and 18b (C-C') shown in black.

a)

b)
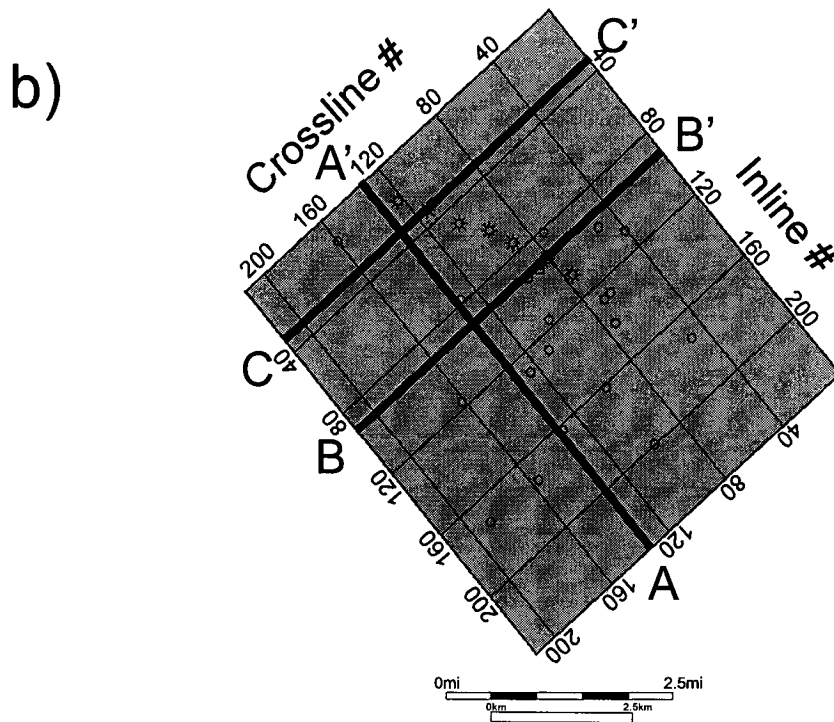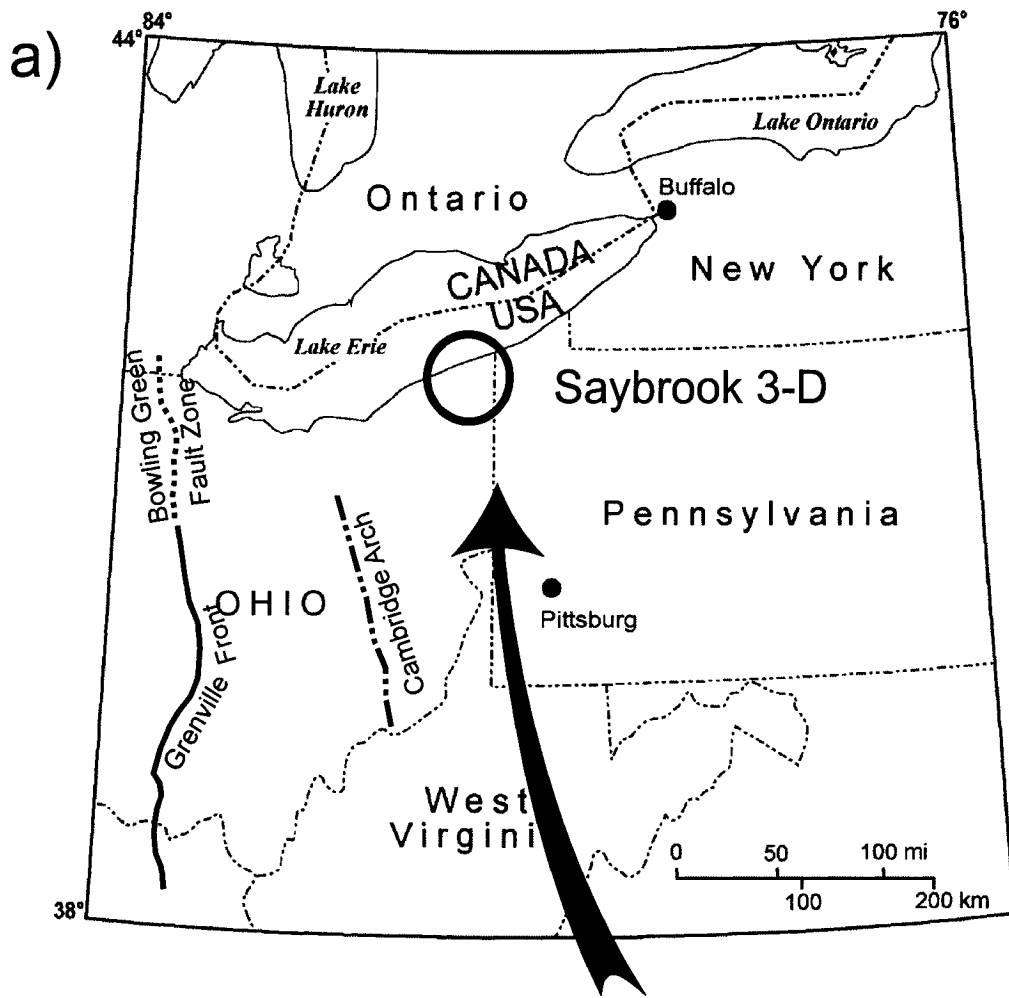
and Gray, 1989). The Lima-Indiana Trenton-Black River Trend occurs along the Bowling Green Fault Zone, with fracture-related reservoirs in its vicinity accounting for up to 45% of the total 500 million barrels that have been produced (Keith, 1989).

The Trenton-Black River was deposited during the Mid-Ordovician (Mohawkian to early Cincinnatian) as shallow sub-tidal bioclastic shelf and platform carbonates (Wickstrom and Gray, 1989; Middleton et al., 1993). The Black River consists of shallow water muddy carbonates, while the Trenton carbonates were deposited in a deeper water setting with shale lamina and fossiliferous intervals throughout. In northwestern Ohio the Trenton-Black River interval generally consists of tan to gray, micritic to finely crystalline limestone. Shale and bentonite layers may be found that can be used locally as log markers (Wickstrom and Gray, 1989). The Utica Shale sharply overlies the Trenton-Black River interval, the contact of which has been interpreted as a submarine hardground (Figure 2; Keith, 1989; Budai and Wilson, 1990). This thick undifferentiated package of shale is considered to have been deposited in response to deepening of the basin and increased clastic influx resulting from erosion of the Taconic Mountains to the east.

The Saybrook discovery well, York UN #3, was drilled in 1997 based on exploration using 2-D seismic lines. Production at Saybrook began in 1997 and is from the Trenton-Black River interval, with the reservoir consisting of fractured, brecciated and vuggy dolomite that is laterally sealed by unaltered limestone and vertically sealed by the Utica Shale and/or unaltered limestone. Originally the

Figure 2: A simplified stratigraphic column for northeastern Ohio from the Late

Cambrian to the Early Silurian (adapted from Larsen, 2000).

14

System	Series	Northeastern Ohio
Silurian	Alexandrian	Clinton Sandstone
Ordovician	Cinncinnatian	Utica Shale
Ordovician	Mohawkian	Trenton-Black River Limestone Gull River
Ordovician	Whiterockian	Wells Creek Formation
Ordovician	Ibexian	Knox Unconformity
Cambrian	St. Croixian	Trempealeau — Knox Dolomite

438mya

505mya

structure of the field was interpreted to have formed from karsting related to Ordovician thrusting and subsequent subaerial exposure (MacKenzie and Grubuagh, 2000). Other producing intervals in the area include the Clinton and Rose Run sandstones. Production peaked in 2001, and by the end of 2002 seven wells had produced 4.8BCF of gas (Table 1).

2.3 Previous Work

A previous geophysical study of Saybrook was completed by Minken (2002). He used various analyses such as amplitude variation with offset (AVO), model-based acoustic inversion and probabilistic neural networks in an attempt to characterize the productive trend. However, the only positive results were found using neural networks to model the photoelectric absorption log. His study was completed using a limited suite of the available wells (only the 12 wells closest to the producing trend were included), and little consideration was given to the structural setting and its influence on dolomite distribution.

2.4 Database and Methodology

The database for this study consisted of a 3-D seismic survey and well logs (Figure 1b). The seismic survey was acquired with a dynamite source and

Table 1: Production data for the seven producing Trenton-Black River wells. Gas production is in MCF and oil production is in barrels. Note that production sharply decreased from 2001 to 2002.

Gas prod.	Riffle UN 1	York UN 3	Downes 1	Downes 3	Dalin E UN 1	Mantell K	Strong 1	Total prod.
1997		16016						16016
1998		373173						373173
1999	216676	339704	92874					649254
2000	312180	171100	525968	113448	132135	63881		1318712
2001	216153	35743	527444	255434	423645	57675		1516094
2002	97320	6816	305696	126005	351471	55221	27471	970000
	842329	942552	1451982	494887	907251	176777	27471	4843249
Oil prod.								
1997		101						101
1998		1052						1052
1999	691	599	537					1827
2000	571	293	1251	101	272	0		2488
2001	112	0	293	73	479	80		1037
2002	192	59	81	69	268	70	0	739
	1566	2104	2162	243	1019	150	0	7244

covered an area of approximately 35mi^2 (56 km^2) with a bin size of 110ft (33.5m) by 110ft (33.5m).

We had digital logs for 27 wells within the 3-D survey area, although not all of the wells penetrated the entire Trenton-Black River interval. All of the wells had caliper, gamma ray, neutron porosity, density porosity, density, and photoelectric absorption logs. Sonic logs were available for only two wells (Schoneman #1 and KR CAL UN #1). "Artificial" sonic logs for other wells were created using multivariate regression to estimate the sonic log values from a combination of the other well logs. In order to identify which logs were the most effective predictors, the well logs (or a non-linear transform of them) were ranked by step-wise linear regression. Then the best logs were cross-validated by excluding one well at a time while the other wells were used to predict the target log values at the missing well. The optimal number of input logs to use was defined at the point when the validation error increased with the addition of a new log (Hampson et al., 2001). It was found that a combination of four logs (the gamma ray, density, neutron porosity, and density porosity logs) best predicted the sonic logs. The prediction had a correlation coefficient of 0.987 and a RMS error of 2.1. The resulting equation was applied to the wells to generate the new sonic logs (Appendix A).

The first task was to pick stratigraphic markers in the well logs. Then sonic and density logs were used to generate synthetic seismograms that were tied to the seismic data. This crucial step allowed the seismic reflectors to be identified that correlated to the top of the Trenton, Black River, Trempealeau and

17

Basement (Figure 3). These horizons were then mapped in the seismic data using a combination of auto-tracking and handpicking – the latter being necessary in areas around the faults. Horizon-based attributes such as dip angle, azimuth, and various measures of curvature were extracted from these horizons to look for subtle structures. The major faults in the area were mapped using both amplitude and coherency data. Various visualization methods were used to analyze relationships between structural features.

A seismic attribute study was undertaken following the structural interpretation. We sought to create a porosity volume for the Trenton-Black River interval using the total average porosity (PHIA), which was generated from the average of the density porosity and neutron porosity logs. We used the methodology of Hampson et al. (2001) to identify the best combination of seismic attributes for predicting PHIA. We then trained a neural network to convert the seismic amplitude data to a porosity volume for the Trenton-Black River interval. Finally, the porosity volume was combined with the fault mapping in order to examine relationships between porosity and structural features.

2.5 Results and Discussion

2.5.1 Logs and Stratigraphy

The Trenton-Black River interval at Saybrook averages 525ft (160m) in thickness and consists of relatively clean limestones with some minor

Figure 3: Synthetic seismograms for the wells that contained original sonic logs, Schoneman #1 and KRCAL UN #1. Both synthetics correlated well with the seismic over the 600ms to 900ms range with correlation coefficients of 0.82 and 0.87 respectively.

Schoneman #1

Synthetic Trace	Actual Trace		P-wave		Density	
		10000us/ft		30000us/ft	2g/cc	3g/cc

KRCAL UN #1

Synthetic Trace	Actual Trace		P-wave		Density	
		10000us/ft		30000us/ft	2g/cc	3g/cc
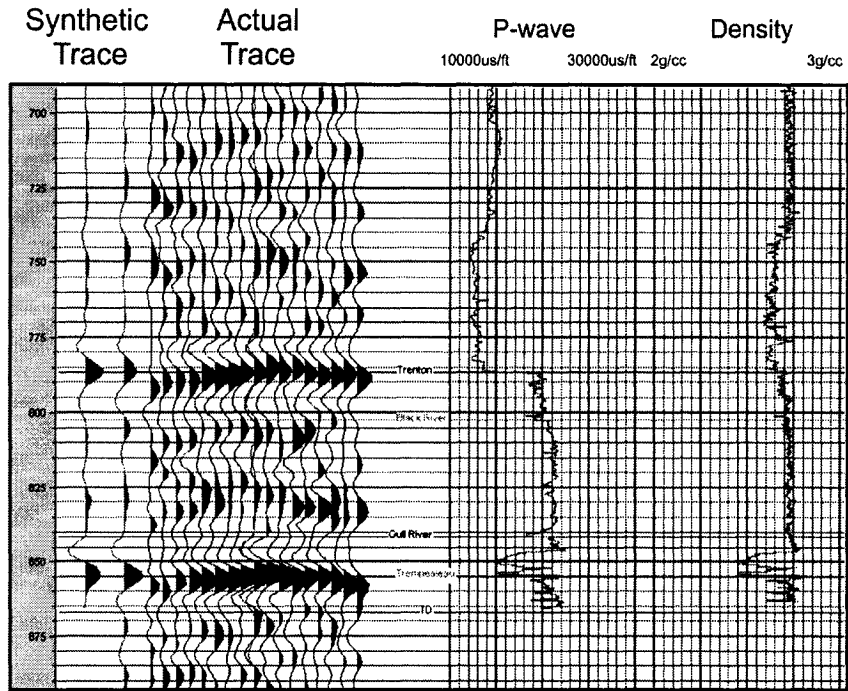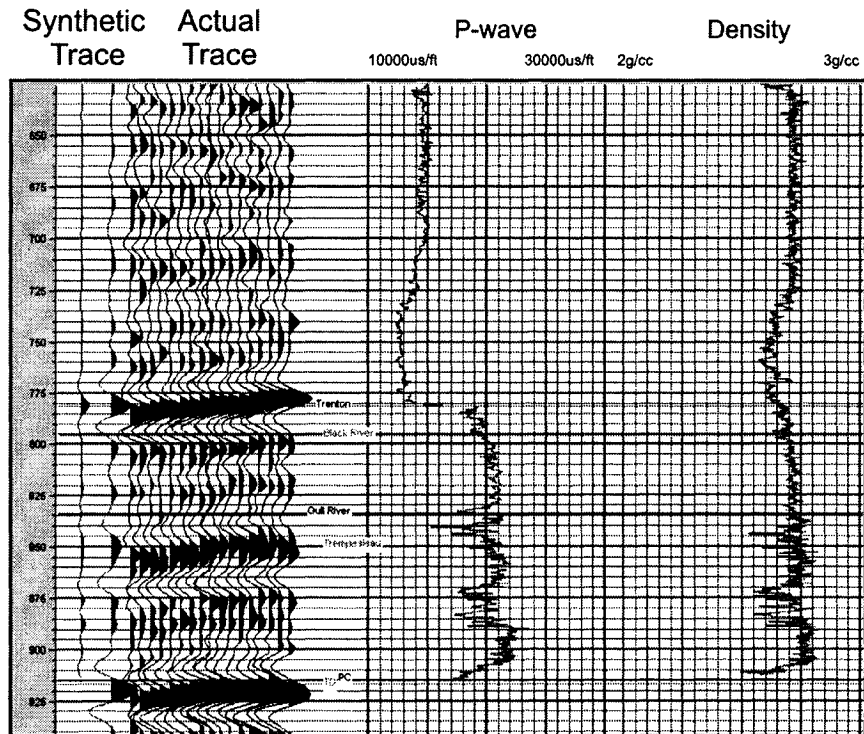
interbedded shale and bentonite layers. It is sharply overlain by the ~1750ft (533m) thick Utica Shale (Figures 3 and 4). The Trenton is characterized by an abrupt lowering in the gamma ray signature from the higher radioactivity of the Utica Shale, whereas the Black River is marked by an even cleaner, blockier gamma ray response than that of the Trenton (Figure 4). However, for the purposes of this study they were essentially treated as one interval.

Neutron-density cross plots show that the reservoir is in dolomite, either in thin dolomite layers (as in Downes #1 and Mantell K #1; Figure 4) or as massive dolomite (e.g. Downes #3; Figure 4). Significant porosity only occurs in the dolomitized zones, with values ranging from 2% to 22% (PHIA). The total dolomite thickness varies from 15ft (4.6m; Mantell K #1) to approximately 345ft (105m; Downes #3) and can be present anywhere from 22ft (6.7m) to 384ft (117m) below the top of the Trenton (i.e., throughout the Trenton-Black River interval). Many of the producing wells were not drilled all the way through the interval, thus some of the lower porous zones may not have been penetrated.

Synthetic seismograms were generated using a zero-phase statistical wavelet that was extracted from the data over the 600ms to 900ms interval (i.e. encompassing the Trenton-Black River). The synthetics were then tied to the seismic data with the primary aim of tying the interval below 600ms. This encompassed the interval of interest and avoided the effects of a section of washed-out evaporite at about 450ms in all of the wells. The correlation for the two wells with original sonic logs was excellent over the 600ms to 900ms interval (calculated correlation coefficients were .87 for Schoneman #1 and .82 for KR

Figure 4: Sample stratigraphic cross-section across the study area, showing five

productive wells and one dry hole (KRCAL UN #1). The top of the

Trenton (also the datum) is characterized by a lowering of the gamma

ray reading from the overlying Queenston Shale. The Black River is

picked where the gamma ray becomes slightly cleaner. The grey lines

to the right of the density logs indicate where dolomite was identified

from neutron-density cross plots.

DOWNES #1   DOWNES #3   RIFFLE UN #1   DALIN E UN #1   MANTELL K UN   KRCAL UN #1

GR   PHIN RHOB   GR   PHIN RHOB   GR   PHIN RHOB   GR   PHIN RHOB   GR   PHIN RHOB   GR   PHIN RHOB

TRENTON

BLACK RIVER

GULL RIVER

TREMPEALEAU

100ft
30m

Porous zones
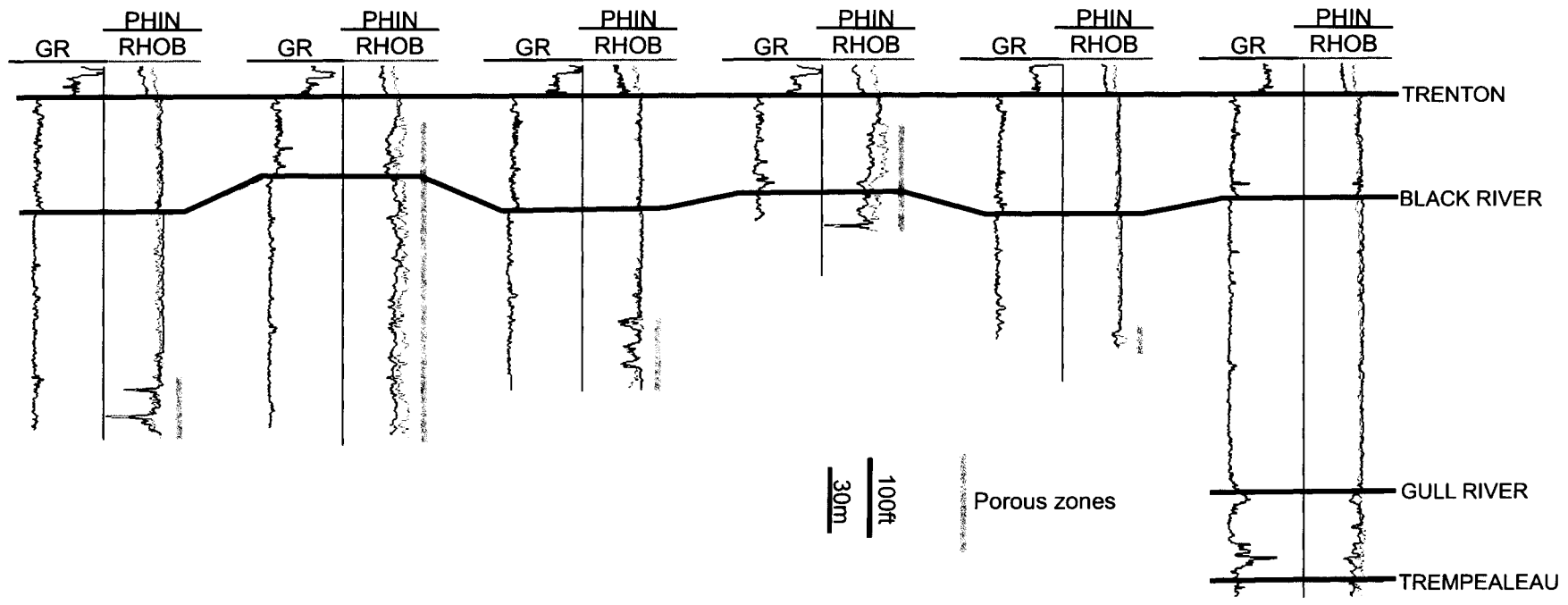
CAL UN #1; Figure 3). In general the synthetics generated from "artificial" sonic logs also tied very well, with correlation coefficients that commonly ranged from 0.66 to 0.84 (see Appendix A for synthetics ties for all of the wells).

The top of the Trenton was identified as a relatively high amplitude peak at about 790ms (Figures 5 and 6) while the top of the Black River corresponded to a zero crossing from trough to low amplitude peak approximately 15ms below the Trenton. A high amplitude peak at about 855ms was determined to approximately represent the Trempealeau, although there were many thin beds in its vicinity that have might affected the seismic character of the Trempealeau on some of the well ties. Another high amplitude peak separating chaotic reflections below from stratified reflections above was chosen to represent the structure of the Basement (Figures 5 and 7).

2.5.2 Fault Mapping and Interpretation

Fault Mapping

Faults were mapped using a combination of timeslices and vertical transects through coherency and amplitude versions of the seismic data. Saybrook Field overlays a basement fault that spans most of the seismic survey, approximately 3.4mi (5.5km) in length (Figure 8). This fault is sinuous in nature with a series of obvious bends across the survey. The overall strike of the main basement fault is approximately 122°-302° (A in Figure 8). There are also two smaller basement faults that are offset from the main trend, one striking

Figure 5: Sample seismic line with horizon picks shown (A-A' in Figure 1b; positive amplitudes in white, negative amplitudes in black). The Basement horizon shows some NE-SW trending structures that appear to be small grabens in cross section. However, these structures are not apparent at the Trenton level.

Crossline 127 · Rife #2

Trenton

Black River

Trempealeau

Basement

0mi · 0.5mi
0m · 500m
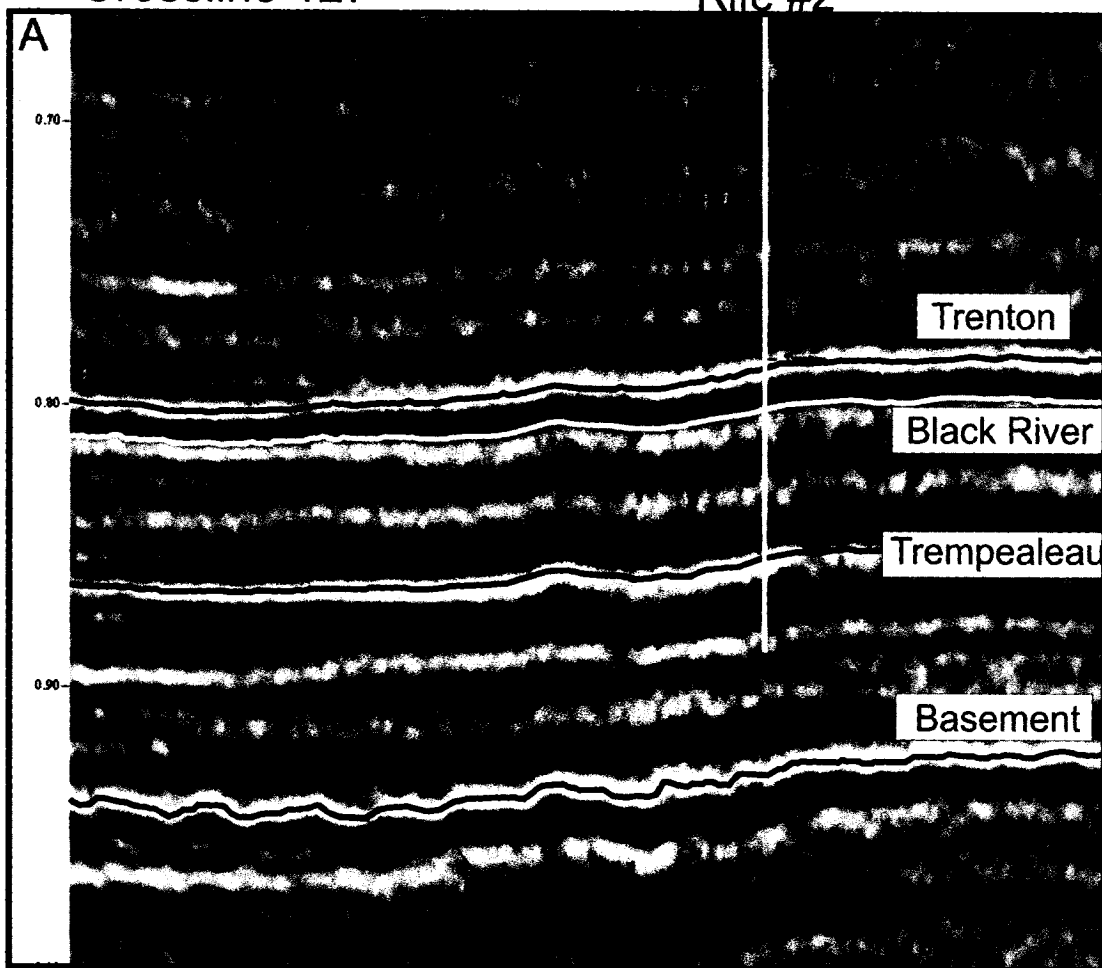
Figure 6: Time structure map of the Trenton horizon. The ridge associated with the productive trend is evident in the center of the survey.

Crossline #

Inline #

746ms

761ms

776ms

791ms

806ms

N

0mi   2.5mi

0km   2.5km
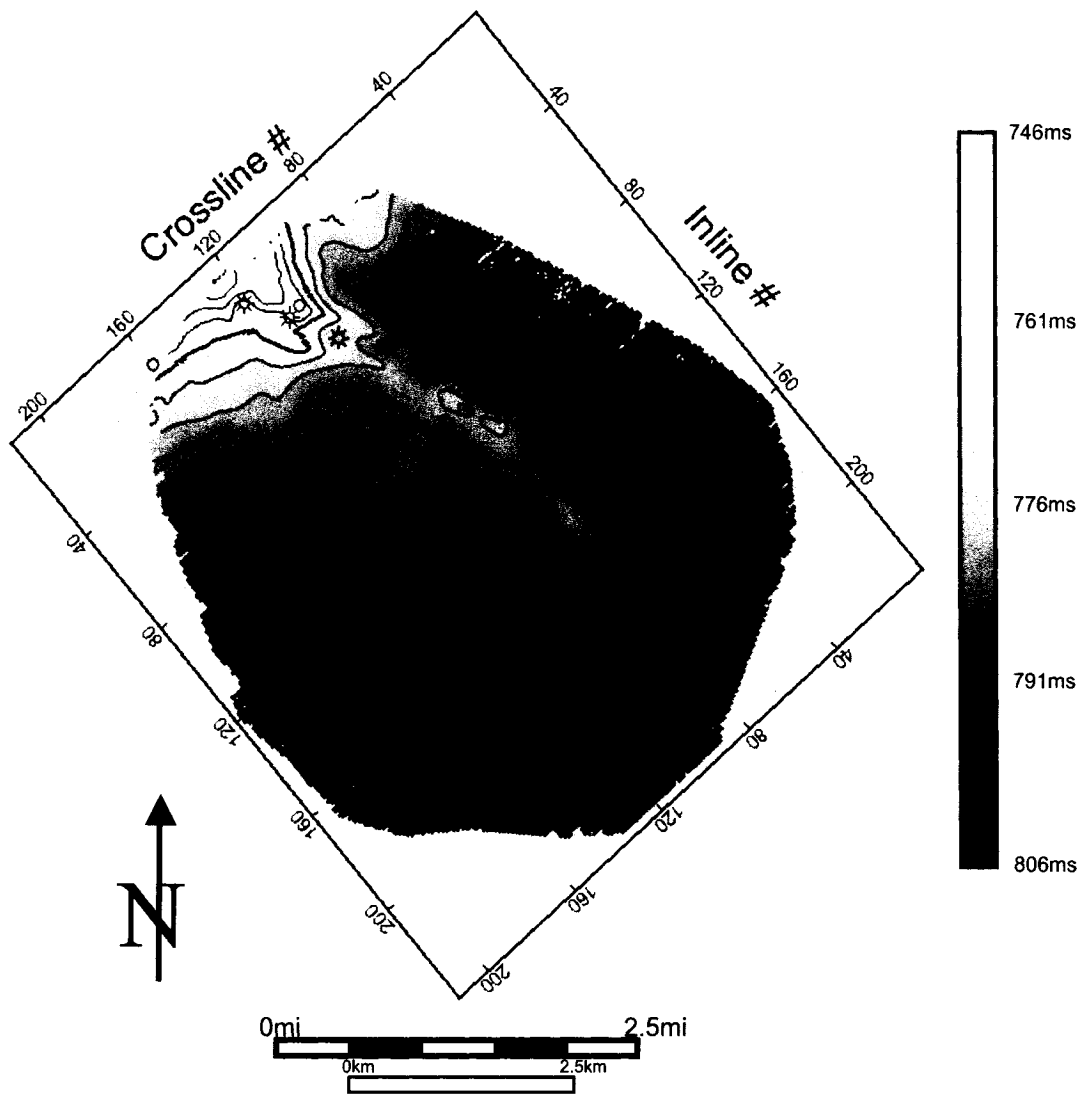
Figure 7: Time structure map of the Top Basement horizon. At this level the prominent basement fault is apparent, as are the NE-SW trending structures noted in Figure 5.

Crossline #

Inline #

40
80
120
160
200

40
80
120
160
200

40
80
120
160
200

40
80
120
160
200

N

0mi   2.5mi
0km   2.5km

883ms

899.5ms

916ms

932.5ms

949ms
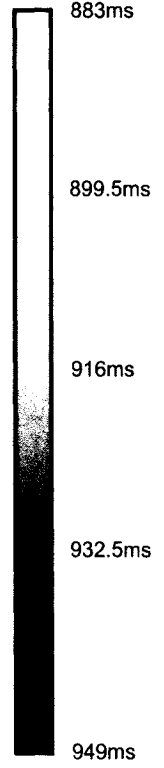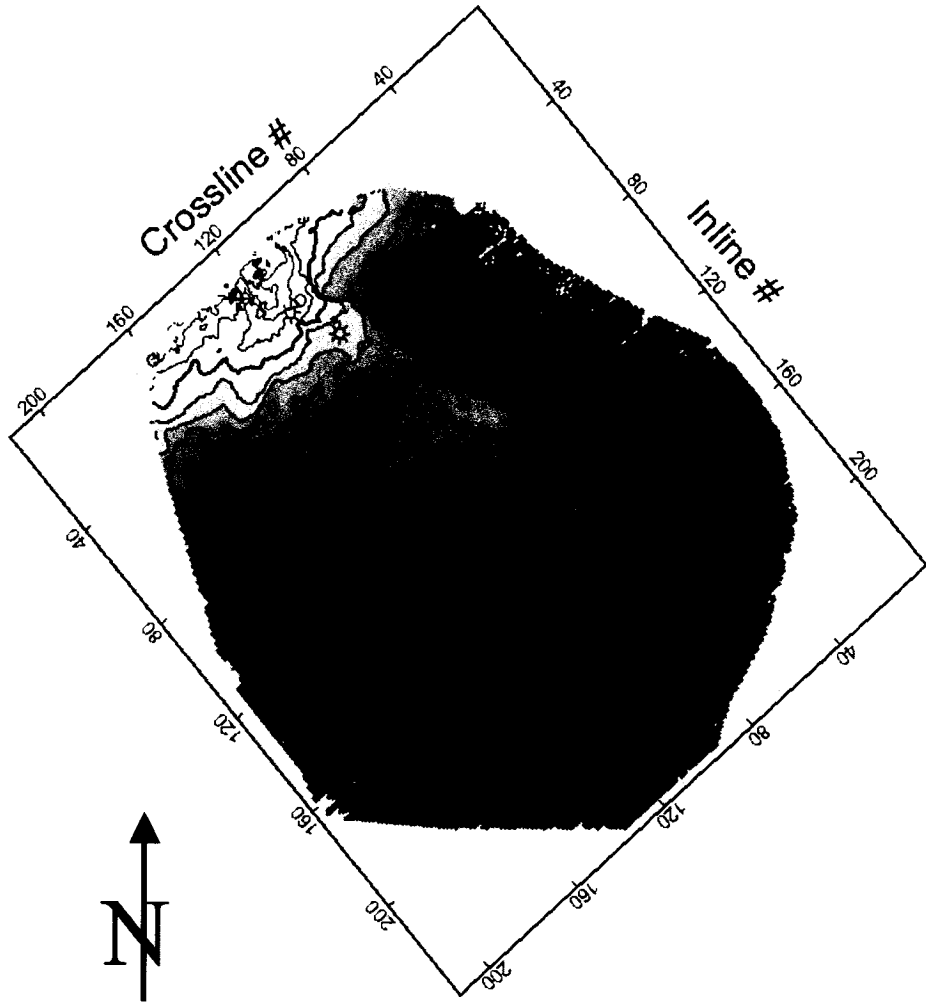
Figure 8: Stratal slice through the coherency volume 18ms above the Top

Basement horizon, with highly coherent reflections shown in white and

less coherent in black. The sinuous nature of the main basement fault

(A) can be seen, along with the step-over faults to the north (B) and

south (C).

B

A

C

small
grabens

N

0mi 2.5mi

0km 2.5km
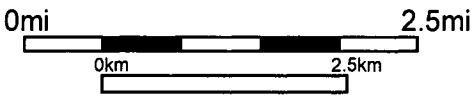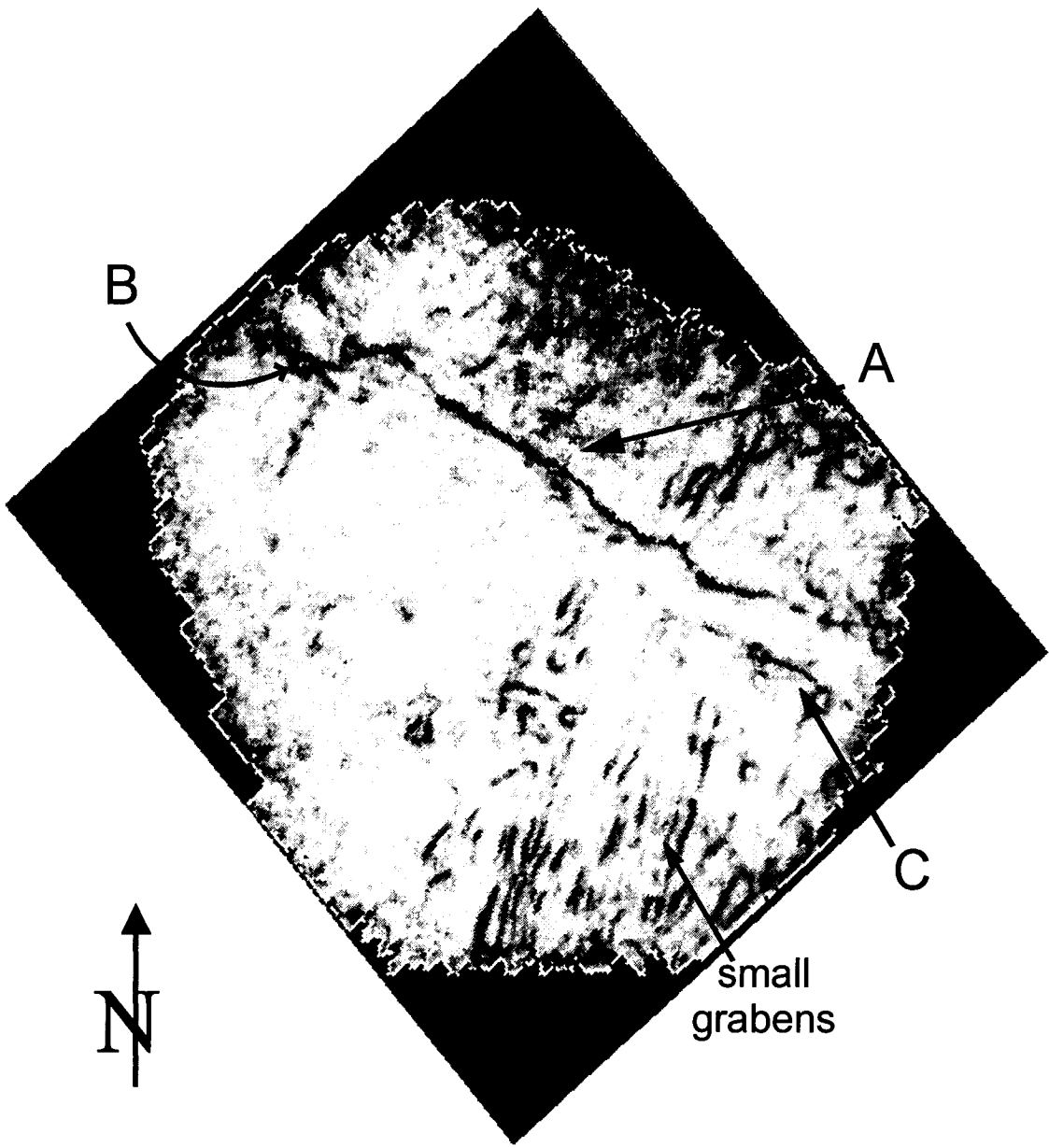
105°-285° to the northwest (B in Figure 8) and another to the southwest (C in Figure 8) that strikes 113°-293°. They both appear to extend past the survey limits, and are about 0.89mi (1.44km) and 1.06mi (1.7km) long respectively in the survey. The basement fault extends upward into the overlying Paleozoic section in a helicoidal manner (Figure 9a, b). At its maximum, it cuts 1350ft (411.5m) into the above strata, (A; Figure 10a, b) and at the Trenton level the general strike is 118°-298°. In addition to this main fault, there are a series of five en echelon faults at the Trenton-Black River level that trend obliquely to the basement fault (Figure 11a). At various points they overlap to form concave-upward positive flower structures in cross-section, mainly in the center and the northwest parts of the survey (Figure 10a, b). The traces of these faults are somewhat sinuous, but on average their strike ranges from 097°-277° to 115°-295°. They vary in length from 0.28mi (0.45km) to 0.93mi (1.5km), and in height from approximately 1000ft (305m) to 300ft (91m). Nineteen smaller faults were picked using coherency timeslices, although many appeared to be near the limit of seismic resolution. These features (shown in purple) seem to be aligned in a slightly different orientation than the main en echelon trend, at about 090°-270° to 100°-280° (Figure11b). The faulted zone is about 1700ft (518m) wide in the middle of the survey, and up to about 2000ft (610m) wide in the north part of the survey where the previously noted offset basement faulting occurred.

In addition to mapping the faults, surface attributes such as curvature, dip and azimuth were extracted from the horizons. These measures have aided in the detection of fractures and faults in the subsurface in the North Sea (Roberts,

Figure 9: a) 3D view of the longest synthetic shear fault showing its helicoidal nature, a common feature in the deformation of overlying strata above single strike-slip basement faults. b) A simplified block diagram of helicoidal deformation above a basement fault (after Mandl, 1988).

a)

b)

Overburden
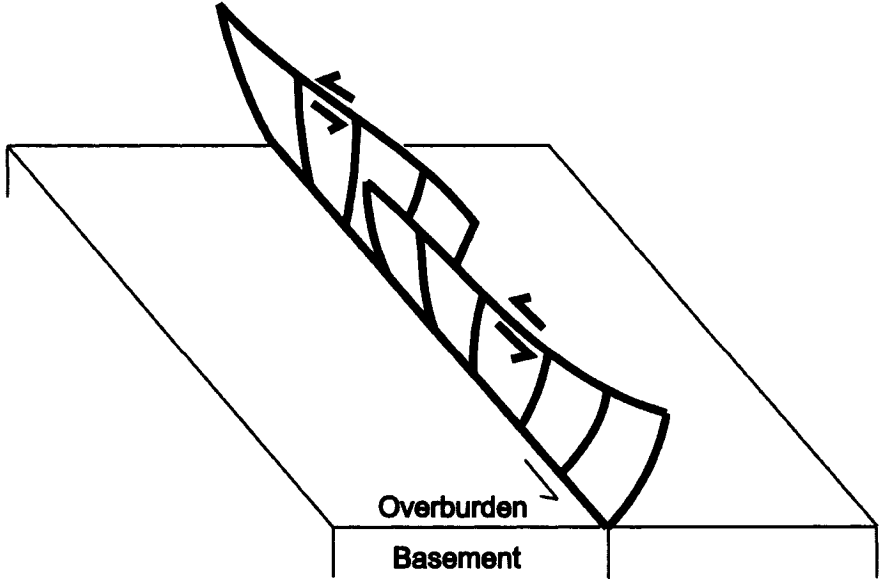
Basement

Figure 10: a) Sample inline through the coherency volume (B-B'), with the

mapped faults shown. The heliocoidal deformation above the longest

basement fault is labeled A. This inline shows a positive flower

structure with a producing well (Strong UN #1) on the upthrown side.

b) The same inline is shown through the reflection seismic data.

A) **Inline 93**

Chapel Hill GC   Strong UN #1

Trenton

Black River

Trempealeau

Basement

1700ft
518m

B)

Chapel Hill GC   Strong UN #1

Trenton

Black River

Trempealeau

Basement
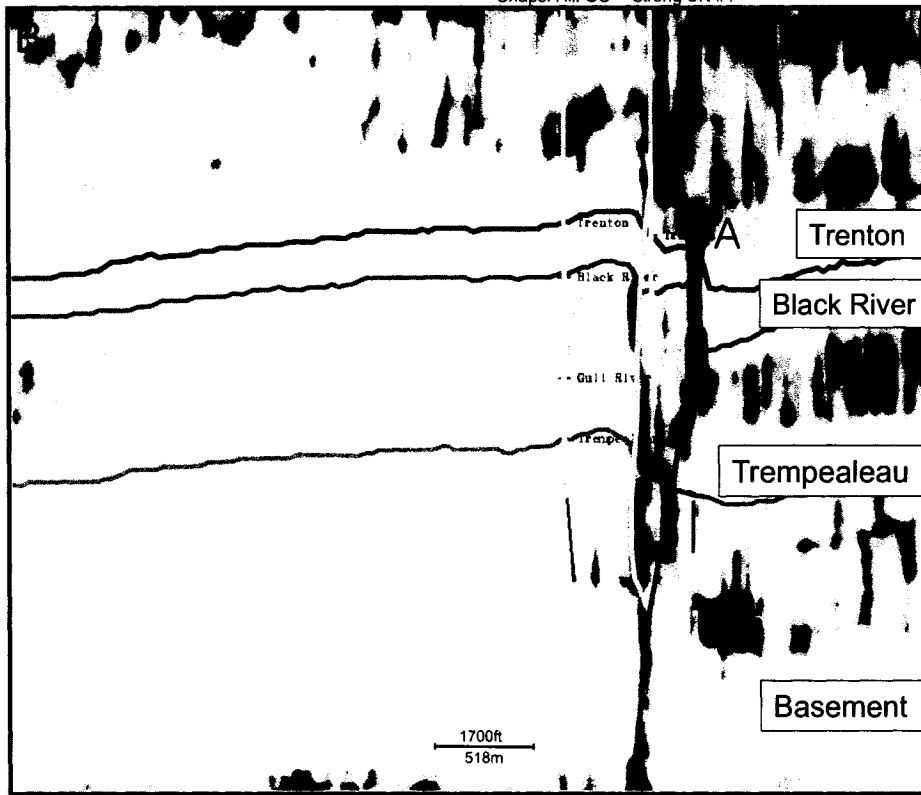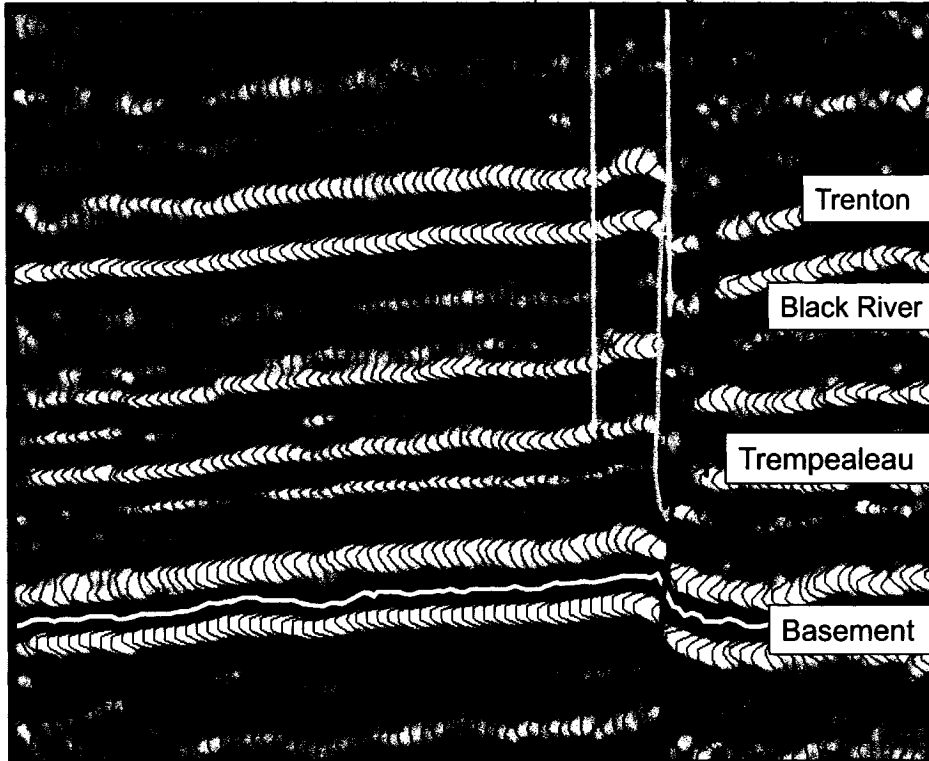
Figure 11: a) Looking down the fault system at Saybrook at the Trempealeau

level and above (Trempealeau time structure is shown). The main

synthetic shear fault is light green, and the less developed shears

are in darker greens. The en echelon nature of these faults is

apparent from this angle. b) The fault zone as it intersects the

Trenton surface, with a similar color scheme as above. The smaller

faults in purple can be seen to trend at a slightly greater angle to the

main trend than the en echelon shear faults; for simplicity, only the

largest of these faults are shown.

a)
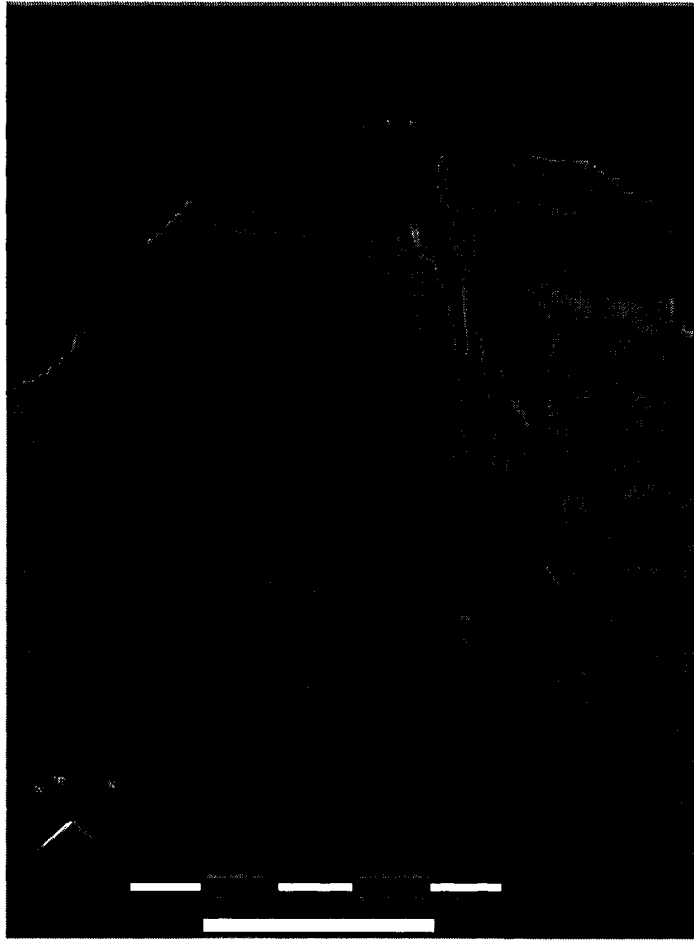
b)
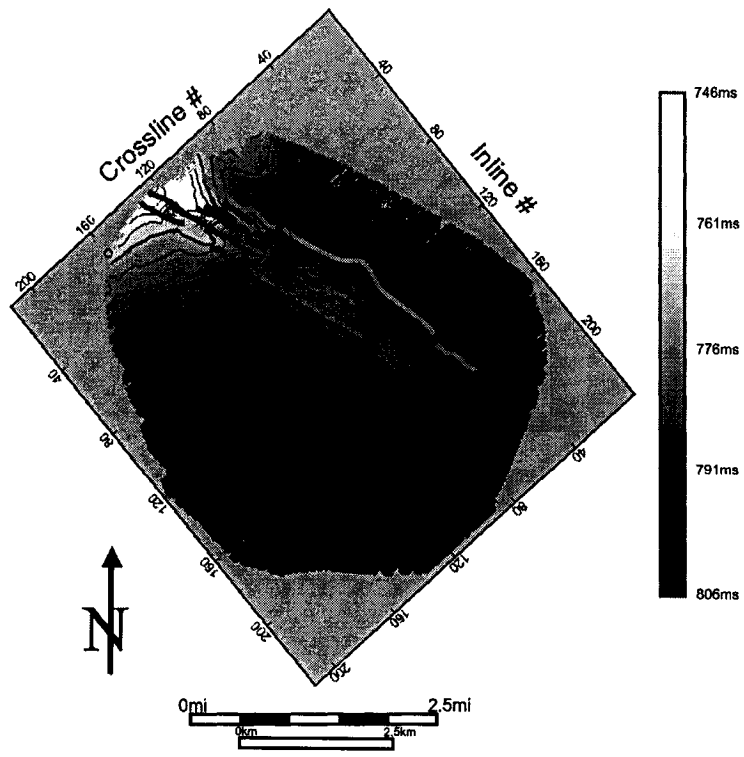
2001) and in the identification of fracture-swarm sweet spots in tight-gas sandstones of New Mexico (Hart et al., 2002). The fault zone is clearly delineated in curvature displays of all horizons, exhibiting a general positive trend (i.e. convex-up) the length of the survey (Figure 12). The maximum curvature of the Trenton horizon was particularly effective in highlighting the areas along the main trend where there were depressions or "lows on the high". These spots displayed negative curvature (concave-up) on the generally positive curvature trend of the structural high that corresponded to the main fault ridge. As indicated on Figure 12, the orientation of the ridges between the collapse structures appear to be parallel to one another, and have a trend of approximately 072°-252°, or 50° from the strike of the main basement fault.

Interpretation

Before examining the fault zone morphology, it is important to consider the conditions that lead to its formation. The origins of the basement fault zone are unclear. Studies of Trenton-Black River reservoirs in southern Ontario and New York have shown that many fields are associated with aeromagnetic highs, such as at the Dover and Romney pools in Kent County, Ontario (Carter et al., 1996). These highs may be caused by the presence of plutonic bodies at depth. Emplacement of plutons could have generated faults and the plutons could provide a heat source for the circulation of hydrothermal fluids. This type of setting was suggested by Minken (2002) as causing the structure seen at Saybrook. However, the slight positive magnetic values that are present in the

31

Figure 12: Maximum curvature extracted from the prestack Trenton horizon,

draped over the 3D surface (the illumination direction is slightly from

the east). Negative curvature is seen in red and orange, while

positive curvature is in blue and green. The main fault ridge is

clearly a positive anomaly (convex-up), while well locations (black

dots) are located in small negative curvature anomalies (concave-up)

along the ridge. Black lines indicate the trends of the ridges

between collapse structures (072°-252°), also note the prominent grid

of acquisition artifacts (yellow).

1.8E-007
1.6E-007
1.4E-007
1.2E-007
1E-007
8E-008
6E-008
4E-008
2E-008
0
-2E-008
-4E-008
-6E-008
-8E-008
-1E-007

N→

0mi   2.5mi

0km   2.5km
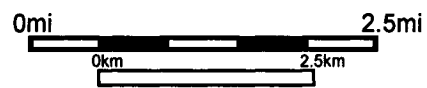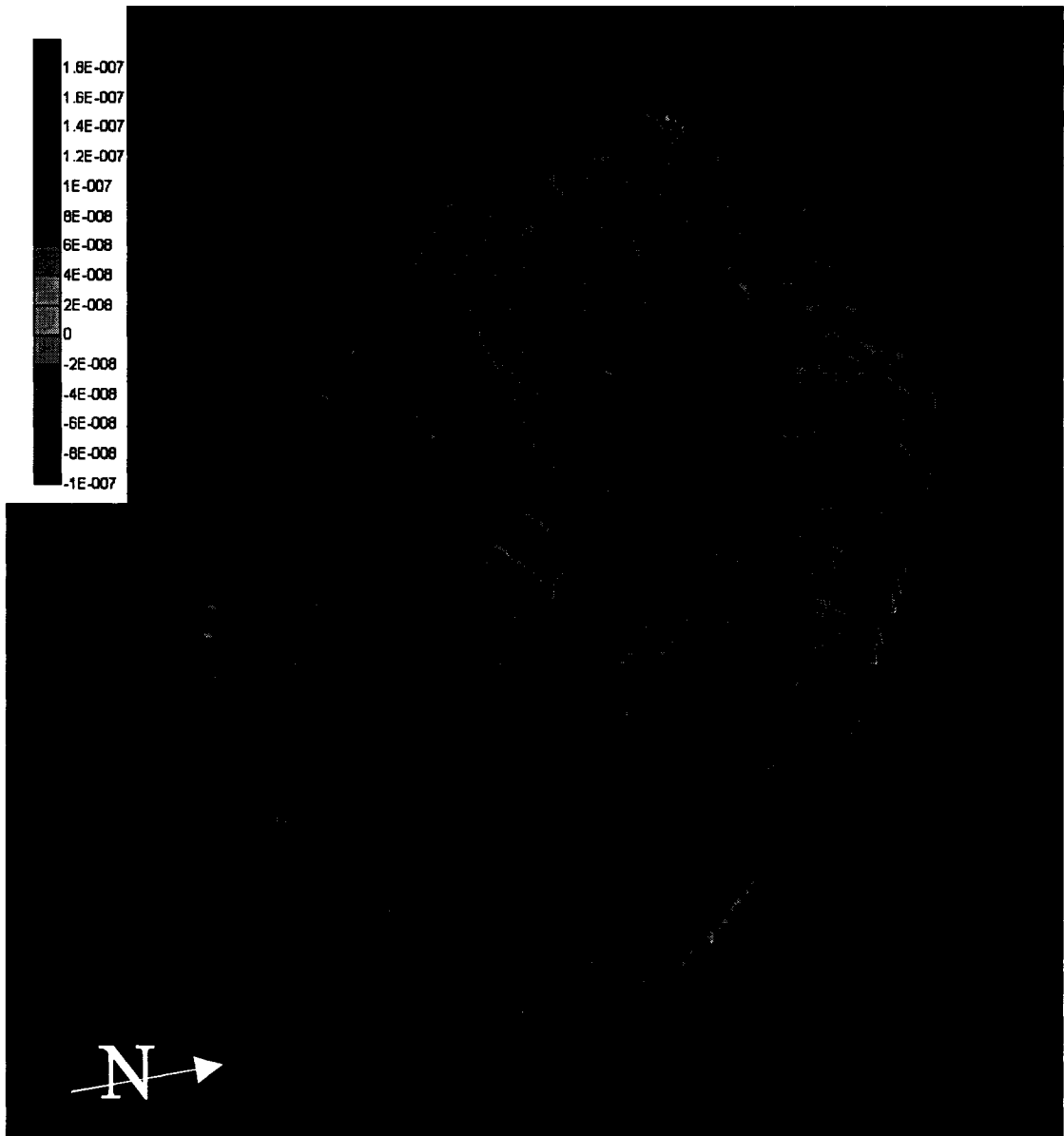
Saybrook area (-75nT to 175nT) are insignificant when compared to values interpreted as plutons in western Ohio (<1000nT; von Frese et al., 1997). Additionally, not all of the Trenton pools in Ontario are directly associated with anomalies (Carter et al., 1996). Alternatively the faulting may have developed originally in response to events that occurred in relation to the Grenville orogeny and/or later Precambrian rifting. The trend of the Saybrook fault is similar to that of other Grenville-aged fault zones in northeastern Ohio, such as the Akron, Suffield, Smith Township and the Highlandtown and Middleburg faults that are oriented at 125°-305° (Root, 1996). Hart et al., (1996) used 3-D seismic data to map northwest-southeast striking faults affecting the Knox Unconformity in western New York. They concluded that these structures were produced by reactivation of a Grenville-aged structure.

The Saybrook fault system is consistent with a left lateral strike-slip model, although it was not possible to quantify the amount of strike-slip displacement. The faulting dies out in the overlying Utica Shale, allowing for the timing of the main movement to be constrained to the Late Ordovician. The principal tectonic activity during that time period was the Taconic Orogeny, suggesting that the faulting seen at Saybrook maybe the result of far field stresses from this event. Evidence of basement reactivation during the Taconic has been recorded by Versical (1991) and Ettensohn et al. (2002) throughout the east central United States. Figure 13 shows the location of Saybrook west of the New York Promontory, which according to Ettensohn et al. (2002) may have led to an increase in the lithospheric flexure that, in turn, caused basement

Figure 13: Paleogeographic reconstruction from the Mid to Late Ordovician of southeast Laurentia, showing the location of Taconic activity on the northeast edge of the New York Promontory (after Ettensohn, 2002). The arrows illustrate the main directions of compression at the time (SE-NW to E-W).

Location of Saybrook

New York Promontory

ST

Ouachita Sea

N

ST

CT

0km   300km

0mi   300mi

ST Sebree Trough

CT Carolina Terrane

Cratonic Margin

Taconic Orogenic Activity

Martinsburg Foreland Basin

Blountian Tectophase Highlands

Sevier Foreland Basin and equivalents
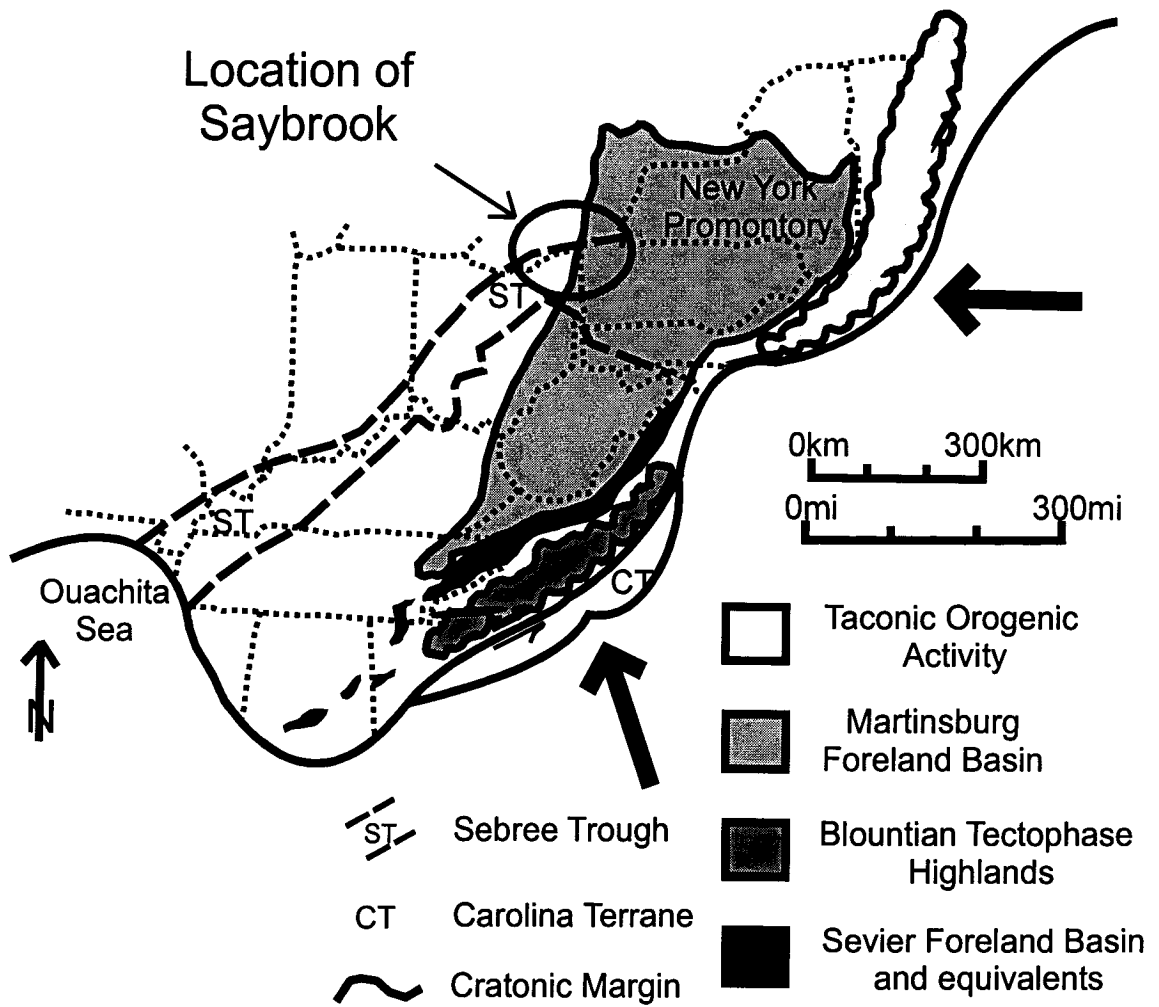
reactivation in the area. The last and most intense activity of the Taconic Orogeny was on the northeastern edge of the New York Promontory, which would have been approximately east of the present location of the study area (Ettensohn et al, 2002). Versical (1991) used calcite twin strain analysis to establish the mean compression direction in Paleozoic strata of the Michigan Basin as SE-NW to approximately E-W. He also found that fault models that combined dip-slip movement and compression at angles of $20°$-$30°$ from a basement fault generated concave-up flower structures (as seen at Saybrook). Using the general strike-slip criteria that the primary stress is oriented at $45°$ to the direction of movement ($122°$-$302°$), the resulting primary stress at Saybrook would be oriented approximately $077°$-$257°$, slightly north of east. However, given a zone of pre-existing weakness (i.e. a basement fault), reactivation may occur under a primary stress orientation that is less than $45°$ (as was measured by Versical (1991)). We conclude that the strike-slip faulting at Saybrook probably developed in response to approximately ESE-WNW compression during the later stages of the Taconic Orogeny.

It is important to consider that the damage zone associated with the seismically imaged faults probably contains more small-scale faults and fractures than could be imaged seismically. The mapping of the main faults completed here may be considered a first order approximation of the true fault zone morphology. Using the nomenclature of Prouty (1989) the deformation above the basement fault would be considered a shear fault zone, thus the faults in the area would be regarded as synthetic shear faults or antithetic shear faults

35

depending upon their angular relationship to the basement fault (Figure 14; Mandl, 1988). The main synthetic shears changed in orientation slightly from the level of the basement fault, as expected (Figure 9). The basement fault has a strike of 122°-302°; the extension of this fault at the Trenton-Black River is oriented at about 118°-298°, although it is somewhat sinuous. The other main synthetic shears at the Trenton-Black River level are oriented from 115°-295° to 097°-277° (7° to 25° from the basement fault). Where these synthetic shears overlap each other and meet at depth, they form the limbs of concave-up flower structures. If the primary stress is oriented at angles less than 45° from the basement fault, antithetic shears may form at angles of 48°-64° from the strike of the basement fault, although their presence would depend upon how evolved the system became (Mandl, 1999). Such values assume that the primary stress is mainly horizontal and depend upon the state of stress prior to shearing, as well as the internal friction angle of the faulted material (Figure 15a, b, c; Mandl, 1999; Ahlgren, 2001). Although not imaged directly seismically, the ridges between the collapse structures were defined using curvature and their orientation (072°-252°) may attest to the presence of the antithetic shear faults. Additionally the smaller faults that were mentioned above also fit with the left-lateral shear model. Their orientations of 090°-270° to 100°-280°, on the order of 20°-30° off of the strike of the basement fault, indicate that they were possibly precursors to the en echelon synthetic shear faults. As strike-slip systems evolve, the later-formed synthetic shears tend to become more in line with the movement of the underlying basement fault (Naylor et al., 1986; Ahlgren, 2001).

Figure 14: The generalized strain ellipse for a left lateral strike-slip system

oriented in the same direction as the Saybrook system, although the

primary stress is shown at 45° from the basement fault (after Prouty,

1989). The expected orientations of the synthetic and antithetic

shear faults are labeled, with extension expected approximately

north-south. If the primary stress were oriented at less than 45° then

the angle between the synthetic shear and the main basement fault

would be smaller.

Extension

Antithetic
shear fault

Synthetic
shear fault

σ_1
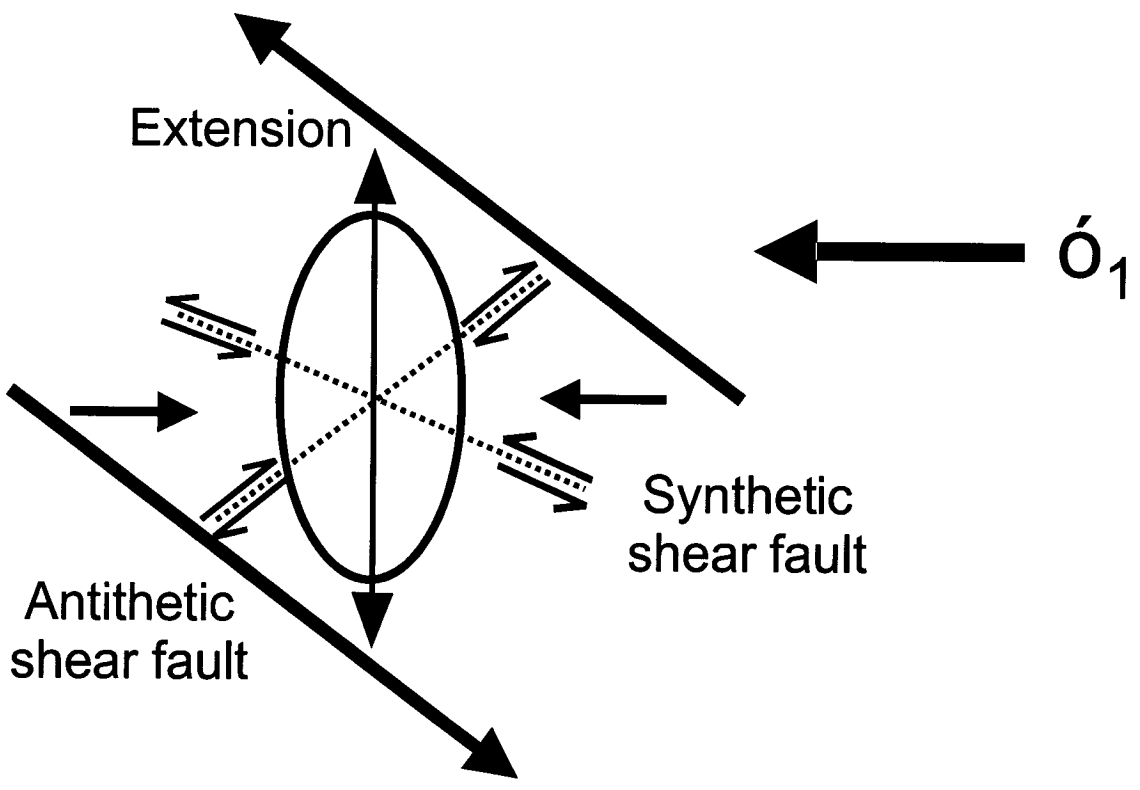
Figure 15: An idealized cartoon of two stages of development of a shear fault zone a) initially with only synthetic shear faults and b) later with antithetic shear faults (adapted from Mandl, 1988 and Ahlgren, 2001). The regularly spaced extension along sub-seismic antithetics combined with minor dip-slip movement may have helped to develop fluid migration pathways. c) The Trenton surface with the intersecting faults shown, between the green (synthetic shear) faults is the likeliest location for antithetic shear faulting to occur.

a)

synthetic
shear faults

b)

antithetic
shear faults

c)

Crossline #

Inline #

746ms

761ms

776ms

791ms

806ms

N

0mi   2.5mi

0km   2.5km
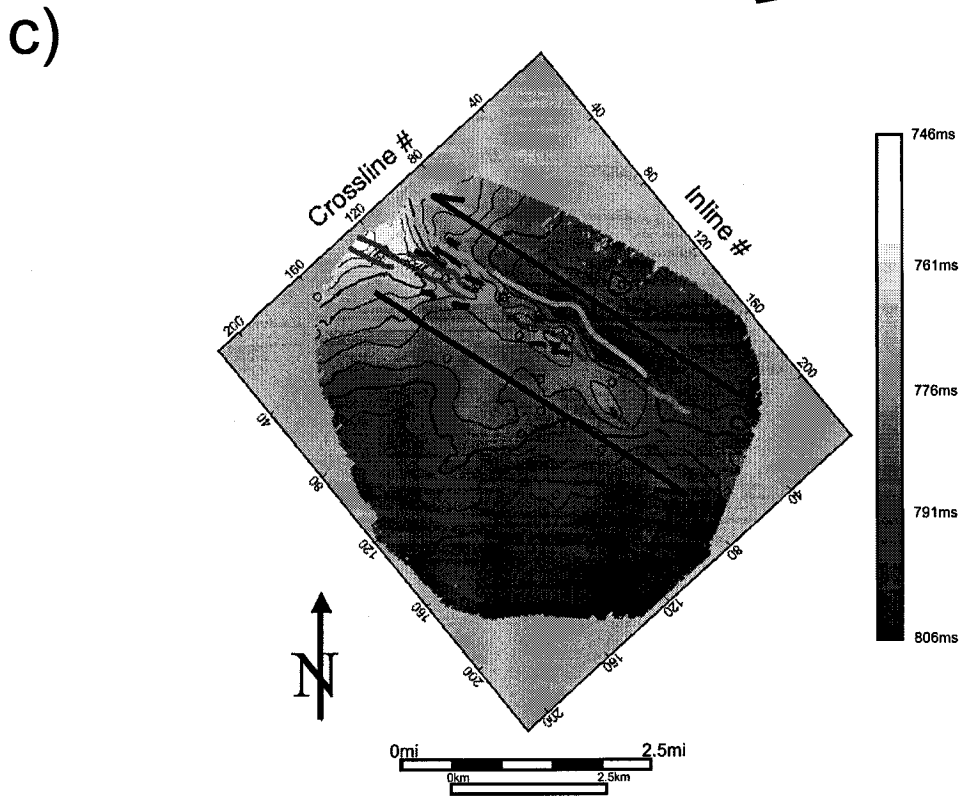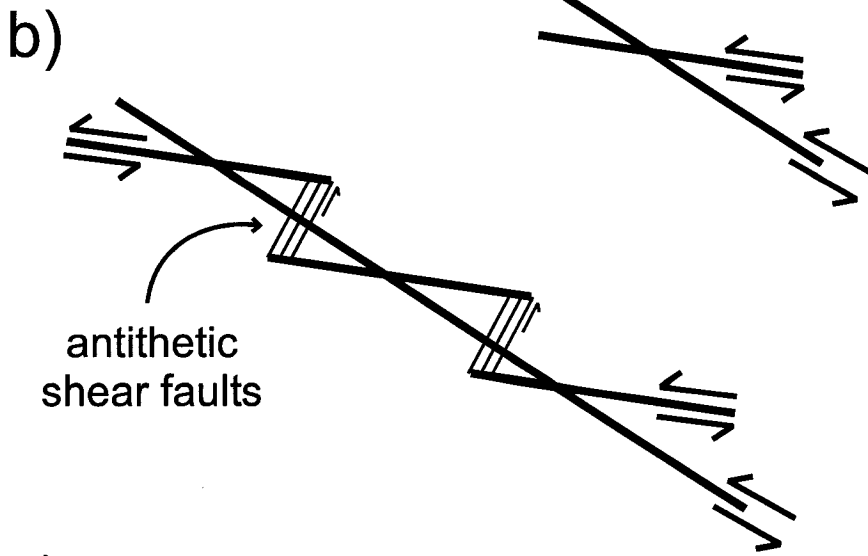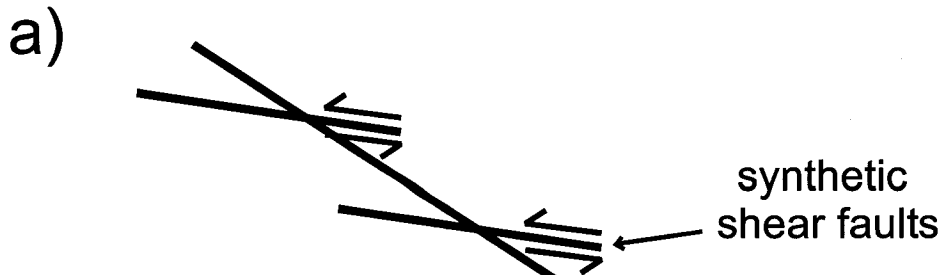
While the main fault movement appears to be constrained to the Taconic Orogeny, some faulting continues upward into the Utica Shale, signifying that there may have been some renewed activity with the Acadian and Alleghenian orogenies (Mid-Devonian and Late Carboniferous/Early Permian respectively). As no core was available for analysis, it is not possible to determine when the dolomitizing fluids were circulated, or what their source was. It is also impossible to establish the precise temperature information needed to conclusively label the dolomite as hydrothermal (Machel and Lonnee, 2001). Other fields in the vicinity, such as in southwestern Ontario (Middleton et al., 1993), have been shown to be related to hydrothermal activity, but the best that can be said at Saybrook is that is a suspected hydrothermal system. Studies in the Michigan Basin and in southwestern Ontario have found that a Silurian source is consistent with isotopic work done in the area (Granath, 1991; Middleton et al., 1993). Activity related to Alleghanian deformation has been suggested as a possible drive to fluid flow, moving the brines northward through the basin (Farquhar et al, 1987; Prouty, 1989; Hurley and Budros, 1990; Budai and Wilson, 1991). Similar basin-wide fluid flow events related to the Antler and Laramide orogenies have been postulated in the WCSB as contributing to hydrothermal dolomitization across that basin (Al-Aasm et al., 2002).

2.5.3 Attribute Study

After establishing the structural context and mapping the horizons, a relationship between log-based physical properties (porosity) and seismic attributes was sought. An attribute is a derivative of the seismic data that may be extracted over an interval or along a horizon (Brown, 1996). The goal of the attribute study was to create a porosity volume of the Trenton-Black River interval using methods described by Hampson et al. (2001). This result allowed us to examine the distribution of porosity in 3-D, an improvement over a porosity map. This type of approach increases the number of data points used in the correlation thus improving the statistical basis of the correlations (Hampson et al., 2001).

The interval of interest was defined from the top of the Trenton to the base of the Black River (identified as the Gull River) or TD, whichever was the lowest level penetrated by the well. The target log was the average porosity log (PHIA), calculated as the average of neutron and density porosity, with a 2ms sample rate. This type of log is an effective means of reducing the influence of lithology on the measured porosity (Hearst et al., 2000). A subset of 18 out of the total 27 wells was used in the porosity prediction. These wells were selected largely based on their tie with the seismic data using the statistical wavelet. Non-producing wells having synthetics that tied with correlation coefficients greater than 0.75 and all producing wells (regardless of how they tied to the seismic data) were used. Two producing wells (York UN #3 and Strong UN #1) were not used as they were both deviated and they could not be adequately tied above the Trenton.

The porosity prediction was undertaken in much the same fashion as the sonic log prediction except using seismic attributes instead of well logs. A probabilistic neural network was trained over the interval using the attributes that were identified from the multiattribute regression. A porosity volume was then created over the entire survey for the interval of interest. Neural networks have proven to be more effective in some cases than multivariate regression in modeling the non-linear relationships that may exist between physical properties and seismic attributes (Leiphart and Hart, 2001; Hart and Chen, *in press*).

Stepwise linear regression and validation testing identified six attributes that were the most effective porosity predictors (Figure 16). These attributes were the RMS (root-mean squared) amplitude, perigram, reflection strength, derivative of reflection strength, integrated trace and the cosine of instantaneous phase. When applied to the data, the resulting prediction (based on multiattribute linear regression) had a 73% correlation, with an average error of 1.36%. These attributes were then used to train the neural network. The neural network had a training error of 0.96% and an overall correlation of 89% (Figure 17a, b; see Appendix B for the application of the neural network at all the wells). This neural network was then applied to the entire seismic survey from the Trenton to the Trempealeau in order to map the porosity distribution over the entire survey (Figure 18a, b and Figure 19).

Figure 16: Graph showing the prediction error (black) and validation error (red) for the multiattribute analysis. Although the validation error decreases slightly for predictions using 7 and 8 attributes, 6 is determined to be the optimal number in order to avoid overtraining the data.

Average Error for All Wells
Operator Length: 3
Black Dot: Analysis Using All Wells
Red Dot: Analysis Leaving Out Target Well

Average Error (fraction)

Number of Attributes
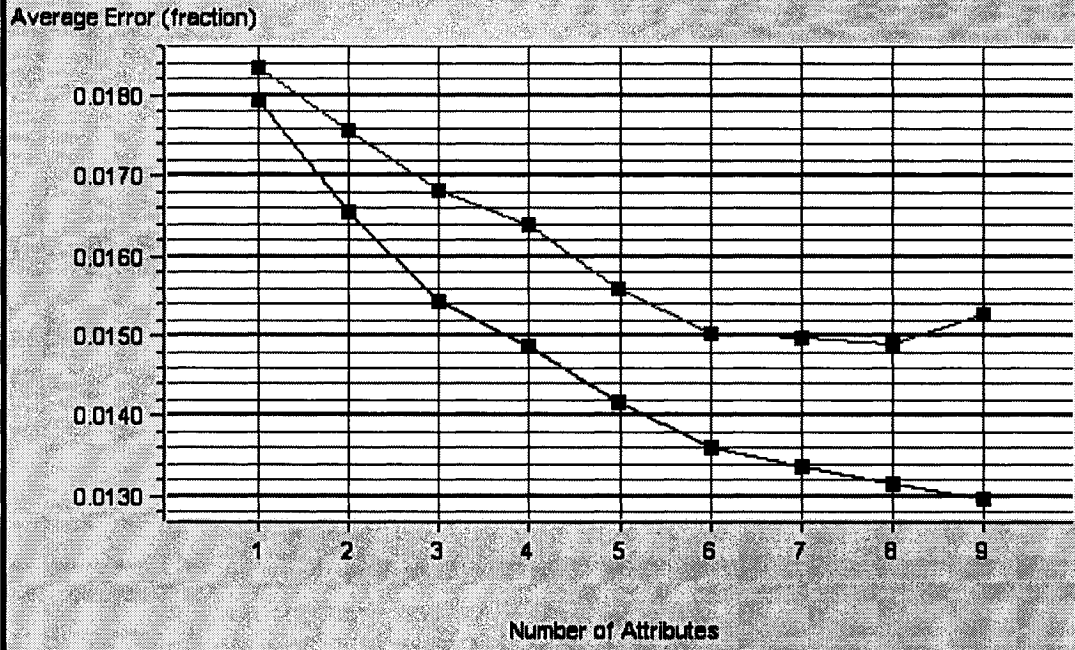
Legend
— ■ — All Well Error   — ■ — Validation Error

Figure 17: a) Selected wells showing the application of the neural network to the

training data, the average error was 0.96% and the correlation was

89%. The prediction (red) closely matches the target log (black;

PHIA – values increase to the right). b) Crossplot of the predicted

versus the actual values of porosity, different colors represent each

well. Values that fall off of the trend indicate areas where the

neural network under-predicted the porosity. This may have been

caused by artifacts generated in wells that terminated within the

Trenton-Black River interval, as at Dalin E UN #1 and Downes #1.

a)
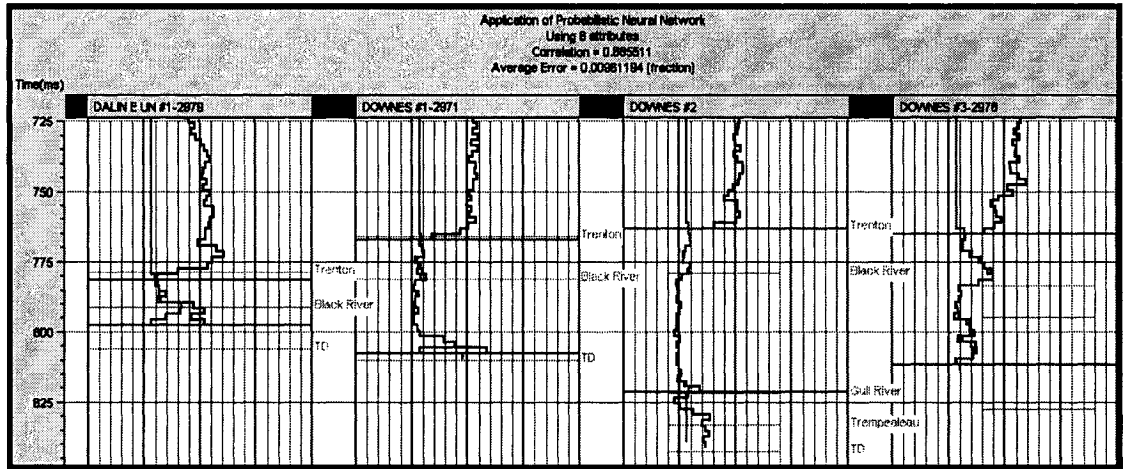
b)
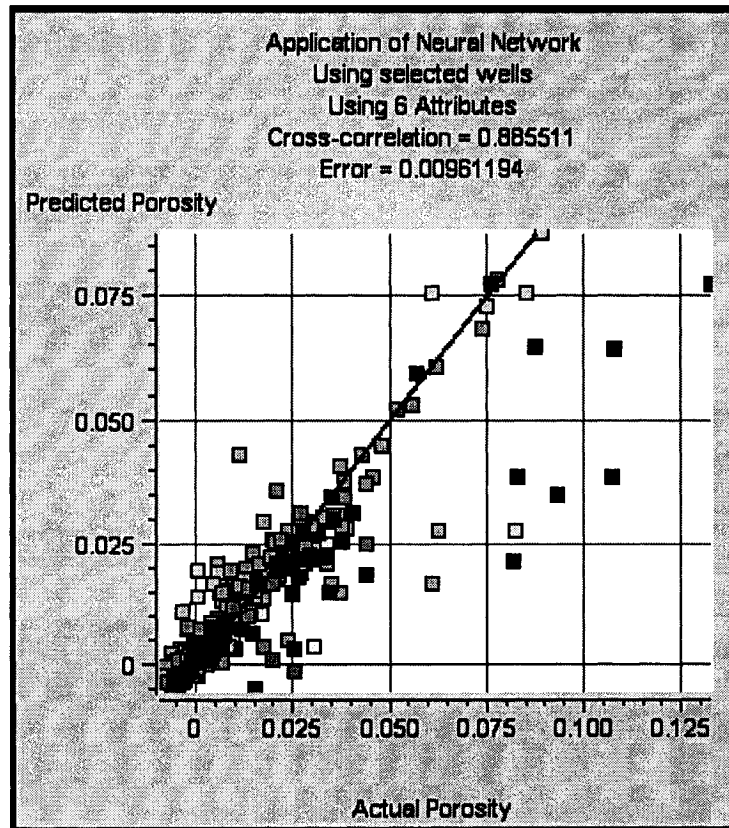
Figure 18: The application of the neural network to the entire seismic survey

generated a porosity volume, high porosity values are in hot colors.

a) Inline 93 (B-B') showing the Strong UN #1 well and b) Inline 33

(C-C') with the Downes #2 and #3 wells shown. The faults are also

seen in these inlines and the best-developed porosity is clearly

between the limbs of the flower structures (i.e. where synthetic shear

faults overlap).
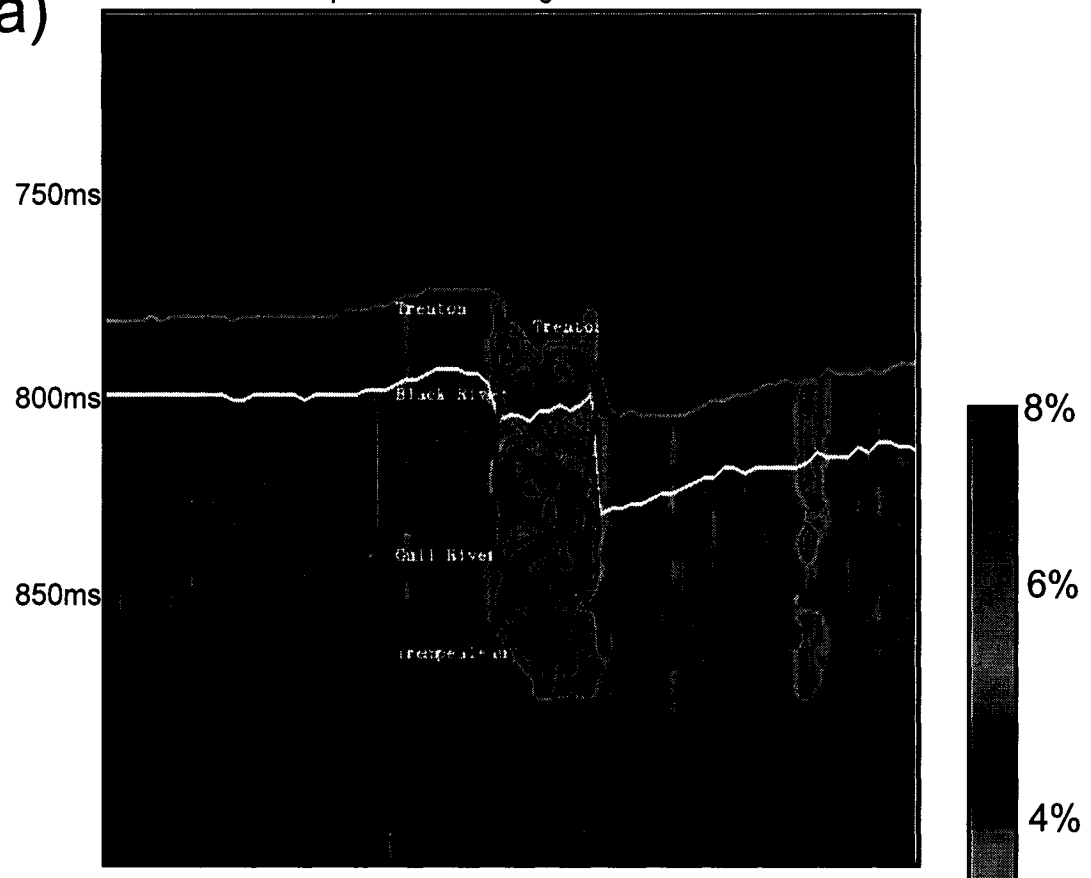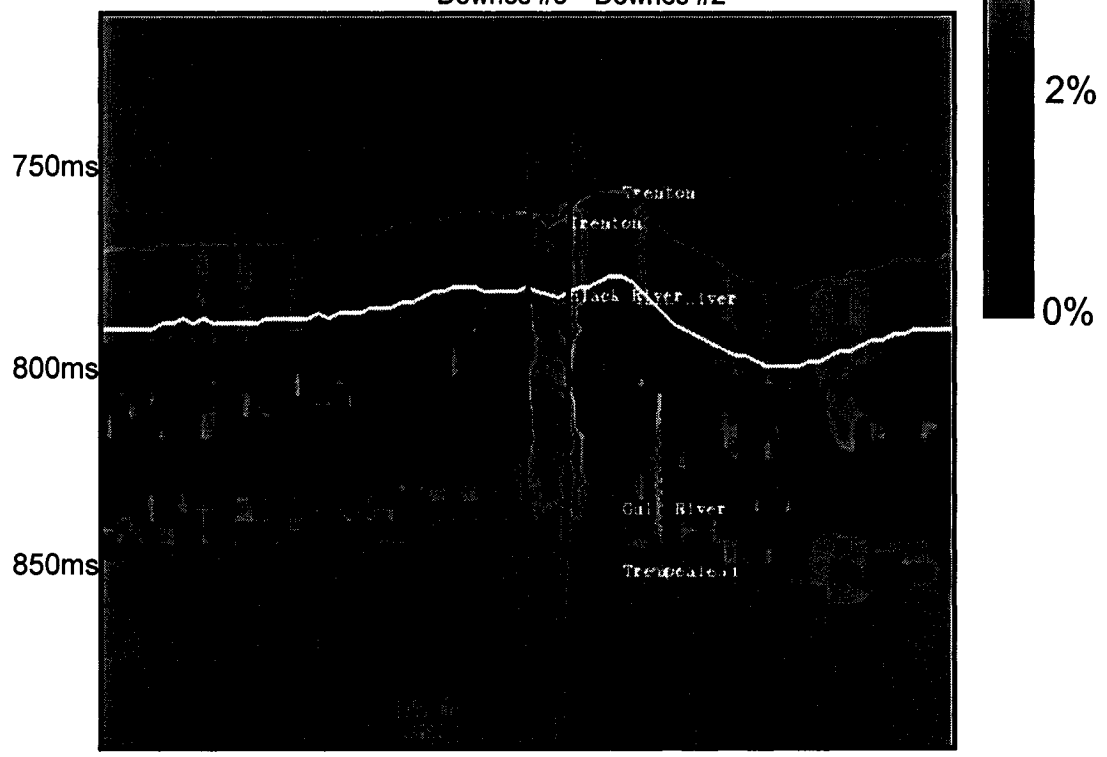
Figure 19: The RMS porosity measured for a window 40ms below the Trenton,

hotter colors represent higher porosity. The linear porosity trend can

be seen, along with some of the noise that was predicted on the

edges of the survey. The latter is particularly evident along the

western margin of the survey.

0mi   2.5mi

0km   2.5km
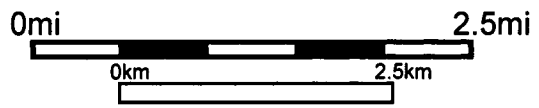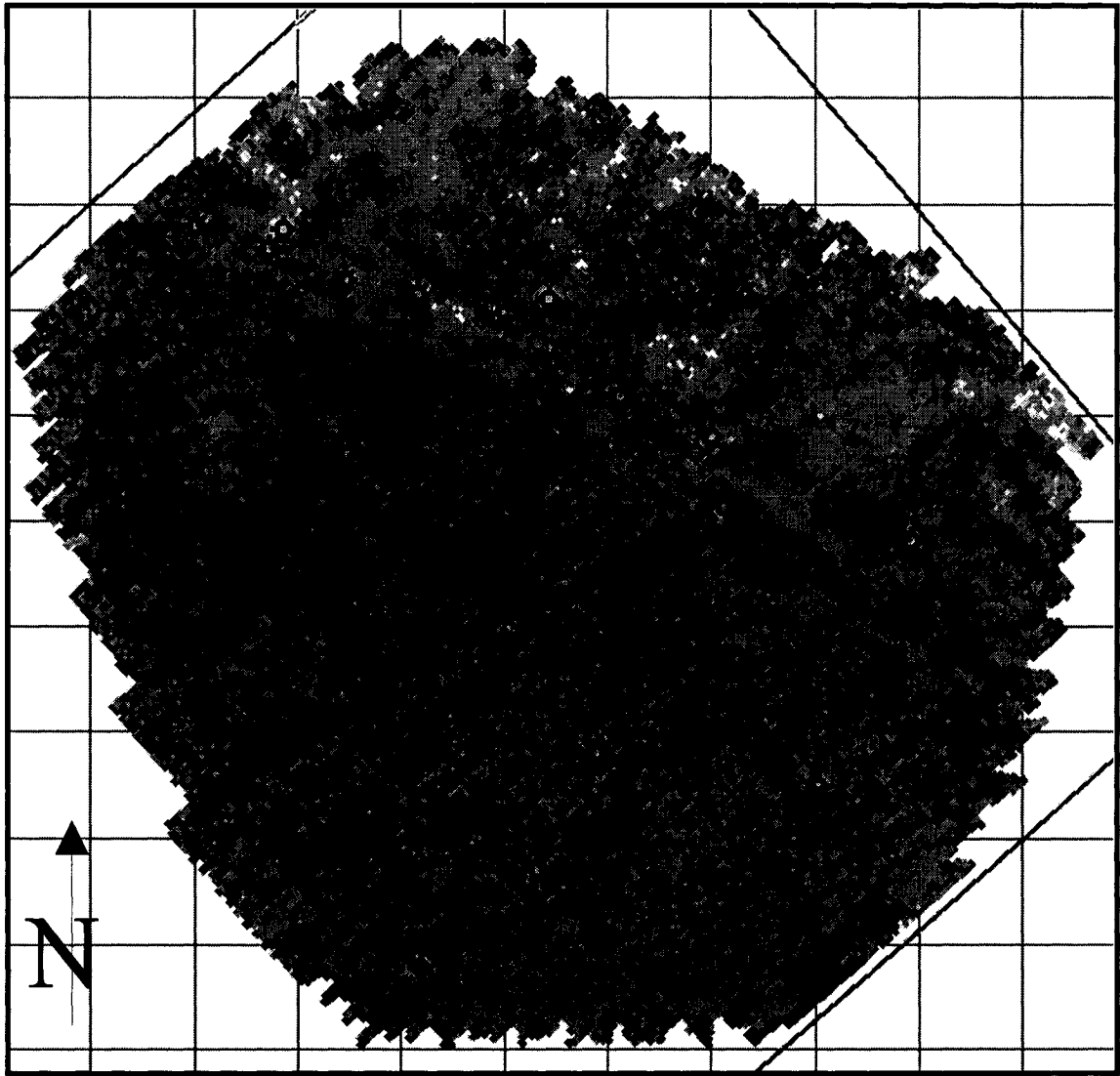
It is important to justify the use of the attributes used in the prediction in order to ensure that they are geologically valid (e.g., Schultz et al., 1994). The single best attribute to use was the RMS amplitude (calculated in a sliding window of 100ms), which has proven to be significant when tracking lithological changes (e.g., from limestone to dolomite) and amplitude anomalies (Chen and Sidney, 1997). The next two best attributes found by the prediction were perigram and reflection strength, which are interrelated. Perigram was first described by Gelchinsky et al. (1985) and is the low-frequency component of reflection strength that is then subtracted from the reflection strength such that it contains both positive and negative samples. The reflection strength is the instantaneous value of the square root of the total energy, and is often used as a phase-independent measure of amplitude. Both of these attributes are useful for detecting phenomena such as thin-bed tuning effects, which may be useful in the Saybrook area given the variable thickness of the porous dolomite (15ft-345ft or 4.6m-105m), and both respond to changes in acoustic impedance, which in turn is directly influenced by lithological changes (as from limestone to dolomite) or other variations in physical properties (Chen and Sidney, 1997). The derivative of the reflection strength is a measure of the rate of change of that attribute. It conveys discontinuities in the amplitude, in contrast to changes in magnitude (as imaged by perigram and reflection strength), which may reflect faulting or fractured rocks (Taner, 2000). The integrated trace is calculated performing integration such that the output trace is the sum of the original samples including the original sample. It tends to reflect contrasts in physical properties and can be

considered a first-pass estimate of acoustic impedance, which is a function of lithology and porosity. Finally the cosine of instantaneous phase is commonly used as a measure of continuity that is independent of amplitude. As such it can be useful in delineating faulted zones and tuning effects (Chen and Sidney, 1997).

Some of the attributes that were found to be optimal predictors may appear to be somewhat redundant, such as perigram, reflection strength, and derivative of reflection strength. However, it can be proven mathematically that the step-wise regression methodology will only select attributes if they add information (Hampson et al., 2001). We conclude that the attributes all 'see' the porosity in slightly different ways.

A comparison of the predicted versus the actual porosity logs shows that in some of the wells, such as Dalin E UN #1 and Downes #1, the neural network under-predicted values at the end of the logs (Figure 17a). This is also evident in the cross plot of predicted versus actual values as those underpredicted values are well below the trend (Figure 17b). This effect may be due to artifacts in the prediction where the wells terminated within the Trenton-Black River interval. Some higher porosity values were also predicted in the upper few milliseconds of the Trenton. The upper part of the Trenton limestone does tend to have slightly higher PHIA porosity (2-3% as at Rife #2 and Merilla L UN #5) than undolomitized rocks lower in the Trenton-Black River (which average 0-2%), although without core the reasons for this difference are unknown.

A RMS amplitude map of the porosity for the 40ms below the Trenton horizon shows several trends (Figure 19). The areas with the highest porosity were found to trend in line with the producing wells. It was also evident that there were lenses of higher porosity along this trend, and areas where the higher porosity values were missing, as in Dalin E UN #1. Towards the edges of the survey the neural network generated some porosity values that were unreasonably high and are most likely related to noise in the data. The prediction accurately illustrates the porosity especially in cases where the trend was just missed, as in the case of Downes #2 and Downes #3. Although only 580ft (177m) separates these two wells, Downes #3 contains porosity while Downes #2 does not (Figure 18b and 19). Transects through the porosity volume showing relationships between porosity and faults are presented and discussed in the following section.

2.6 Discussion: Faults and Porosity

The regularity of the locations of the small collapse structures where the porosity is preferentially developed would suggest some structural control on the development of the porosity. Rotation of parallel antithetic shear faults can occur in an area of direct shear (Ahlgren, 2001). Discrete packages of rocks may form that rotate slightly in the opposite direction of the main shear (Figure 15a, b) (Schreurs, 1994; Alhgren, 2001). With a left lateral strike-slip system, antithetic rotation would occur in conjunction with north-south extension (Figure 14). This

movement combined with minor dip-slip movement of the Saybrook fault system would pull the overlying cover downwards and cause dilation along the faults, thus facilitating the upward migration of fluids. If Mg-rich fluids rose along these conduits, entered the formation and became concentrated in the structural highs, dolomitization could proceed (Warren, 2000). The associated brecciation and dissolution in these conduits could lead to the creation of the small collapse structures seen along the main ridge at Saybrook. This dolomitization may have been responsible for obliterating most of the direct evidence of antithetic movement. Furthermore, antithetic shear faults usually have little offset and are typically smaller in size than synthetic shear faults, making them more difficult to image seismically (Schreurs, 1994; Mandl, 1999; Ahlgren, 2001). Another factor to consider is that the amount of deformation along a fault is not constant (Ahlgren, 2001). Thus antithetic faults may have formed preferentially in areas where there was better development of the synthetic shears, as in the center of the main fault trend and in the northwest portion of the area. Cross-sections through the porosity volume show the relationship of the faults to the porosity in the vicinity of the wells. These cross-sections illustrated that the porosity was best developed in areas between the synthetic shear faults (i.e. the limbs of flower structures; Figure 18a, b).

Exporting the created porosity volume into a program that permitted the faults and seismic to be viewed together in three dimensions, allowed better visualization of the relationship between the faults and the predicted porosity. Values below about 5% porosity were made transparent so that the highest

porosity (producing) areas could be highlighted. While some of the predicted noise was isolated through this procedure, especially on the edges of the survey, in general the porosity is observed to be closely associated with the mapped fault network. The highest porosity values are concentrated in the areas of intense faulting, especially where the synthetic shear faults overlap and meet at depth to create flower structures (Figure 20a-c). This may indicate that fluid migration pathways were better developed in these areas. It is also apparent that although the main fault trend strikes approximately 122°-302°, the porosity development does not follow this trend. Instead it is better developed along the obliquely striking en echelon synthetic shear faults at an average strike of 105°-285°. This trend continues in the northwest to where the left lateral offset of the basement fault is located (B; Figure 8) and where there are also overlapping synthetic shear faults at the Trenton level (Figure 18b, Figure 20a-c). By examining the relationship between the porosity and fault system in plane view, it can be seen to support the proposed model of porosity development discussed above.

2.7 Conclusions

This study established a relationship between a seismic attribute-based porosity prediction and the structural framework of a suspected hydrothermal dolomite field. This was accomplished through first mapping the faults in the area and then training a neural network to create a porosity volume of the

Figure 20: a-c) A series of 3 slices through the porosity volume illustrating the changes in porosity development through the Trenton-Black River section, the color scale ends at 8% porosity and values above that are white. The slice in a) is taken 10ms below the Trenton surface and shows the best development of porosity in the center as well as in the northwest part of the survey. The next slice b) is 30ms below the Trenton and the porosity in the northwest is less apparent than in a). In c) which is 60ms below the Trenton, there is no evidence of it at all.

a) 10ms

b) 30ms

c) 60ms

>8%

4%

2%

0%

N

0mi   2.5mi
0km   2.5km
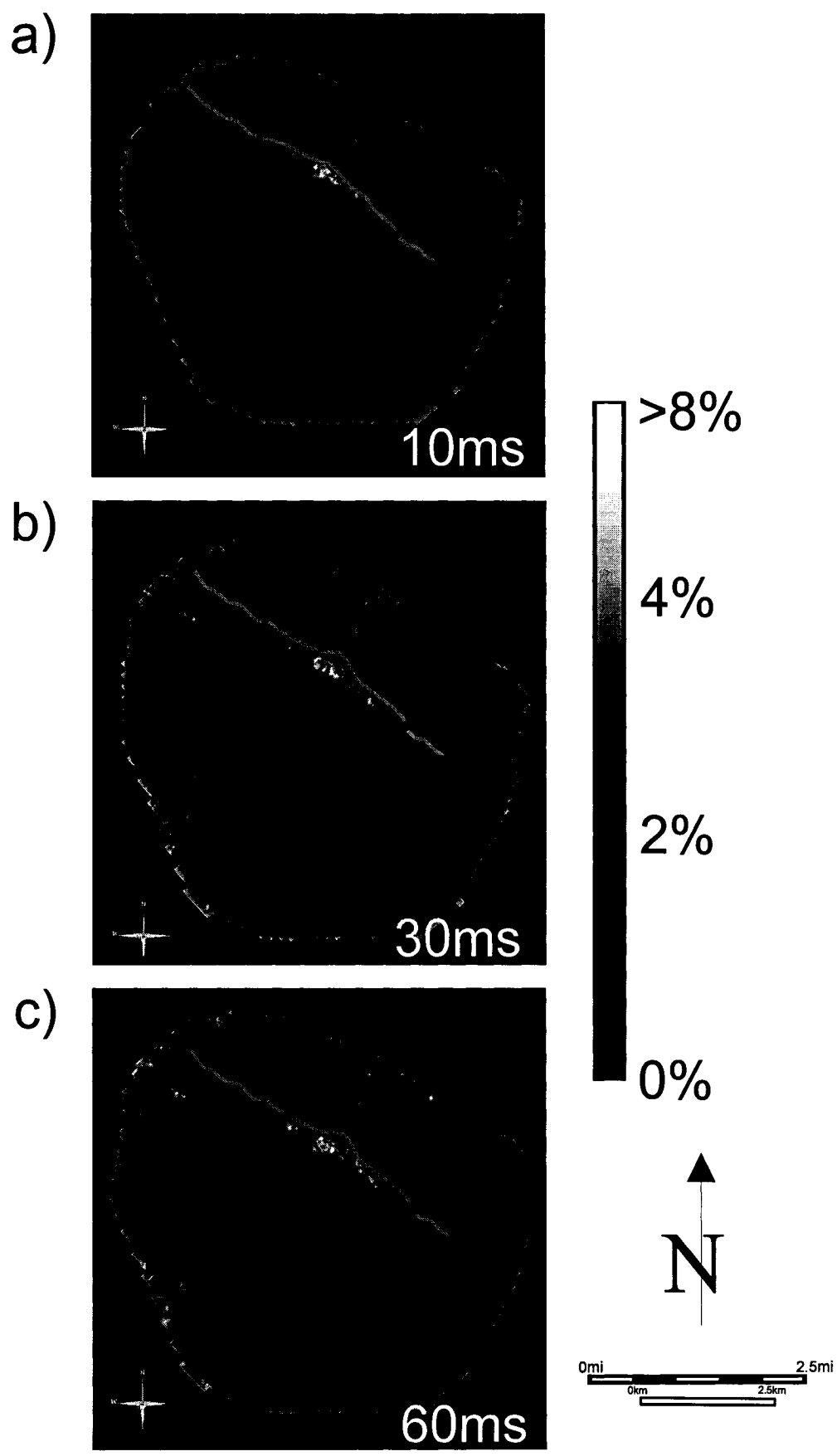
Trenton-Black River interval. The neural network used six attributes identified through step-wise linear regression and was found to adequately predict the PHIA porosity of the wells included in the training set. The predicted trend closely followed that of the producing wells in the field.

The porosity prediction was used as a proxy for dolomite distribution given that only dolomites contain significant porosity in the area. Reactivation of the basement fault that underlies the field appears to have created a ready network of fluid pathways that allowed the Mg-rich fluids to circulate and dolomitize the limestone host rocks. It is proposed that the interaction of synthetic, antithetic and dip-slip movement along the fault zone was responsible for creating these pathways. Seismic porosity imaging in which the best porosity appears to be developed in the areas between synthetic shears, where antithetic faults would be most likely to form, supports this hypothesis. This is especially apparent in areas where the synthetic shears form flower structures, indicating that these structures may have been more efficient fluid migration pathways.

Through the combined use of neural networks to predict porosity and fault mapping in 3-D, it is apparent that faulting is likely the key control on porosity development, and hence dolomite distribution at Saybrook. For plays similar to Saybrook in which the reservoir development is related to a strike-slip fault environment, detailed fault mapping should help to illuminate the impact of these structures.

Chapter 3 – Conclusions

1. The main objective of this study was to combine a seismic attribute-based porosity prediction with a 3-D seismic based structural interpretation in order to better define the dolomite distribution at Saybrook Field in Ohio. This was accomplished through the use of multivariate step-wise regression to determine the best porosity predicting attributes and probabilistic neural networks. These were used to better model their potentially non-linear behaviour and a porosity volume was generated for the entire Trenton-Black River interval.

2. Fault mapping and curvature analysis of the horizons were used to identify the major trends, a set of en echelon faults that spanned most of the survey. The faults at the Trenton-Black River level were interpreted to have formed in response to reactivation of the underlying basement fault due to compressive events during the Taconic Orogeny. The deformation was consistent with a left-lateral strike slip system and the en echelon faults were considered to be synthetic shear faults (after Prouty, 1989). In some locations the synthetic shears overlap to produce flower structures. Curvature analysis of the Trenton horizon also revealed the presence of parallel ridges oriented approximately 50° from the basement strike that were interpreted as evidence for the presence of antithetic shear faults.

3. A variety of visualization techniques were used to identify relationships between porosity distribution and faults, including maps, transects through

the volume and a 3-D integration of the mapped faults and higher porosity values. These techniques allowed the areas between synthetic shear faults to be identified as the locations of higher porosity. Where these synthetic shears meet at depth to create flower structures, the best porosity is developed. The proposed mechanism for porosity development involves the combined motion of antithetic shear faults and minor dip-slip movement to create dilational fluid migration pathways. The episodic movement of dolomitizing fluids through these pathways are thought to have been responsible for the porosity and hence the dolomite distribution.

4. This study reinforces the effectiveness of neural networks in integrating well-based physical properties with seismic attributes in order extrapolate physical relationships away from well control. In addition, the advantage of a volume-based approach is demonstrated in that it allows more flexibility when displaying the data and integrating it with other information (e.g. fault interpretation).

5. Finally, we propose that this approach may be useful in understanding other reservoirs that formed in similar environments (e.g. other Trenton-Black River reservoirs or the Slave Point of the WCSB). Integration of the structural interpretation and with a seismic-based porosity model may help to further illuminate the control of structure on porosity or dolomite distribution.

References

Al-Aasm, I., Lonnee, J., Clarke, J., 2002. Multiple fluid flow events and the formation of saddle dolomite from the Middle Devonian of the Western Canada Sedimentary Basin. Marine and Petroleum Geology, v. 19, p. 209-217.

Ahlgren, S.G., 2001. The nucleation and evolution of Riedel shear zones as deformation bands in porous sandstone. Journal of Structural Geology, v. 23, p. 1203-1214.

Berger, Z., and Davies, G., 1999. Hydrothermal dolomites; the development of linear hydrothermal dolomite (HTD) reservoir facies along wrench or strike slip fault systems in the western Canadian sedimentary basin: Reservoir, v. 26, p. 34-38.

Brown, A.R., 1996. *Interpretation of Three-Dimensional Seismic Data, 4th ed.* American Association of Petroleum Geologists Memoir 42, 424p.

Boreen, T.D., Colquhuon, K., 2003. The Ladyfern Gas Field – Canada is still hiding mammoths. AAPG, 2003 Annual Meeting, Abstracts, p. A17.

Budai, J.M., and Wilson, J.L., 1991. Diagenetic history of the Trenton and Black River Formations. *In:* Early sedimentary evolution of the Michigan Basin. P. A. Catacosinos and P.A. Daniels Jr. (eds.). Geological Society of America Special Paper 256, p. 73-88.

Carter, T., Trevail, R., Easton, R., 1996. Basement controls on some hydrocarbon traps in southern Ontario, Canada. *In:* Basement and Basins of Eastern North America. B.A. van der Pluijm and P.A. Catacosinos (eds.). Geological Society of America Special Paper 308, p.95-107.

55

Chen, Q., and Sidney, S., 1997. Seismic attribute technology for reservoir forecasting and monitoring: The Leading Edge, v. 15, p. 445-456.

Ettensohn, F.R., Hohman, J.C., Kulp, M.A., Rast, N., 2002. Evidence and implications of possible far-field responses to Taconian Orogeny: Middle-Late Ordovician Lexington Platform and Sebree Trough, east-central United States. Southeastern Geology, v. 41, p. 1-36.

Farquhar, R.M., Haynes, S.J., Mostaghel, M.A., Tworo, A.G., Macqueen, R.W., Fletcher, I.R., 1987. Lead isotope ratios in Niagara Escarpment rocks and galenas: implications for primary and secondary sulphide deposition. Canadian Journal of Earth Sciences, v. 24, p. 1625-1633.

Gelchinsky, B., Landa, E., Shtivelman, V., 1985. Algorithms of phase and group correlation. Geophysics, v. 50, p. 596-608.

Granath, V.,1991. Geochemical constraints on the origin of dolomite in the Ordovician Trenton and Black River limestones, Albion-Scipio area, Michigan. AAPG Bulletin, v. 75, p. 584-585.

Hampson, D., Schuelke, J., and Quirein, 2001. Use of multi-attribute transforms to predict log properties from seismic data. Geophysics, v. 66, p. 220-236.

Hart, B.S., and Balch, R.S., 2000. Approaches to defining reservoir physical properties from 3-D seismic attributes with limited well control: An example from the Jurassic Smackover Formation, Alabama. Geophysics, v. 65, p. 368-376.

Hart, B.S., and Chen, M.A. *in press*. Understanding seismic attributes through forward modeling. The Leading Edge.

Hart, B.S., Pearson, R.A., and Rawling, G.C., 2002, 3-D seismic horizon-based approaches to fracture-swarm sweet spot definition in tight-gas reservoirs. The Leading Edge, v. 21, p. 28-35.

Hearst, J., Nelson, P.H., Paillet, F.L., 2000. *Well Logging for Physical Properties: A Handbook for Geophysicists, Geologists and Engineers.* John Wiley and Sons Ltd: West Sussex, England, 483p.

Hurley, N., Budros, R., 1990. Albion-Scipio and Stoney Point fields, USA, Michigan Basin. *In:* Stratigraphic Traps I: Treatise of Petroleum Geology Atlas of Oil and Gas Fields. E.A. Beaumont and N.H. Forster (eds.). American Association of Petroleum Geologists, p. 1-37.

Jacobi, R.D., Smith, G., Fountain, J., Fagan, J.P., 2004. Fault systems in New York State and carbonate reservoirs: Trenton/Black River and younger plays. AAPG, 2004 Annual Meeting, Abstracts, p. A70.

Keith, B.D., 1989. Reservoirs resulting from facies-independent dolomitization: Case histories from the Trenton and Black River carbonate rocks of the Great Lakes Area. *In:* The Trenton Group (Upper Ordovician Series) of Eastern North America. B.D. Keith (ed.). American Association of Petroleum Geologists, Studies in Geology No. 29, p. 267-276.

Larsen, G.E., 2000 (Hull, D.N., 1990, chief compiler). Generalized Column of Bedrock Units in Ohio: http://www.ohiodnr.com/geosurvey/pdf/stratcol.pdf.

Leiphart, D.J., and Hart, B.S., 2001. Case History: Comparison of linear regression and a probabilistic neural network to predict porosity from 3-D seismic attributes in Lower Brushy Canyon channeled sandstones, southeast New Mexico: Geophysics, v. 66, p. 1349-1358.

Machel, H., Lonnee, J., 2002. Hydrothermal dolomite – a product of poor definition and imagination. Sedimentary Geology, v. 152, p. 163-171.

MacKenzie, P., and Grubaugh, W., 2000. Discovery of a new field in the Trenton-Black River Interval, Northeastern Ohio: AAPG Bulletin, v. 84, p. 1388.

Mandl, G., 1988. *Mechanics of Tectonic Faulting: Models and Basic Concepts.* Elsevier: Amsterdam, Netherlands, 407p.

Mandl, G., 1999. *Faulting in Brittle Rocks: An Introduction to the Mechanics of Tectonic Faulting.* Springer-Verlag: Berlin, Germany, 434p.

Middleton, K., Coniglio, M., Sherlock, R., Frape, S., 1993. Dolomitization of Middle Ordovician carbonate reservoirs, southwestern Ontario. Bulletin of Canadian Petroleum Geology, v. 41, p. 150-163.

Minken, D.A., 2002. A 3-D seismic case study investigating AVO, acoustic inversion, and probabilistic neural networks in the Trenton-Black River interval, NE Ohio. (M.Sc. thesis): University of Oklahoma, 147p.

Pearson, R.A., and Hart, B.S., 2004. 3-D seismic attributes help define controls on reservoir development: Case study from the Red River Formation, Williston Basin. *In:* Seismic Imaging of Carbonate Reservoirs and Systems. G.P. Eberli, J.L. Masaferro, and J.F. Sarg (eds.). American Association of Petroleum Geologists Memoir.

Prouty, C., 1989. Trenton exploration and wrenching tectonics – Michigan Basin and environs. *In:* The Trenton Group (Upper Ordovician Series) of Eastern North America. B.D. Keith (ed.). American Association of Petroleum Geologists, Studies in Geology No. 29, p. 207-236.

Qing, H., Mountjoy, E., 1994. Formation of coarsely crystalline, hydrothermal dolomite reservoirs in the Presqu'ile Barrier, Western Canada Sedimentary Basin. AAPG Bulletin, v. 78, p. 55-77.

Roberts, A., 2001, Curvature attributes and their application to 3D interpreted horizons. First Break, v. 19, p. 85-99.

Ronen, S., Schultz, P.S., Hattori, M., and Corbett, C., 1994. Seismic guided estimation of log properties, part 2: Using artificial neural networks for nonlinear attribute calculation: The Leading Edge, v. 13, p. 674-678.

Root, S., 1996. Recurrent basement faulting and basin evolution, West Virginia and Ohio: The Burning Springs-Cabridge fault zone. *In:* Basement and Basins of Eastern North America. B.A. van der Pluijm and P.A. Catacosinos (eds.). Geological Society of America Special Paper 308, p.127-137.

Russell, B., Hampson, D., Scheulke, J., Quirein, J., 1997. Multiattribute seismic analysis. The Leading Edge, v. 16, p. 1439-1443.

Scheulke, J., and Quirein, J., 1998. Validation: A technique for selecting seismic attributes and verifying results. 68th Annual International Meeting of the Society of Exploration Geophysicists (expanded abstract), p. 936-939.

Schreurs, G., 1994. Experiments on strike-slip faulting and block rotation. Geology, v. 22, p. 567-570.

Schultz, P.S., Ronen, S., Hattori, M., Corbett, C., 1994. Seismic-guided estimation of log properties: Part 1: A data-driven interpretation methodology. The Leading Edge, v. 13, p.305-315.

Smith, L.B., Lugert, C.M., Nyahay, R.E., 2003. Integrated characterization of

hydrothermal dolomite reservoirs in Trenton-Black River carbonates of New York. AAPG, 2003 Annual Meeting, Abstracts, p. A160.

Taner, M.T., 2000. Attributes Revisited: retrieved from http://www.rocksolidimages.com/pdf/attrib_revisited.htm.

Versical, R.T., 1991. Basement control on the development of selected Michigan Basin oil and gas fields as constrained by fabric elements in Paleozoic limestones. (MSc Thesis): Western Michigan University, 104p.

von Frese, R.R.B., Jones, M.B., Kim, J.W., Li, W.S., 1997. Spectral correlation of magnetic and gravity anomalies of Ohio. Geophysics, v. 62, p. 365-380.

Warren, J., 2000. Dolomite: occurrence, evolution and economically important associations. Earth-Science Reviews, v. 52, p.1-81.

Wickstrom, L.H., and Gray, J.D., 1989. Geology of the Trenton Limestone in northwestern Ohio. In: The Trenton Group (Upper Ordovician Series) of Eastern North America. B.D. Keith (ed.). American Association of Petroleum Geologists, Studies in Geology No. 29, p. 159-167.

Appendices

Appendix A: Synthetic-Seismic Ties

In order to calibrate the seismic data (measured in time) and the well log data (measured in depth), synthetic seismograms needed to be generated by using sonic logs. Because there were only two actual sonic logs in the dataset, sonic logs needed to be estimated from other logs for the remaining 25 wells. As mentioned in Chapter 2, this required using a multiattribute step-wise linear regression, which identified a combination of four logs as being the optimal predictors (Figure A1a). These logs were the gamma ray, density, neutron porosity, and the density porosity. They were combined into an equation of the form:

$$(\text{P-wave})^2 = 0.0632479(\text{gamma ray})^2 - 1678.08(\text{density})^2 + 5.97485 \qquad (1)$$

$$(\text{neutron porosity})^2 - 6.1116(\text{density porosity})^2 + 14743.2$$

The correlation coefficient between the actual and the predicted sonic logs was 0.987 and the RMS error was 2.1 (Figure A1b). Applying this equation to all the wells generated the sonic logs used to create the synthetics.

The synthetic trace is created by first converting the logs to time using the equation:

$$v = d/(\Delta t/2)$$

v=velocity (ft/s), d=depth (ft), t=time (s)

Then the acoustic impedance (AI) is derived for each sample:

$$AI = \rho v$$

ρ=density

Then the reflection coefficients (RC) are derived by comparing the relative changes in acoustic impedance at sample n to that of sample n+1:

Figure A1: a) Graph showing the prediction and validation error for the

multivariate analysis. The increase in validation error after adding

the fifth log indicates that four logs are the optimal predictors. b)

Applying equation (1) to the actual sonic logs (blue) shows that the

predicted sonic logs (red) are close matches.

a)

Average Error for All Wells
Operator Length: 1
Black Dot: Analysis Using All Wells
Red Dot: Analysis Leaving Out Target Well

Average Error (us/ft)

Number of Attributes

b)

Schoneman #1

5000ft/s   25000ft/s

KRCAL UN #1

5000ft/s   25000ft/s

Trenton
Black River

Gull River
Trempealeau
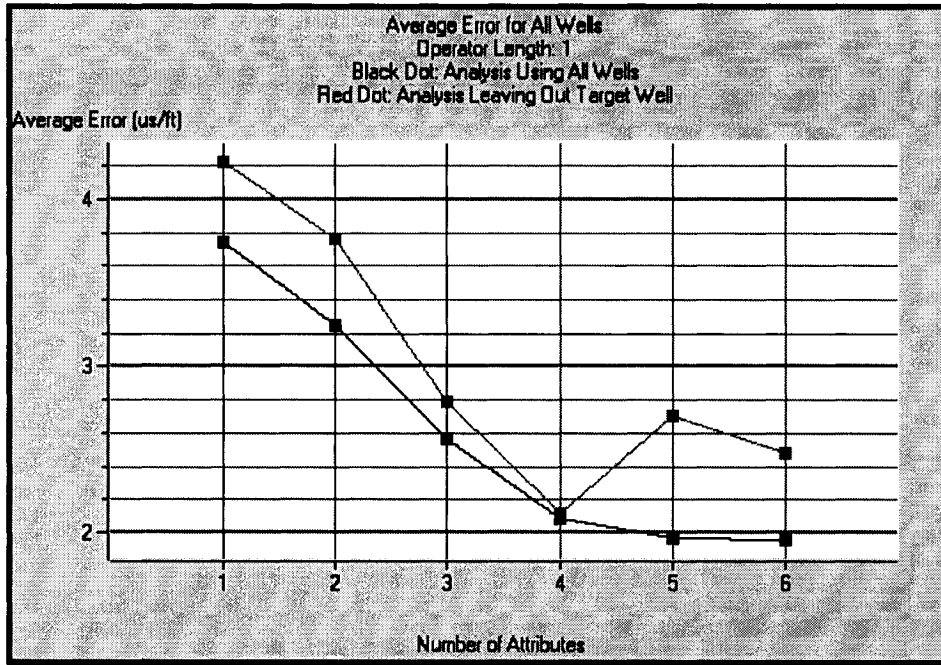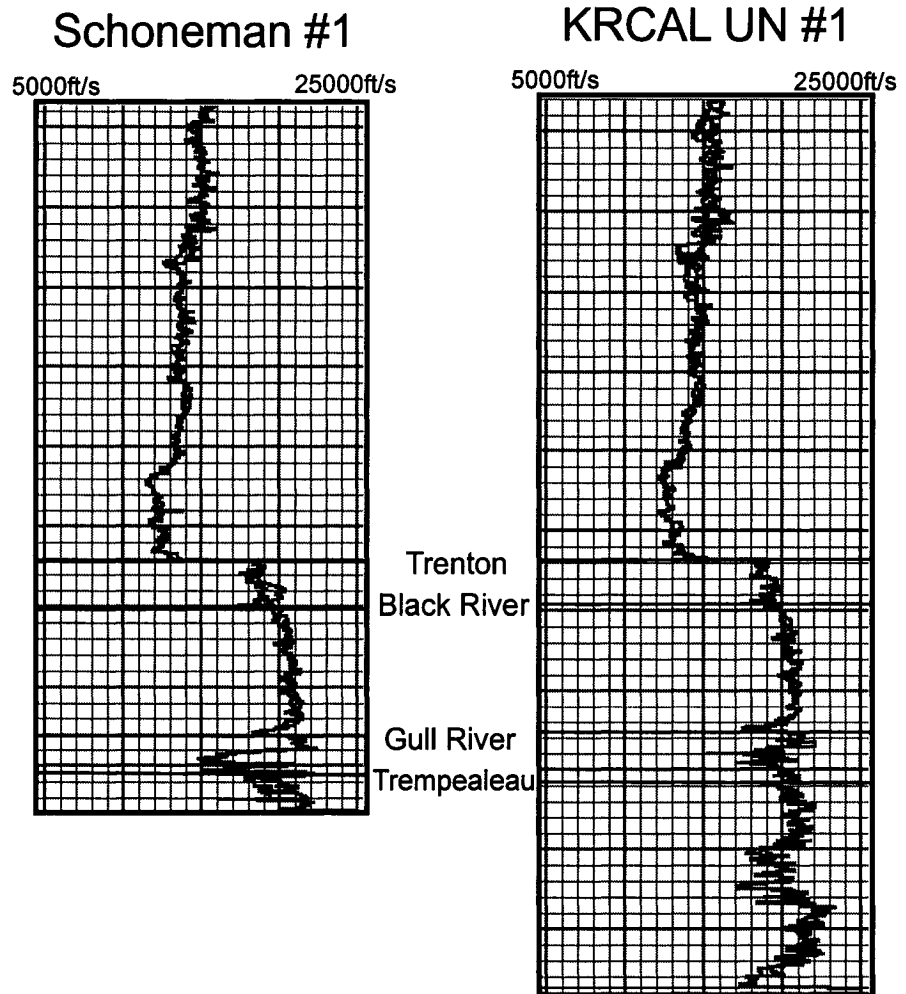
$$RC=(\rho_{n+1}V_{n+1}-\rho_nV_n)/ (\rho_{n+1}V_{n+1}+\rho_nV_n)$$

these values are then put in series so that the changes in reflection coefficients are placed at the correct time.

The next step in creating a synthetic involved extracting a wavelet from the data to be convolved with the calculated changes in reflection coefficients (Russell et al., 1997). The wavelet applied was a statistical wavelet that was extracted over the entire survey from 600ms-900ms. The wavelet was assumed to be zero-phase with a length of 200ms and a taper length of 25ms (Figure A2a, b).

A large washout from a thick evaporite interval at about 2100-2600ft (~450ms) created some anomalous values in the well logs. Thus the interval from 600ms to 900ms was focused on in order to avoid effects of the washout when tying the synthetics. Smaller spikes (from small washouts, vugs etc.) were edited in Hampson Russell's eLog package, which was also used in the synthetic calibration. Almost all of the wells required a static shift to match events at the Trenton. Very little other manipulation of the synthetic trace was required in most cases.

The success of the tie was determined mainly from the correlation coefficient that was calculated over the interval from 600ms until the approximate end of the well log (and hence the synthetic). In most cases the statistical wavelet gave values above 0.75 for the correlation coefficient (Table A1; Figure A3a-n).

Figure A2: Statistical wavelet extracted from the survey over a window 600-

900ms long. a) The wavelet length was 200ms with a taper length of

25ms. The phase and frequency spectrum of the wavelet are shown

in b), although the statistical wavelet will always be zero-phase.

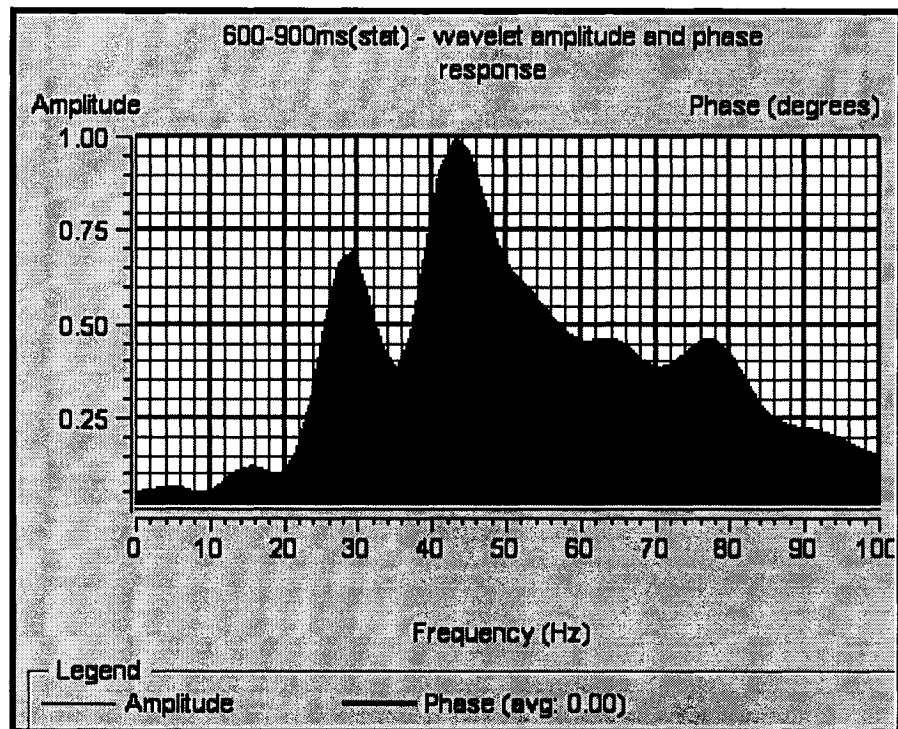a) 600-900ms(stat) - wavelet time response

b) 600-900ms(stat) - wavelet amplitude and phase response
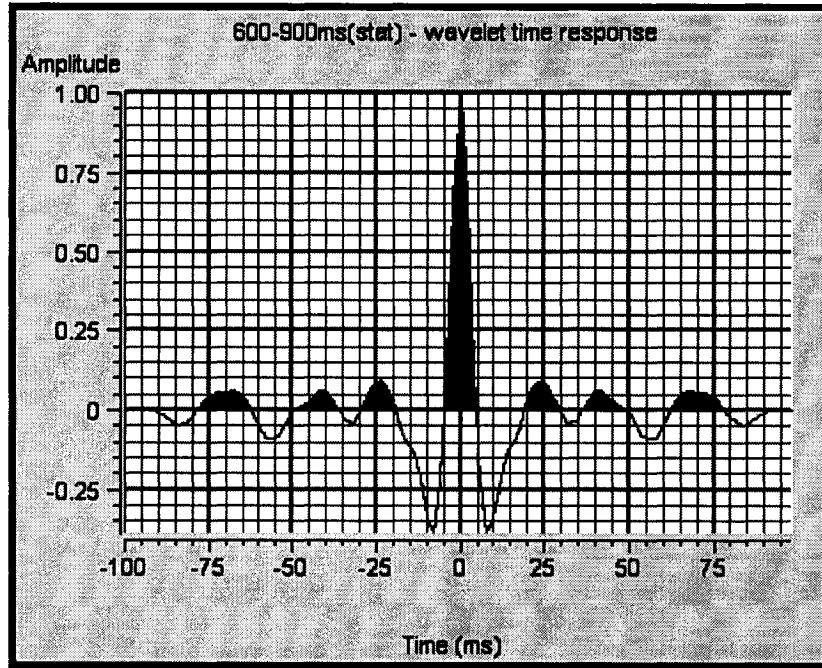
Table A1: The following table shows all of the correlation coefficients for the

seismic to well ties for the training set and the validation set.

| Well Name	Seismic-Well Correlation
Training Set	
BERWALD #1-2951	0.7777
BERWALD #1D-3002	0.7571
BICHSEL UN #1-2955	0.8616
CAMPBELL-HUMPHREY #1-2962	0.8234
CANDELA UN #1-3017	0.7595
CHAPEL HILL G C #1-3006	0.7937
DALIN E UN #1-2979	0.801
DOWNES #1-2971	0.7524
DOWNES #2	0.7554
DOWNES #3-2978	0.5083
KRCAL UN #1-2954	0.8736
MANTELL K UN #1-2961	0.6943
MAROFSKY UN #1-3046	0.7659
MERILLA L UN #5-2975	0.7753
RIFE #2-3013	0.7816
RIFFLE UN #1-2953	0.4876
SCHONEMAN #1-2977	0.818
WRIGHT G UN #1-2980	0.8374
Validation Set	
CHIARAMONTE #1-2987	0.7182
CUTLER UN #1-2997	0.7147
DOWNES R #5-3041	0.7372
MARRISON-ODONNELL U	0.6901
PERKINS UN #1-3014	0.7452
ROWLEY #1-2999	0.6643
STRONG UN #1-3047	0.6642
SULLIVAN UN #2-3022	0.7379
YORK UN #3-2232	0.5548

In the case of the some of the producing wells, once the pay interval was reached the well was not drilled further, resulting in a limited interval over which to tie the synthetic and a poor correlation. This effect was seen at Downes #3 and Riffle UN #1 (Figures 3Ai, k). Pearson and Hart (2004) and Tebo and Hart (*in press*) reported similar problems when working with sonic logs that did not extend throughout the interval of interest.

Figure A3: a to n) Synthetic seismograms correlated over the interval of interest, the generated sonic logs are shown with heavier green lines signifying 250ft intervals (5000-25000ft/s). For Sullivan UN #2 (l) the caliper log is also shown to illustrate the minor washouts in the Trenton-Black River interval, which may have affected the seismic tie.

a) Berwald #1 0.78
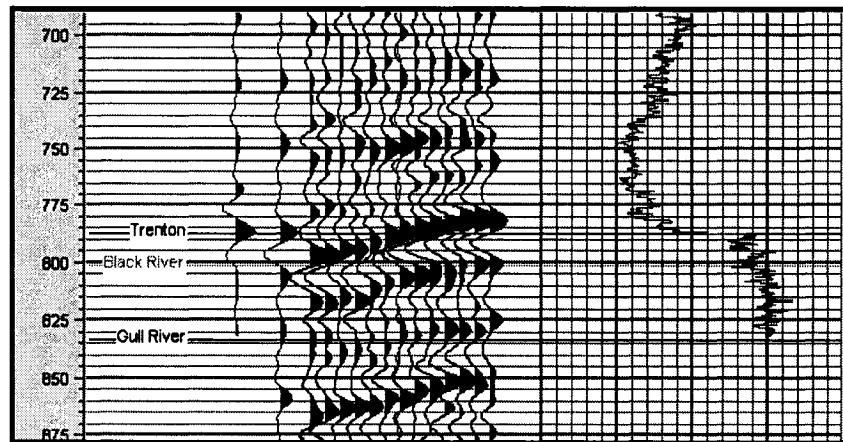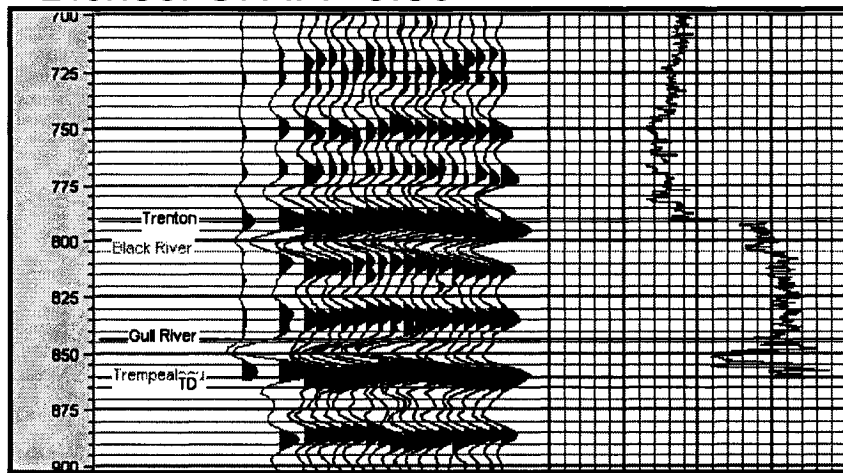

b) Berwald #1D 0.76
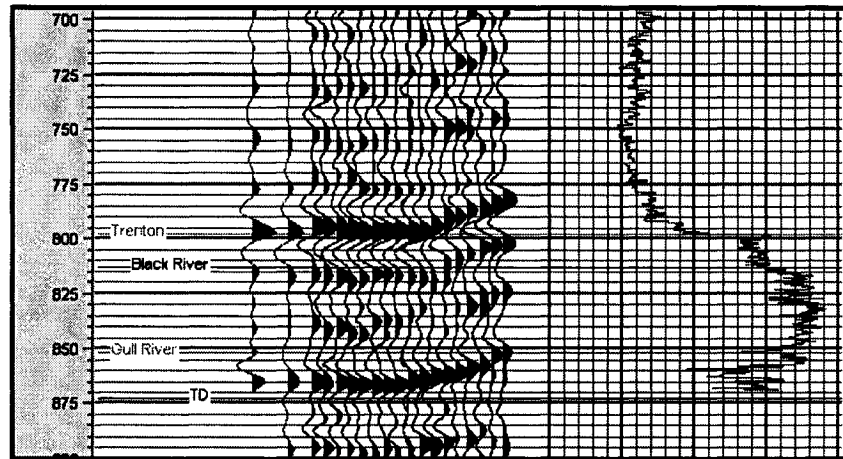
c) Bichsel UN #1 0.86

d) **Campbell-Humphrey #1 0.82**
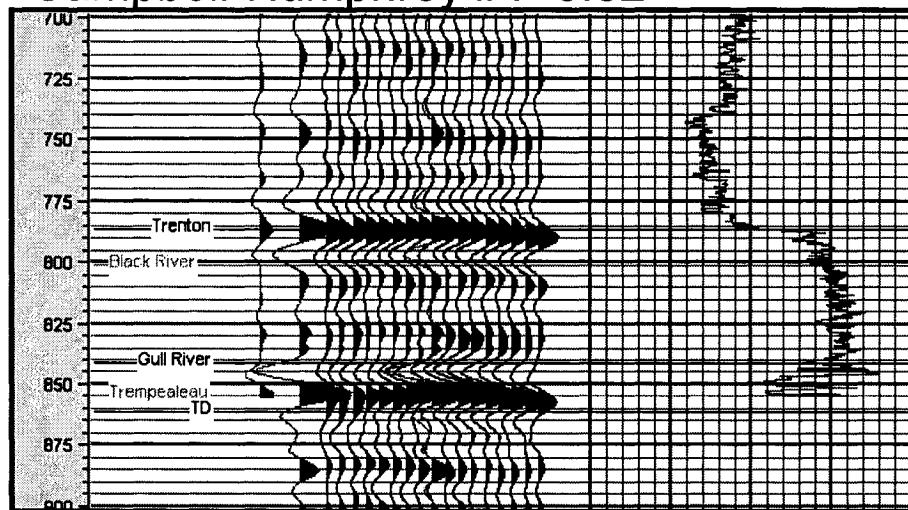
e) **Candela UN #1 0.76**
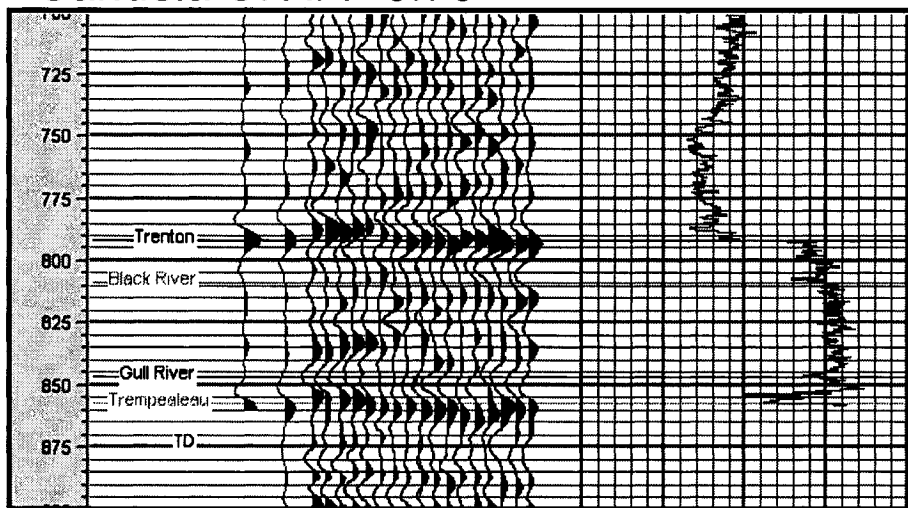
f) **Dalin E UN #1 0.81**
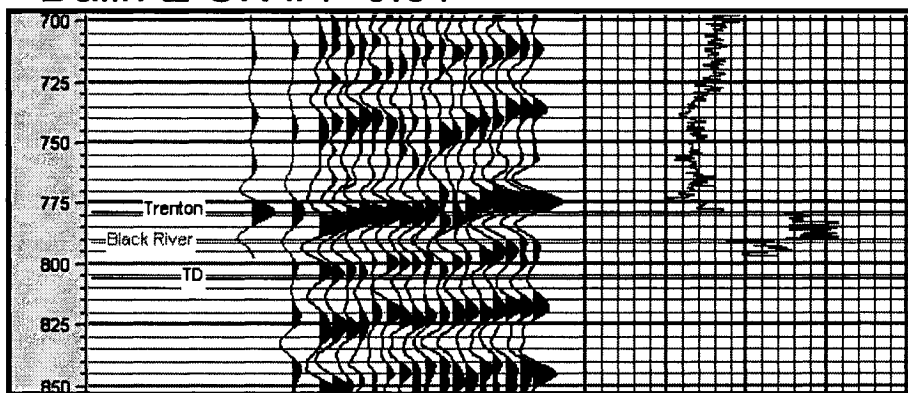
g) **Downes #1 0.75**
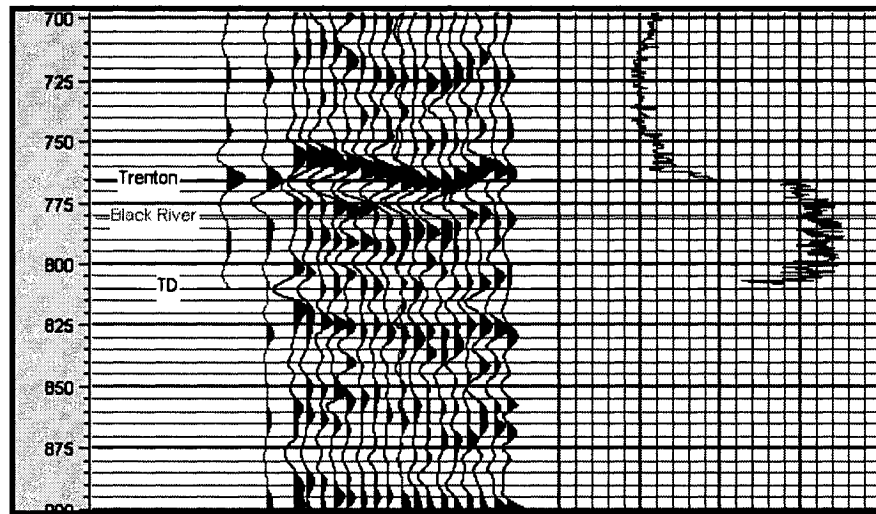
h) **Downes #2 0.76**

l) **Downes #3 0.51**
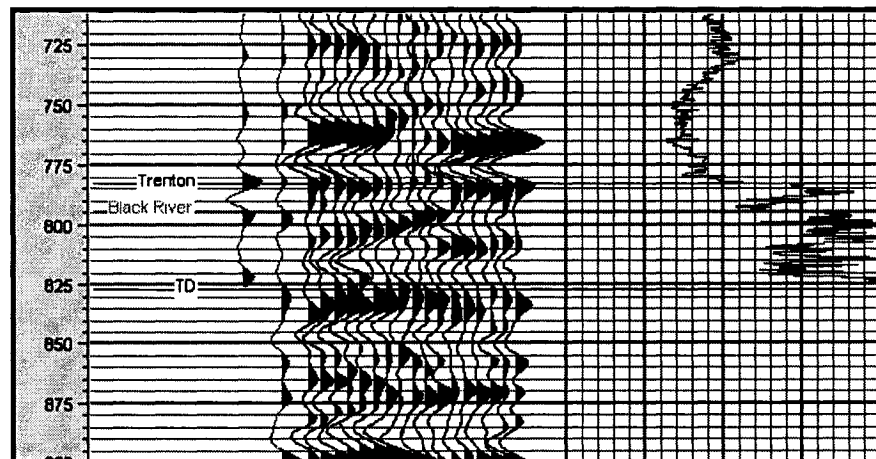
j) **Mantell K UN #1   0.69**

k) **Riffle UN #1   0.49**

l) **Sullivan UN #2   0.71**

m) **Strong UN #1 0.66**

n) **York UN#3 0.55**
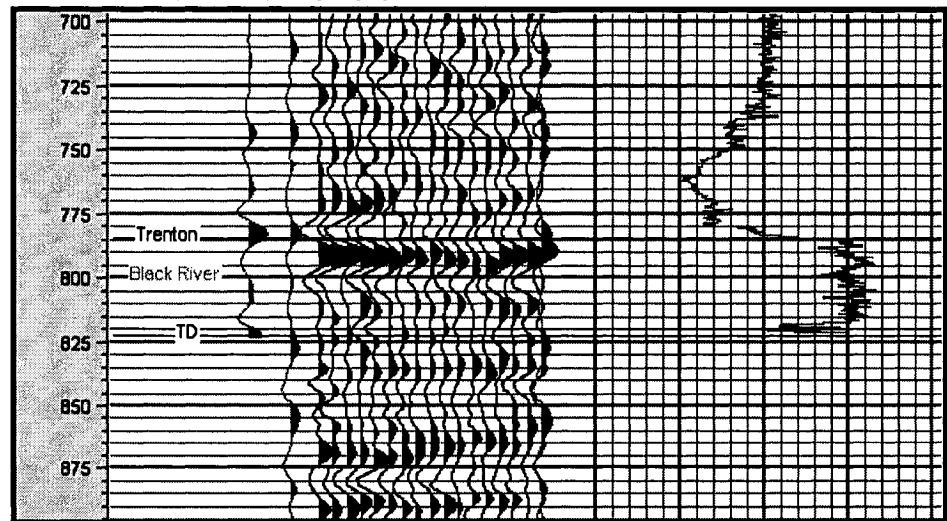
Appendix B: Application and Validation of the Probabilistic Neural Network

(PNN)

Before the neural network could be trained the optimal number of attributes needed to be determined. This was completed by using a multiattribute step-wise regression in Hampson and Russell's Emerge software package (Hampson et al., 2001), as explained in Chapter 2. Addi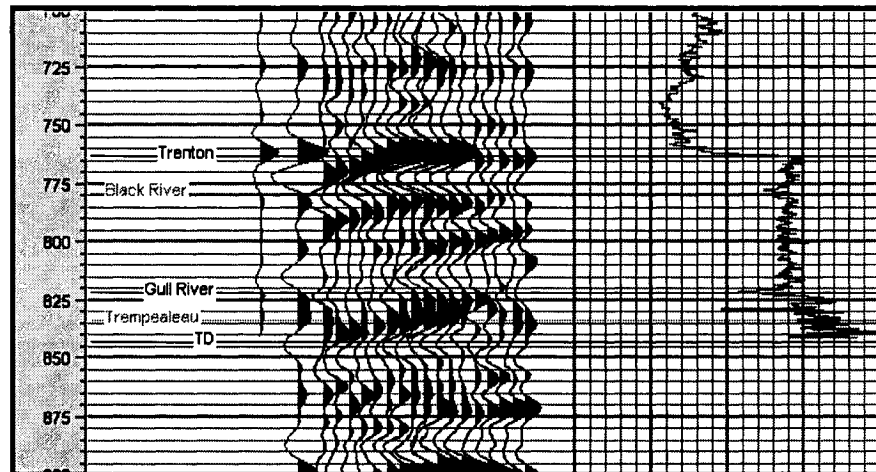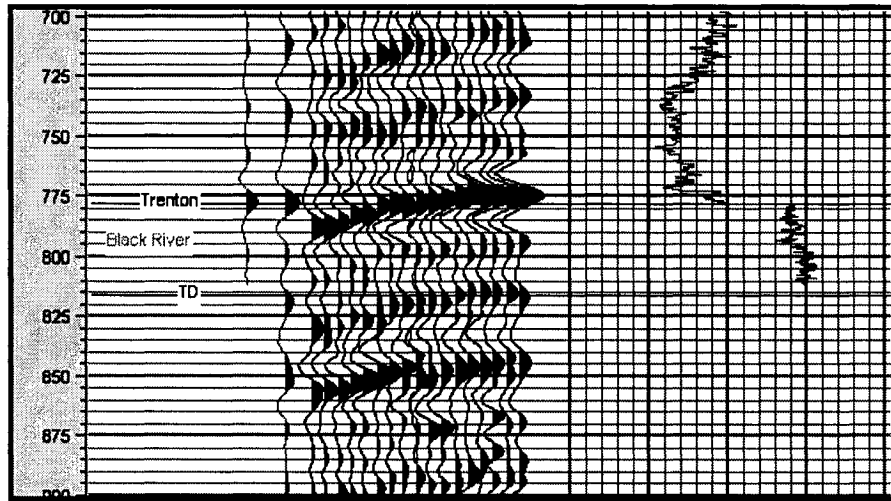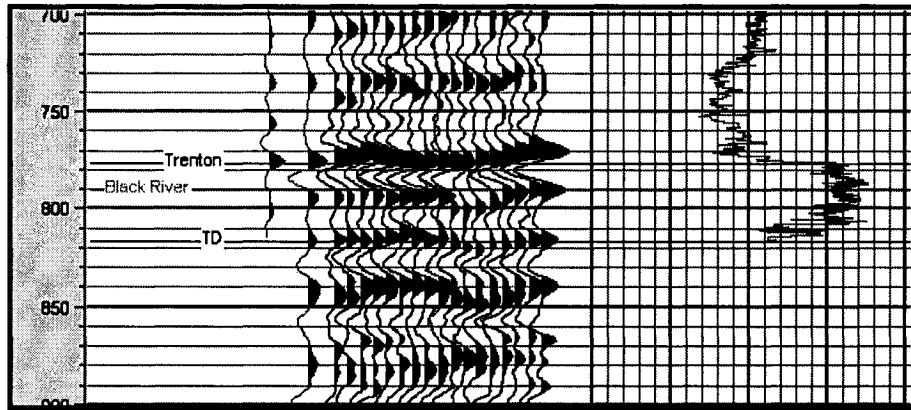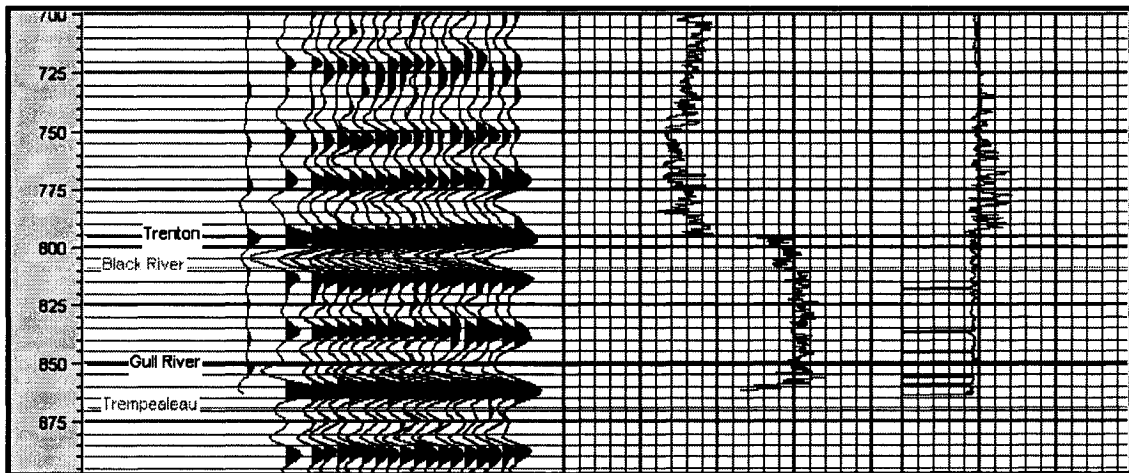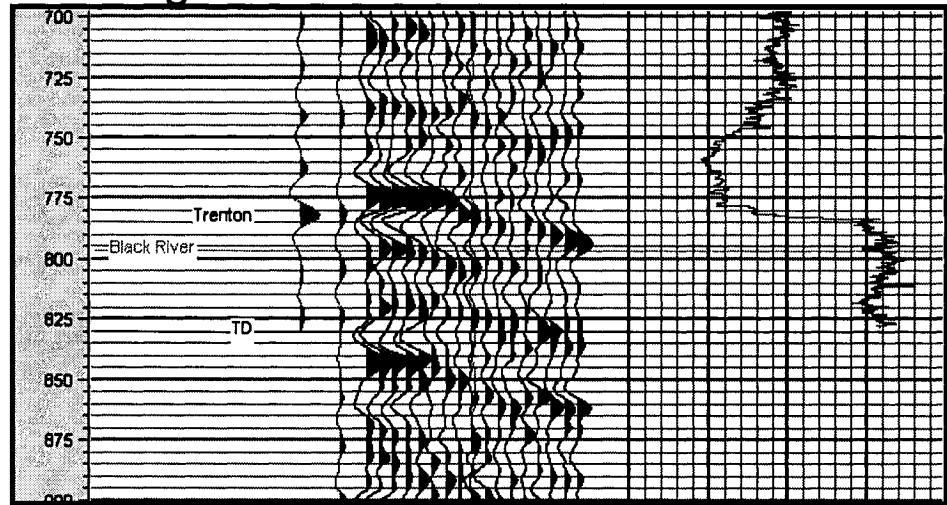tional attributes were added from Landmark's PostStack Pal, including the absolute amplitude, arc length, energy halftime, RMS amplitude, quality factor, response frequency, response phase, amplitude acceleration, perigram, and perigram*cosine of phase. The equation that was generated from the multiattribute analysis had the following form:

$$\text{Porosity (PHIA)}= m_3{}^*\text{log(RMS Amp)} + m_3{}^*1/(\text{Perigram}) + m_3{}^* \text{(Reflection Strength)}^{1/2} + m_3{}^*\text{Derivative of Reflection Strength} + m_3{}^*\text{Integrate} + m_3{}^*\text{Cosine Instantaneous Phase} + \text{Constant}$$

where $m_3{}^*$ represents the convolutional operator (length 3), and the constant (0.296323). For the results and discussion, please see Chapter 2. The application of the neural network for all of the wells in the training set is shown in Figures B1. The validation of the neural network is accomplished by excluding each well from the training set and then attempting to predict the porosity values at that location (Figure B2).

While the training result of the neural network was excellent, the validation result using the wells not included in the prediction was not as accurate. This may be due to the fact that the wells that were not included had poor seismic to well ties, which may have been due to a combination of factors (Table B1). In general, the wells in the training set were chosen based on two measures, how

Figure B1: The neural network was applied to all of the wells in the training set over the interval from the top of the Trenton to the top of the Gull River. The resulting correlation was 89% with an error of 0.0096 v/v (porosity increases to the right –0.1 to 0.3 v/v).
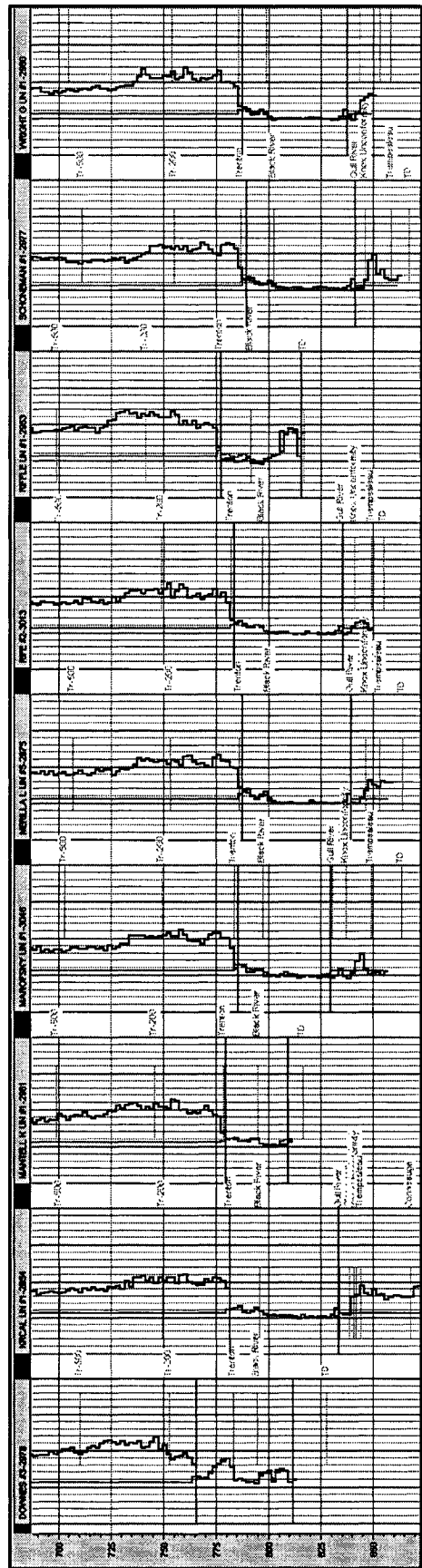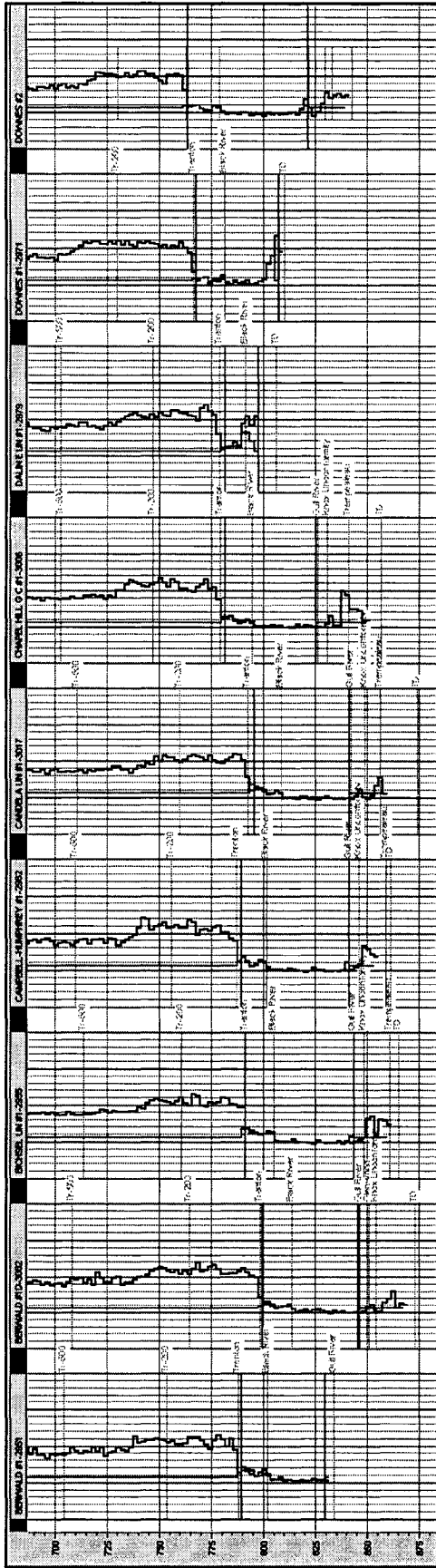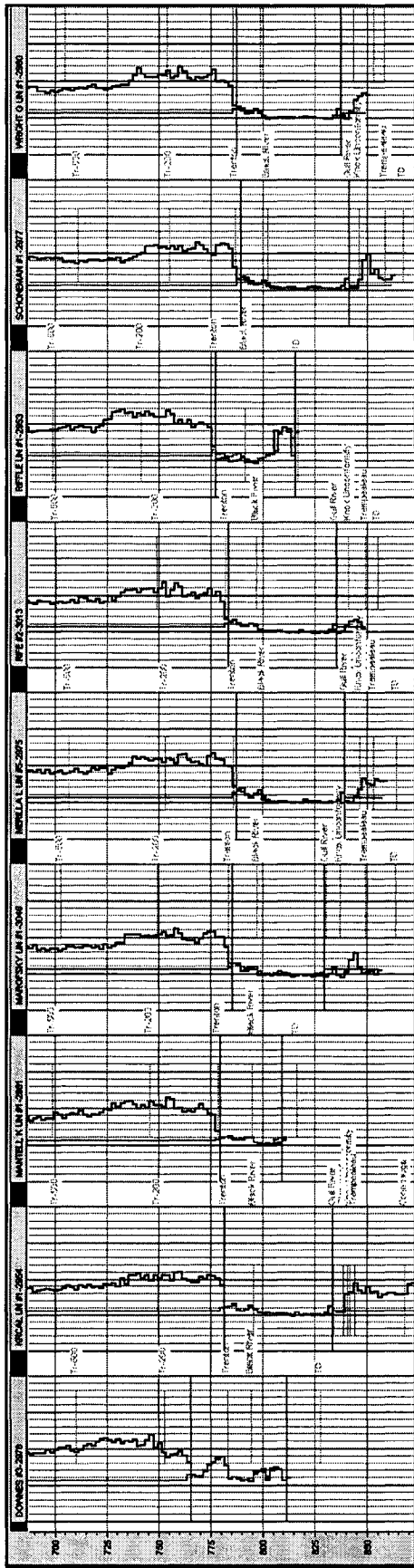
Figure B2: The validation of the neural network was completed by exclusion

testing, one well was removed from the training set and the

remaining wells were used to predict the porosity at that location.

The correlation was 77% with an error of 0.0099 v/v   (porosity

increases to the right –0.1 to 0.3 v/v).
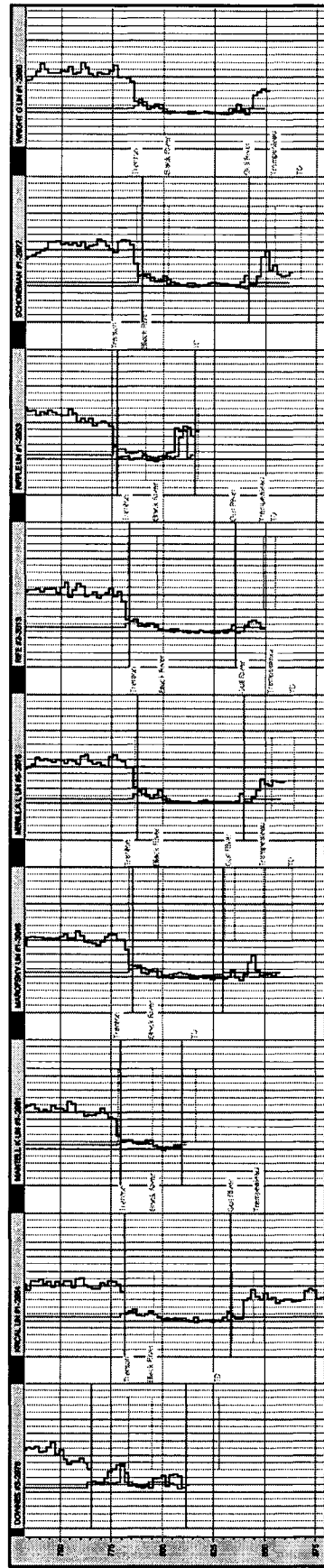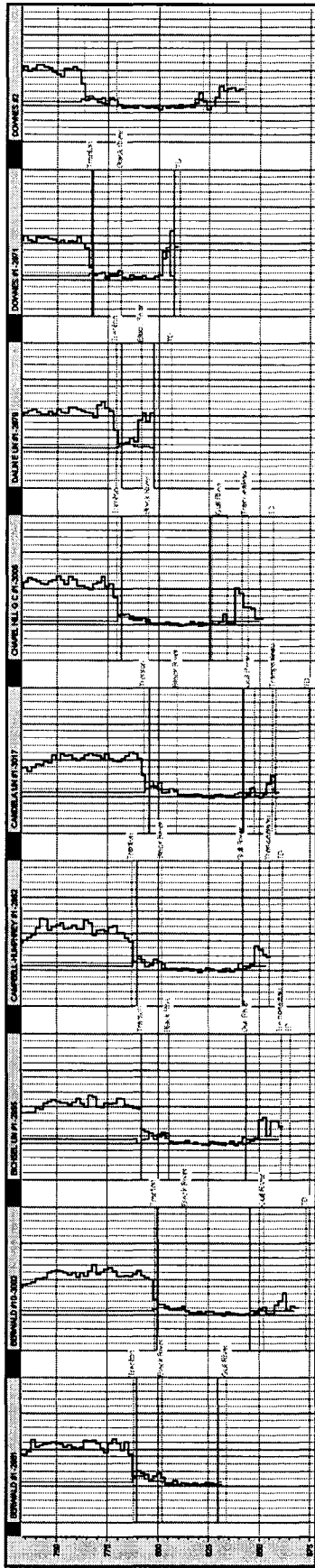
Table B1: The prediction errors (v/v) and correlation coefficients from the neural

network are shown, as well as the seismic-well tie correlation.

Well Name	Prediction Error	PNN Correlation Coefficient	Seismic-Well Correlation
Training Set			
BERWALD #1-2951	0.0050408	0.959353	0.7777
BERWALD #1D-3002	0.0061115	0.915346	0.7571
BICHSEL UN #1-2955	0.0120037	0.856318	0.8616
CAMPBELL-HUMPHREY #1-2962	0.0042812	0.927082	0.8234
CANDELA UN #1-3017	0.0040944	0.942453	0.7595
CHAPEL HILL G C #1-3006	0.0029625	0.956714	0.7937
DALIN E UN #1-2979	0.0323982	0.836555	0.801
DOWNES #1-2971	0.0132963	0.931093	0.7524
DOWNES #2	0.0090014	0.830868	0.7554
DOWNES #3-2978	0.0104309	0.856351	0.5083
KRCAL UN #1-2954	0.0126407	0.716481	0.8736
MANTELL K UN #1-2961	0.0072948	0.63884	0.6943
MAROFSKY UN #1-3046	0.0063848	0.952034	0.7659
MERILLA L UN #5-2975	0.007356	0.874218	0.7753
RIFE #2-3013	0.0044675	0.93428	0.7816
RIFFLE UN #1-2953	0.0152433	0.891547	0.4876
SCHONEMAN #1-2977	0.0063243	0.841633	0.818
WRIGHT G UN #1-2980	0.0049208	0.88749	0.8374
Validation Set			
CHIARAMONTE #1-2987	0.0071301	0.885878	0.7182
CUTLER UN #1-2997	0.0124799	0.650322	0.7147
DOWNES R #5-3041	0.0319359	0.0265463	0.7372
MARRISON-ODONNELL U	0.0103829	0.764242	0.6901
PERKINS UN #1-3014	0.0088875	0.644169	0.7452
ROWLEY #1-2999	0.0141291	0.369574	0.6643
STRONG UN #1-3047	0.0394693	-0.0838135	0.6642
SULLIVAN UN #2-3022	0.0151038	0.753786	0.71
YORK UN #3-2232	0.0473647	-0.0130896	0.5548

well the synthetics correlated with the seismic data and whether or not they contained significant porosity. However, there were some wells that were not included that were significant producers such as the York UN #3 and Strong UN #1 wells, which due to deviated well bores just above the Trenton, did not correlate well (0.55 and 0.66 respectively; Appendix A, Figure 3Am, n). Other wells chosen for the validation set had well logs that were unreliable in the interval around the Trenton due to minor washouts (as in the case of Sullivan UN #2; Appendix A, Figure 3Al), or were situated on the edge of the survey (Downes #5).

By applying the neural network to the validation set we could see that it adequately predicted the porosity in five of the wells (74% correlation), but was quite inaccurate in four of the wells (7.5% correlation; Figure B3). Of these four wells, two were the deviated York UN #3 and Strong UN #1, one was Downes #5 which was located at the noisy edge of the survey, and the last was Rowley #1 that had only a very limited synthetic (~20ms) to tie to the seismic. Thus we propose that the remaining 5 wells would be a more representative gauge of the predicting power of the neural network. The 74% correlation of these wells is satisfactory for predicting the porosity given that they were not included in the training, and these findings reinforces our confidence in the results of the training set.

In order to better quantify the relationship between the seismic-well correlation and the accuracy of the neural network the prediction error was plotted versus the well tie correlation. For the wells not used in training, there

Figure B3: The result of applying the neural network to the wells not included in the training set met with mixed results, five of the wells correlated adequately with an average correlation of 74%, while the remaining four only had a 7.5% correlation likely due to problems with the seismic to well tie (porosity increases to the right –0.1 to 0.3 v/v).
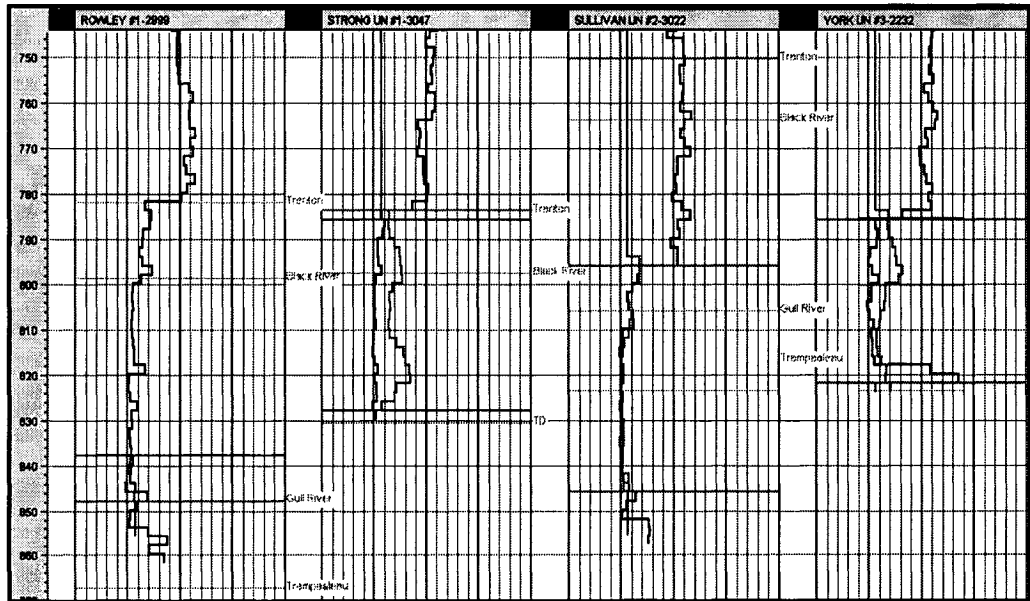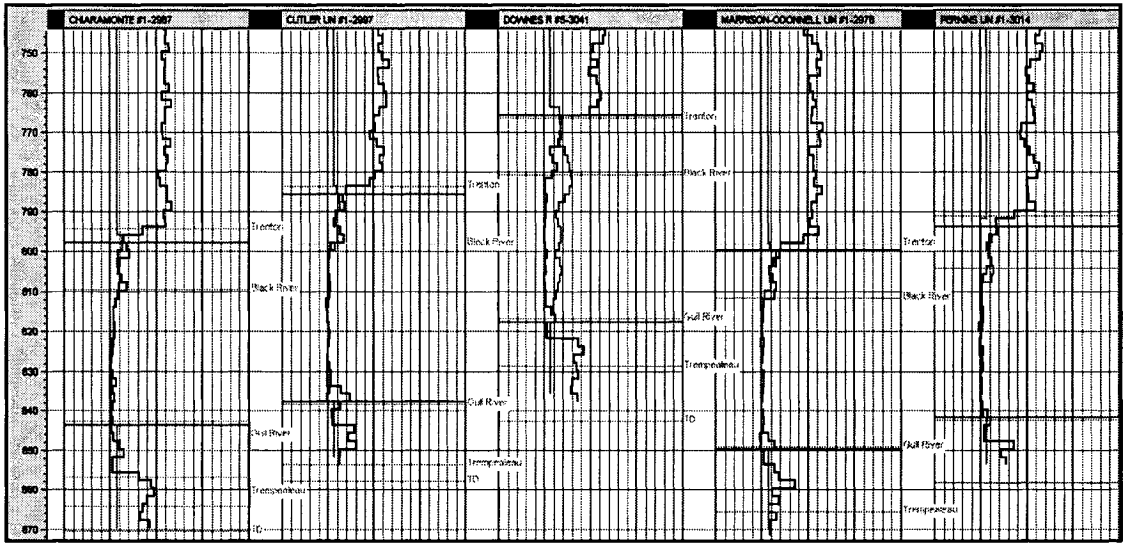
was a weak inverse relationship between the two, that is, the lower the well tie correlation the greater the prediction error (Table B1; Figure B4). A similar relationship was not seen in the training set, which indicates that the neural network was robust enough to accommodate the more tenuous ties of Downes #3 and Riffle UN #1.

Figure B4: Cross plot of the prediction error versus the well tie correlation for the final neural network. The blue diamonds represent the training set and the validation set is shown as purple squares. The trend line correlates the relationship between the two variables for the validation set only.

Prediction error vs. Well tie correlation for the Neural Network
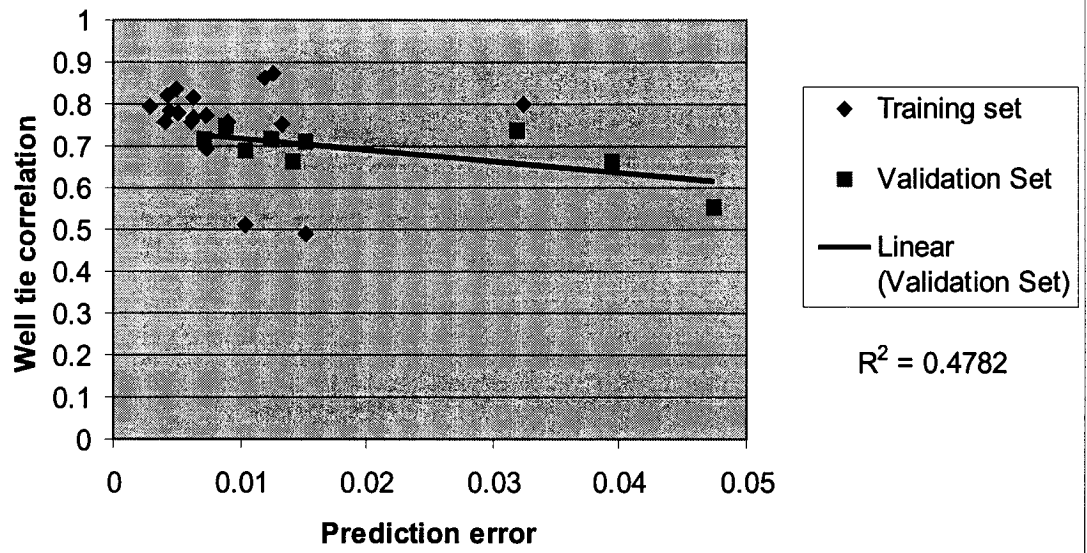
Appendix C: Effect of Operator Length

Another factor that appeared to be important in the porosity prediction was the length of the convolutional operator that was used in the multivariate regression. The operator is embedded in the resulting equation:

$$T = m_0 + m_1 {}^*A_1 + m_2 {}^*A_2 + m_3 {}^*A_3$$

where T is the target log, m_i are operators of a specified length and * denotes the convolution (Hampson et al., 2001). It is responsible for relating the adjacent sample (or group of samples) of the seismic attribute to each sample of the target log (Figure C1) (Hampson et al., 2001).

A number of different operator lengths were tested during the analysis, and those that worked best had a length of three or four. For purposes of comparison a neural network was trained using the same set of wells, but with the three different operator lengths, 3 and 6 and 8 (Figures C2a, b, c). Once applied to the data, it was observed that the statistical match of the neural networks trained with the longer operators was poorer (correlation coefficients of 0.82 and 0.76 respectively) than that of the shorter operator (correlation coefficient of 0.89). These results were consistent throughout the various iterations completed during the analysis. A possible reason for this could be related to the nature of porosity zones (dolomite) at Saybrook, which varied in thickness from 15ft (4.6m) to 345ft (105m). A longer operator may have acted to overly smooth the data so that the thin dolomitized units were obscured by using too many samples above and below the target values.

Figure C1: A schematic representation of the use of a convolutional operator

(three-point) to relate the seismic attributes to the target log (PHIA)

(adapted from Hampson et al., 2001).

Target Log
(PHIA)

Seismic Attributes
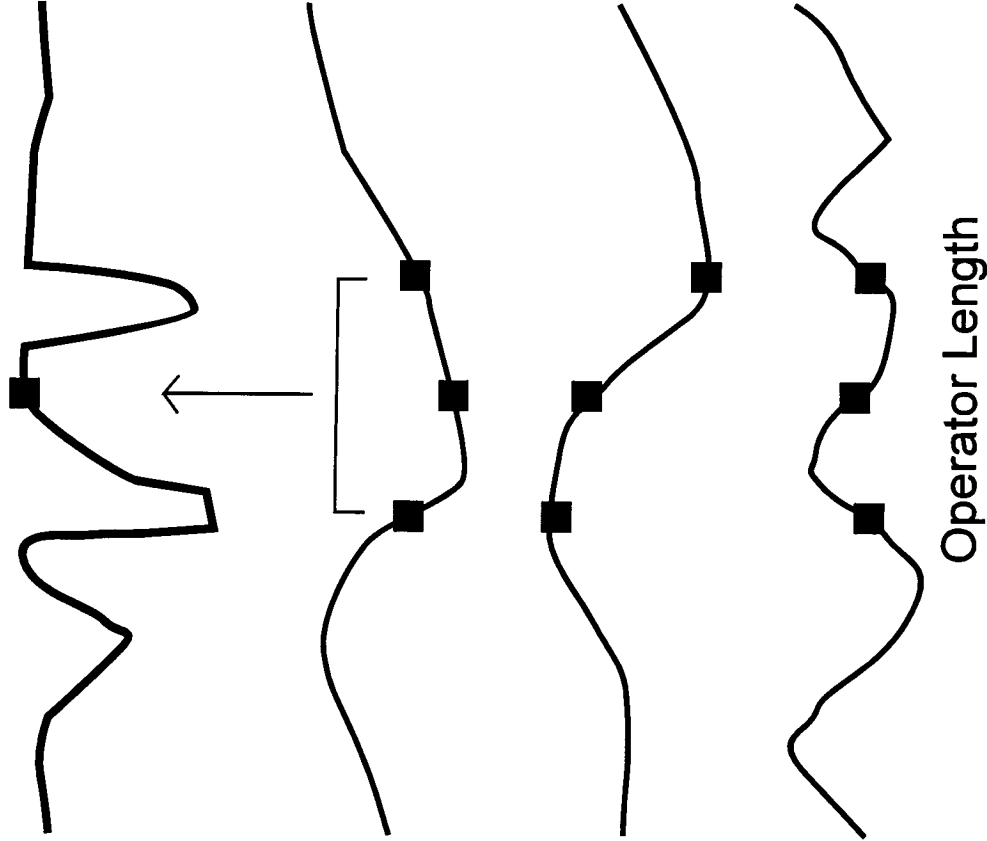
Operator Length

Figure C2: Three different operator lengths, 3, 6 and 8 were used for the

multiattribute analysis in the same training set. Using the optimal

number of attributes identified for each operator length, a neural

network was trained for each scenario. a) The results using an

operator length of 3 were those described in Chapter 2. The neural

network predicts the porosity trends fairly accurately, including some

of the thinner beds in Downes #1 (89% correlation). b) The effects of

using a slightly longer operator (6) are apparent in that the thinner

porous intervals are no longer predicted as accurately, as in the base

of Downes #1 and Downes #3. The correlation is still adequate at

82%. c) The effects noted in b) are even more apparent with a

slightly longer operator (8). The porosity at the base of the Dalin E

UN #1, Downes #1 and Downes #3 is now significantly

underpredicted (76% correlation).

a)
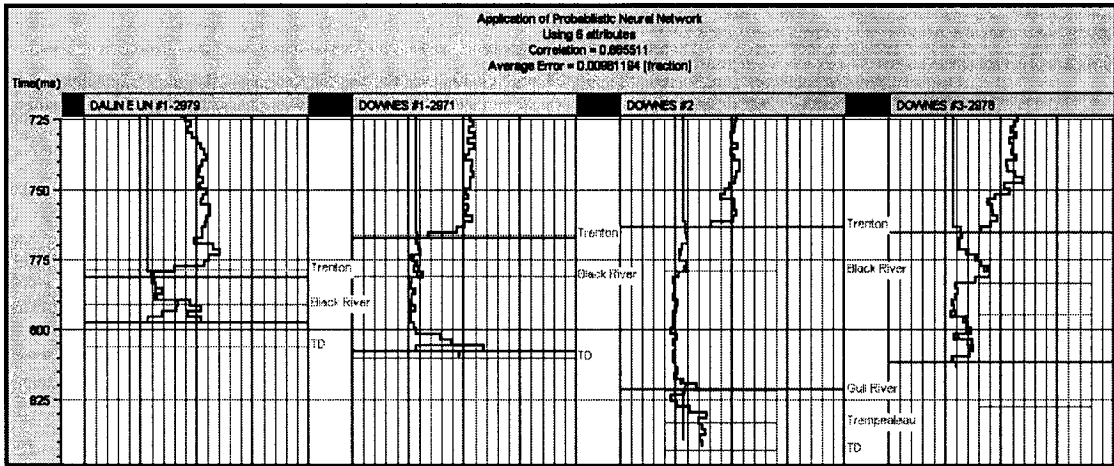
b)
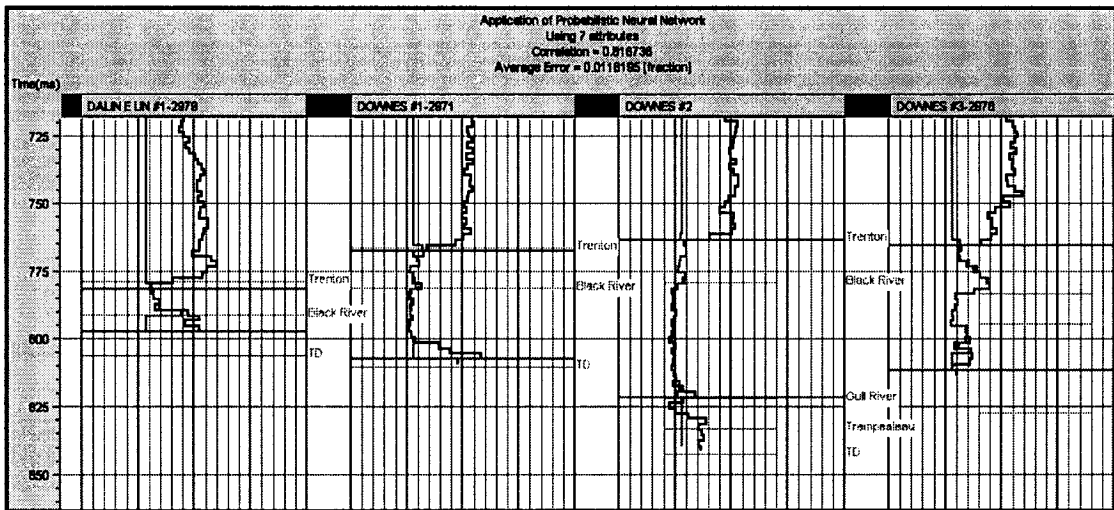
c)
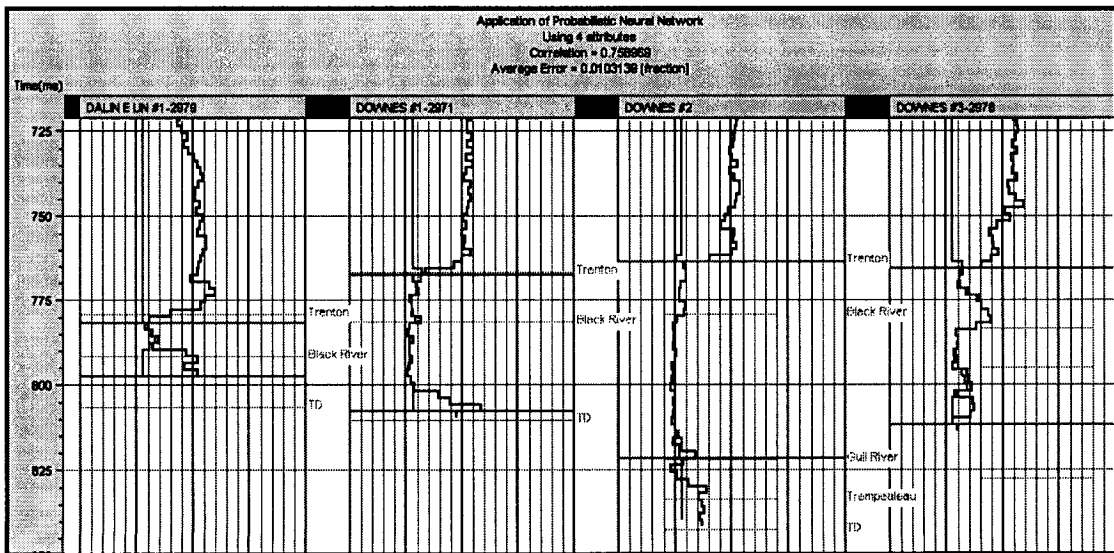
Appendix D: On Hydrothermal Dolomites

Hydrothermal dolomites have clearly proven to be of economic significance. Deposits have been found to host significant reserves of oil and gas around the world, as well as serving as the host for considerable lead-zinc sulfide ore deposits (Mississippi Valley Type [MVT] deposits). These types of plays have recently come into the spotlight with the discovery of the Ladyfern Field in northeast British Columbia in 2000. The estimated 750 BCF reserve was the largest find in fifteen years in the Western Canada Sedimentary Basin (WCSB). The key concept behind hydrothermal dolomite formation is that they form through the alteration of limestone by a hot, magnesium-bearing fluid. These fluid-rock interactions can result in dolomite bodies with highly variable shapes that cut across both facies and formational boundaries (Keith, 1989). Problems arise when trying to define temperature criteria to use for classifying fluids as hydrothermal, and in the determination of possible sources of these fluids.

The hydrothermal dolomitization model shares the same basic problems as any type of dolomitization model. That is, the identification of a source of magnesium, and a transport mechanism that can accommodate the amounts of fluids necessary for dolomitization. However, it is important to first define what constitutes a hydrothermal dolomite before examining the model's shortcomings. At first glance it may be difficult to determine what sets a hydrothermal dolomite apart from other types of dolomites, for example, Allan and Wiggins (1993) do not distinguish between hydrothermal dolomite and burial dolomitization. They define burial dolomite as that which forms at any time during burial due to

elevated temperatures that help relieve kinetic barriers and by "raising the Ca/Mg ratio at which dolomitization can occur". Another broad definition assumes that all saddle dolomite, whether replacive or cement, is hydrothermal in origin and can be used as a proxy for hydrothermal activity (from Davies, 1997 cited in Machel and Lonnee, 2002, and Al-Aasm et al., 2002). However, both these definitions appear to be too vague, and in some cases partially contradictory, to accurately define a hydrothermal dolomite.

The following definition is found in the AGI Glossary of Geology (1999), which states that a hydrothermal fluid is "a subsurface water whose temperature is high enough to make it geologically or hydrologically significant, whether or not it is hotter than the rock containing it. It does not have to be generated by magmatic processes". This definition, while relaying the importance of a hydrothermal fluid, does not establish specific criteria that can be used when trying to decisively determine whether or not a fluid event can be classified as hydrothermal. According to Machel and Lonnee (2002), the "all saddle dolomite is hydrothermal" bandwagon is doomed for several reasons. These include the facts that: several partially contradictory definitions of hydrothermal have been used over the years (for more definitions see Machel and Lonnee, 2002); not all saddle dolomite is hydrothermal; and hydrothermal dolomitization cannot account for the amount of magnesium needed to create the quantity of dolomite present in the WCSB. Machel and Lonnee (2002) developed a definition of hydrothermal that relays the temperature specific criteria necessary for classification in response to this "bandwagon". In its strictest sense,

hydrothermal refers to "aqueous solutions that are warm or hot relative to their surrounding environment" (White, 1957). It is notable that this definition contains no genetic implications with respect to the fluid source, and that these solutions must be significantly higher in temperature (5-10°C) than the surrounding rocks. This definition inherently involves the rigorous determination of the temperature of dolomite formation, which would then be compared to the temperature of the surrounding rocks at the time of dolomitization. The dolomite formation temperature would have to be established through isotope and/or fluid inclusion data, while the ambient temperature would be ascertained through either fluid inclusion data in other minerals, vitrinite reflection data, or the reconstruction of the maximum burial depth and then application of the geothermal gradient (Machel and Lonnee, 2002). Those dolomites that do not fit the definition of hydrothermal may then be considered either 'geothermal' or 'hydrofrigid', respectively indicating a formation within 5-10°C of the ambient rocks or at temperatures lower than that of the surrounding rocks. If saddle dolomite forms at temperatures ranging from 80-100 degrees, by the above definition it cannot be exclusively considered hydrothermal in origin (Figure D1), as this classification would also depend on the ambient formation temperature at the time.

Some researchers have imposed structural constraints on the hydrothermal dolomite model based on the observation that many such deposits occur in relation to faulting, especially strike-slip faulting (Davies and Berger,

Figure D1: Diagram illustrating the relationship between the temperature of

formation of saddle dolomite and the ambient rock temperature.

These two variables will dictate whether the dolomite is considered

hydrothermal or otherwise (after Machel and Lonnee, 2002).

Hydrothemal	Geothemal	Hydrofrigid	Ambient Temperature (degrees Celsius)
150			0-20
			100
	150		
			200
		150	
			300

1999). Such relationships can be significant as strike-slip faults are usually deep-seated basement features and would be capable of creating or enhancing fault networks to aid in the movement of the dolomitizing fluids and hydrocarbons (Prouty, 1989, Berger and Davies, 1999). A common manifestation of these tectonic environments is seen in the formation of flower structures or en echelon shear faults (as described in Chapter 2). These features clearly form important components of some hydrothermal dolomite reservoirs, as seen in Chapter 2.

The hydrothermal dolomitization model is in most cases considered an open system in order to allow for the movement of enough magnesium to the site of dolomitization (Middleton et al., 1993; Montanez, 1994, Al-Aasm et al., 2002). Thus the fluids responsible for dolomitization can originate from other locations and later migrate to the site. The fluids that would be produced from the compactional dewatering of basinal shales and evaporites (or modified original evaporitic brines) are an example of this. These fluids may be magnesium-rich as the transformation of montmorillonite to illite, as well as the dissolution of salts such as carnallite, polyhalite and kieserite, can all result in magnesium ions going into solution (Warren, 2000). One problem is that for more regional dolomitization these sources have mass balance issues in that they cannot provide sufficient magnesium to account for large volumes of dolomite (Allan and Wiggins, 1993). However, in the case of some localized Trenton-Black River dolomites in southwestern Ontario, compactional dewatering is cited as a possible fluid source given the high salinities found in fluid inclusions in the

dolomite (Middleton et al., 1993). These fluids are thought to have traveled updip to the basin margins where they reached the Ordovician strata through faults and fractures.

Another possible fluid and magnesium source that has been cited is the downward movement of younger fluids into the host formation. This was proposed for the Albion-Scipio field in the Michigan Basin based on the strontium isotope ($^{87}Sr/^{86}Sr$) ratio that was measured (Granath, 1991). The strontium ratio plotted between Silurian and Ordovician aged seawater indicating that the dolomitizing fluid may have been a mixture of the two. Other fluid sources include the upward movement of basement fluids and the reworking of nearby and/or older dolomites through pressure solution (Allan and Wiggins, 1993). In order to establish an influence of nearby dolomites, it would beneficial to have isotope data from the two areas that could be compared to check for any relationships. Understanding the geology in a study area and the timing of dolomitization can aid in identifying fluid and magnesium sources. It may be that there were no other dolomites present at the time of dolomitization that could have been reworked, which would rule out this process as a source of magnesium.

Different mechanisms have been suggested for the movement of fluids to the site of dolomitization. These range from regional tectonic influences to more localized fault relationships. The compaction and uplift model, also called the "squeegee model", relies upon a regional tectonic event causing compression and uplift, combined with pressure pumping from the weight of clastic wedge

deposition to drive fluids through formations (Garven and Freeze, 1984). The uplifted thrust sheets would also result in topographically driven fluid flow and would reinforce the movement caused by tectonic compression. However, sufficient porosity and permeability (or faults and fractures) must be present in order for the fluids to travel large distances. This model has been proposed in the Presqu'ile barrier and Pine Point dolomites as the mechanism responsible for fluid flowing to that area (Qing and Mountjoy, 1994). Their study proposed multiple stages of dolomitization, which were inferred to have formed in relation to different orogenic events. The main stage of dolomitization that resulted in the coarsely crystalline replacement and saddle dolomite would then correspond to the period of greatest sediment thickness (to provide fluids) and tectonic loading and uplift (to provide a driving force), which was identified as during the Late Cretaceous to Early Tertiary Laramide orogeny (Figure D2). The isotope and fluid inclusion homogenization temperatures also illustrated a marked cooling eastward trend that would be consistent with the upward flow of deeper fluids mixing with formation waters (Figure D3). In addition, the strontium isotopes showed an eastward (ie. shallower) decrease in radioactivity. This is also consistent with a radiogenic basement fluid source that later mixed with formation waters updip. The Presqu'ile dolomites were shown to be hydrothermal as the temperatures of homogenization were consistently found to be significantly higher than that of the surrounding rocks at the time of dolomitization (Qing and Mountjoy, 1994). The dolomitization in Upper Knox carbonates in the Southern Appalachian Basin have also been interpreted as

Figure D2: Schematic cross-section through the Western Canada Sedimentary

Basin during the Tertiary, after compression and uplift. Arrows show

the path of proposed fluid flow, also called the "squeegee model"

(from Qing and Mountjoy, 1994 modified from Garven and Freeze,

1985, 1989).

West   East
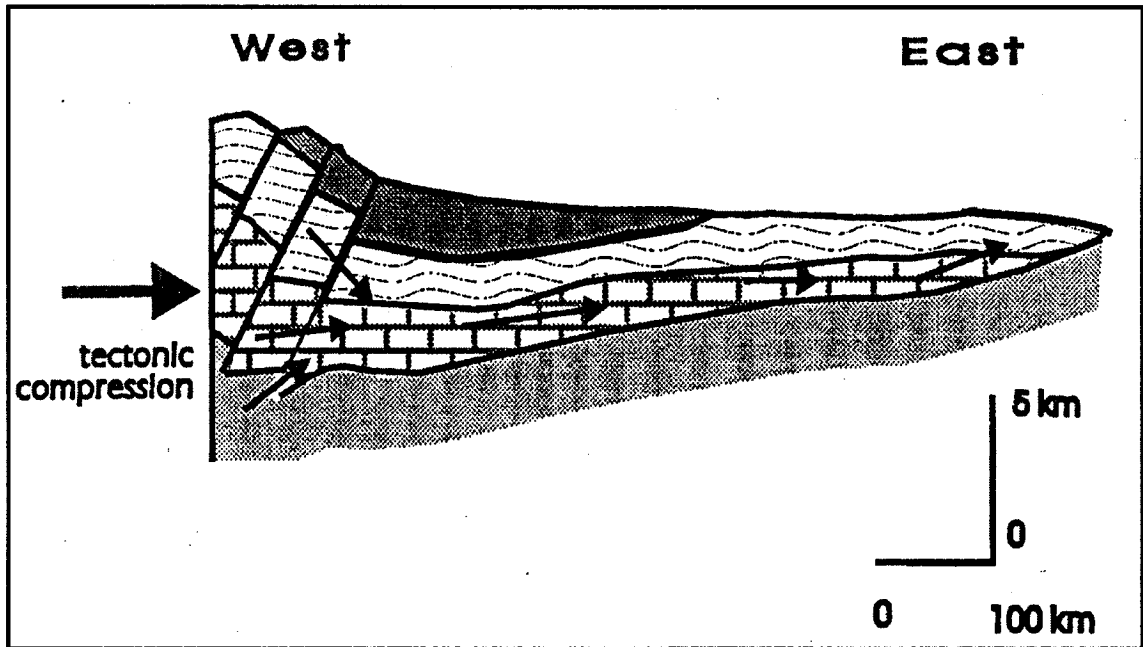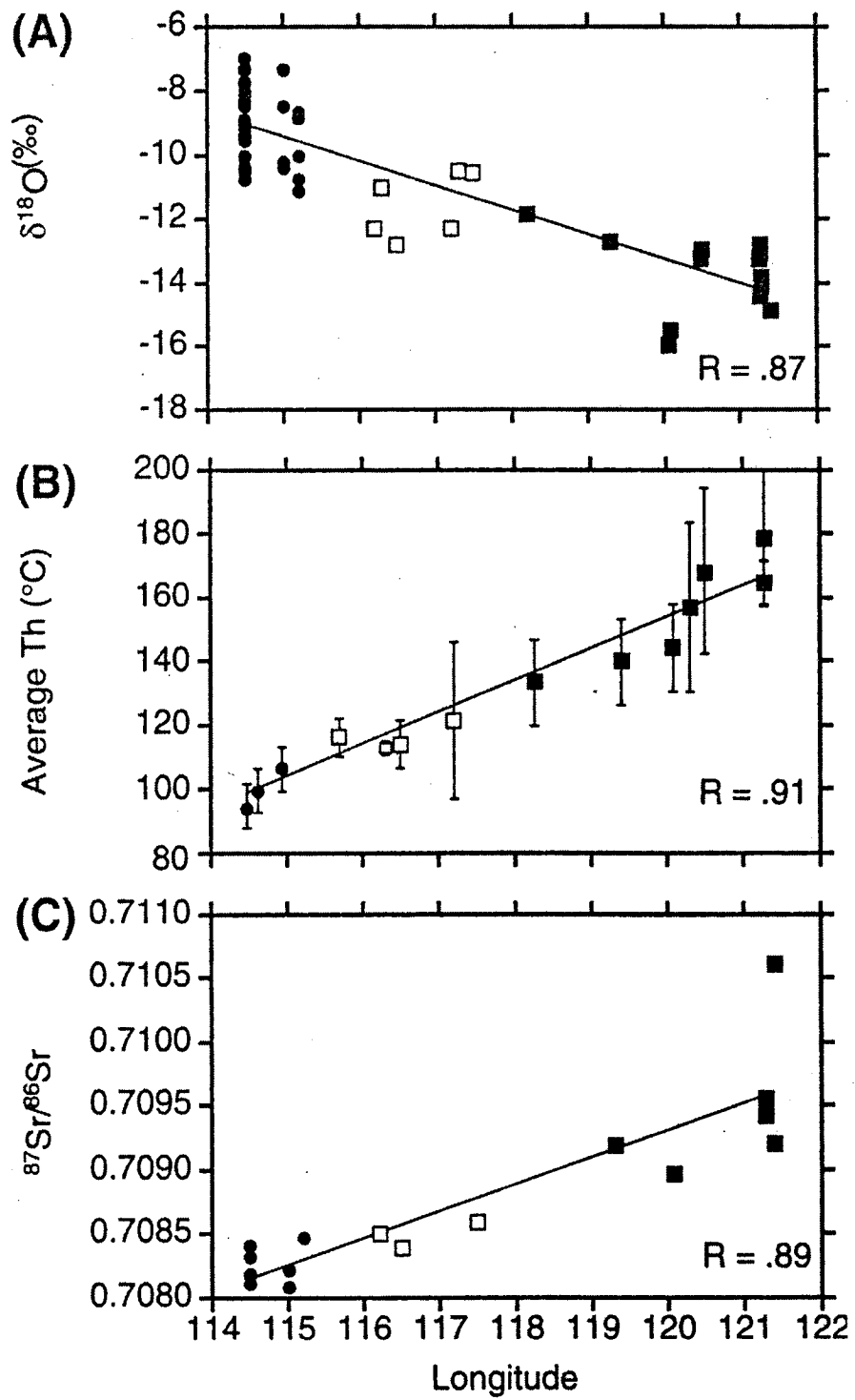
tectonic
compression

5 km

0

0   100 km

Figure D3: Various cross plots of isotope and inclusion homogenization

temperatures versus longitude. Dots are samples from Pine Point,

open squares are form west of Pint Point and dark squares are from

NE British Columbia, note the distinct trends from east to west (from

Qing and Mountjoy, 1994).

(A) R = .87

(B) R = .91

(C) R = .89

resulting from large-scale fluid flow related to a tectonic event (Montanez, 1994). In this case it was the Alleghenian tectonism inthe Late Paleozoic that was responsible for the development of replacement dolomite and zoned dolomite cements.

A recent study of the Sulphur Point and Slave Point formations in northwestern Alberta attempted to identify regional fluid flow events with the development of saddle dolomites in the two formations (Al-Aasm et al., 2002). Through the comparison of oxygen, carbon and strontium isotope values, it was seen that two different isotopic signatures were evident (Figure D4). This led to the conclusion that different fluid flow events could be responsible for the development of dolomite in these formations. The timing of the events, constrained by crosscutting relationships with styolites, appeared to be consistent with the development of the Antler orogeny in the Late Devonian to Early Mississippian (Slave Point) and the Late Cretaceous to Early Tertiary Laramide orogeny (Sulphur Point). It was not clear whether or not the criteria used in the study were consistent with the hydrothermal definition of Machel and Lonnee's (2002). However, the study does contribute to the case of regional tectonic events impacting on the development of localized dolomite reservoirs.

Davies and Berger (1999) have found that many hydrothermal dolomites are also fault related, as mentioned above, and these faults could act as pathways for basement fluids to travel through. At the Albion-Scipio Field it was inferred that the fluids ascended along the faults given that the dolomite and other secondary minerals increased in abundance with depth (Prouty, 1989). In

Figure D4: Fluid inclusion and isotope measurements from dolomites in the Sulphur Point (circles) and Slave Point (squares) formations. The two distinct clusters were interpreted to indicate origins from distinct fluid flow events related to the Antler and Laramide orogenies (from Al-Aasm et al., 2002).
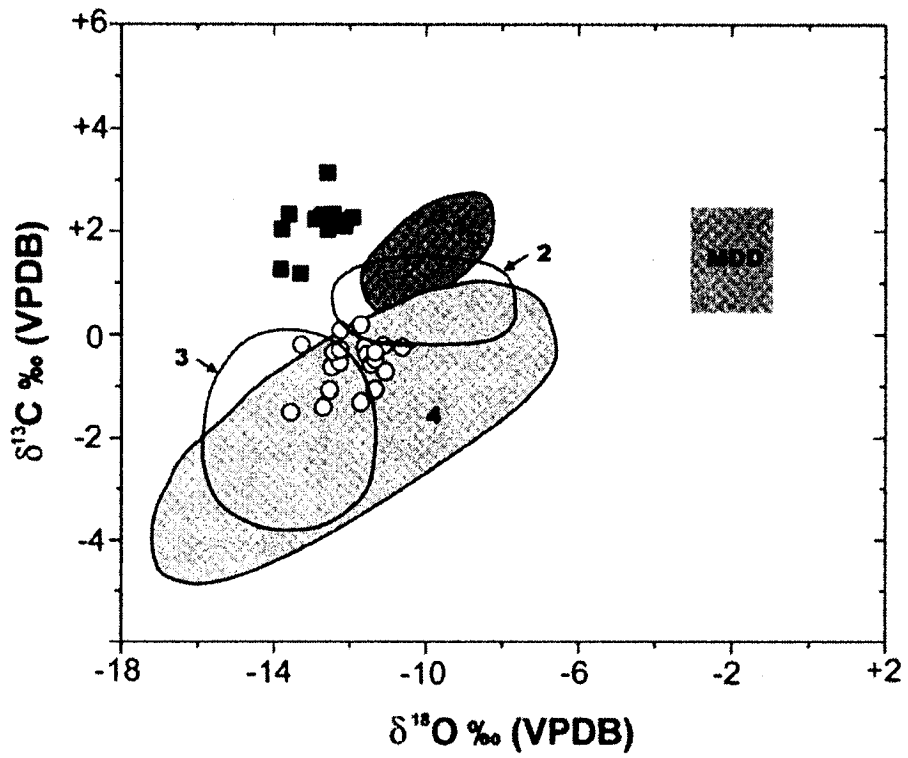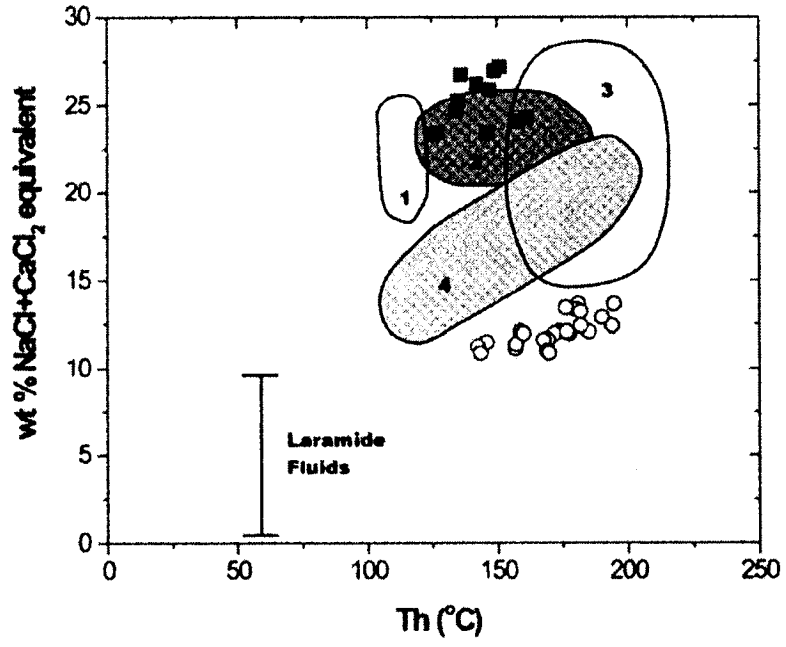
addition, the dolomitization appeared to be most extensive peripheral to the faults and had near vertical interfaces with adjacent undolomitized limestones. The well coverage (some 1500) over the $58km^2$ area has allowed the construction of a map that illustrates the complex, compartmentalized nature of the field (Figure D5). A left lateral shear stress regime has been applied to explain the morphology of the field (Hurley and Budros, 1990). These faults were thought to have been reactivated during the Taconic orogeny in the Late Ordovician with dolomitization occurring thereafter (Prouty, 1989). The system at Saybrook appears to be remarkably similar to that which has been documented at Albion-Scipio. Other Trenton-Black River dolomite reservoirs in Ohio, New York and southern Ontario have shown similar relationships to basement faulting (Carter et al., 1996). However, the various isotope work has not been completed in all these locations that would be necessary in clearly establishing a hydrothermal origin according to Machel and Lonnee (2002). At Saybrook, the lack of core prevents the completion of this type of analysis, hence the qualifier "suspected" must be used.

Another example of a fluid flow mechanism commonly is thermal convection. Convection moves fluid by creating buoyancy from thermally imparted density differences; hot fluids rise while cooler fluids move downwards. This can create convection cells with the re-circulation of fluids occurring over time, depending upon the permeability of the rocks as well as the efficiency of the heat source. This brings to light one of the uncertainties of this model, which is the heat source. Middleton et al. (1993) acknowledge that convection may

Figure D5: Diagram illustrating the compartmentalized nature of the Albion-

Scipio field in the Michigan Basin. The lines indicate the trace of

synclinal axes and the arrows show the inferred orientation of the

shear stress of the reactivated basement fault (from Hurley and

Budros, 1990).

R4W

T2S

T3S

ALBION

R3W   R2W

PULASKI
BREAK

8 km
5 mi

T4S

STONEY
POINT

T5S   SCIPIO

T6S
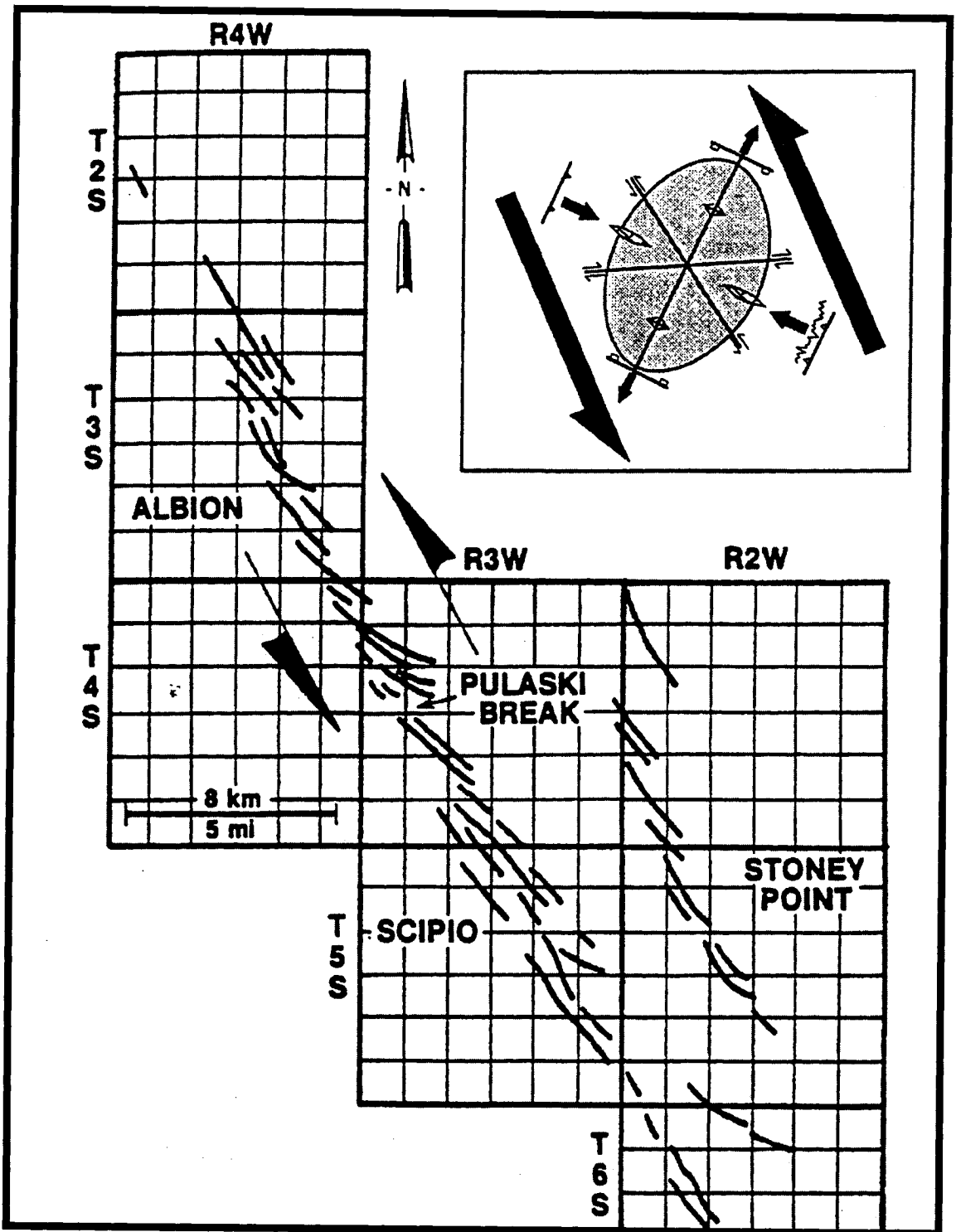
have played a role in the movement of fluids in the Trenton-Black River; however, evidence of a possible heat source is not seen. They speculate that an igneous intrusion in the upper part of the Precambrian basement could be responsible, but there has been no conclusive evidence to support this (Middleton et al., 1993).

It is important to have a clear definition of what a hydrothermal dolomite is, before a given deposit can be classified as such. If one uses Machel and Lonnee's (2002) definition of hydrothermal as an aqueous solution that is significantly (5-10 degrees) hotter than the surrounding rocks, then certain values must be determined before this label is applied. This includes establishing the burial history of the formation in order to constrain the ambient temperature, as well as determining the timing of dolomitization within this burial history. Then the proper isotope analysis must be completed in order to ascertain the temperature of the dolomitizing fluids (values may need pressure corrections). These analyses will also, hopefully, provide insight into the source and movement of the dolomitizing fluid. Many questions remain with respect to these types of deposits. The exact fluid migration mechanisms are not well understood and in some cases there seems to be more than one possible fluid source. It also is important to develop a clear picture of the structural setting of these deposits as faults can play an important role in the movement of fluids. Given the economic significance of recent hydrothermal dolomite discoveries, future work will hopefully provide further insight into these complex reservoirs and deposits.

References

AGI, 1999. Illustrated Dictionary of Earth Science. American Geological Institute. CD-ROM edition.

Al-Aasm, I., Lonnee, J., Clarke, J., 2002. Multiple fluid flow events and the formation of saddle dolomite from the Middle Devonian of the Western Canada Sedimentary Basin. Marine and Petroleum Geology, v. 19, p. 209-217.

Allan, J., Wiggins, W., 1993. Dolomite Reservoirs: Geochemical Techniques for Evaluating Origin and Distribution. American Association of Petroleum Geologists Continuing Education Course Note Series 36: Tulsa, Oklahoma, p. 90-109.

Carter, T., Trevail, R., Easton, R., 1996. Basement controls on some hydrocarbon traps in southern Ontario, Canada. *In:* Basement and Basins of Eastern North America. B.A. van der Pluijm and P.A. Catacosinos (eds.). Geological Society of America Special Paper 308, p.95-107.

Davies G., Berger, Z., 1999. The development of linear hydrothermal dolomite (HTD) reservoir facies along wrench or strike slip fault systems in the Western Canada Sedimentary Basin. CSPG Review, v. 26, p. 34-38.

Garven, G., and Freeze, R.A., 1984. Theoretical analysis of the role of groundwater flow in the genesis of stratbound ore deposits – I. Mathematical and numerical model. American Journal of Science, v. 284, p. 1085-1124.

Granath, V., 1991. Geochemical constraints on the origin of dolomite in the
Ordovician Trenton and Black River limestones, Albion-Scipio area,
Michigan. AAPG Bulletin, v. 75, p. 584-585.

Hurley, N., Budros, R., 1990. Albion-Scipio and Stoney Point fields, USA,
Michigan Basin. *In:* Stratigraphic Traps I: Treatise of Petroleum Geology
Atlas of Oil and Gas Fields. E.A. Beaumont and N.H. Forster (eds.).
American Association of Petroleum Geologists, p. 1-37.

Keith, B.D., 1989. Reservoirs resulting from facies-independent dolomitization:
Case histories from the Trenton and Black River carbonate rocks of the
Great Lakes Area. *In:* The Trenton Group (Upper Ordovician Series) of
Eastern North America. B.D. Keith (ed.). American Association of
Petroleum Geologists, Studies in Geology No. 29, p. 267-276.

Machel, H., Lonnee, J., 2002. Hydrothermal dolomite – a product of poor
definition and imagination. Sedimentary Geology, v. 152, p. 163-171.

Middleton, K., Coniglio, M., Sherlock, R., Frape, S., 1993. Dolomitization of
Middle Ordovician carbonate reservoirs, southwestern Ontario. Bulletin of
Canadian Petroleum Geology, v. 41, p. 150-163.

Montanez, I., 1994. Late diagenetic dolomitization of Lower Ordovician, Upper
Knox carbonates: a record of the hydrodynamic evolution of the Southern
Appalachian Basin. AAPG Bulletin, v. 78, p. 1210-1239.

Prouty, C., 1989. Trenton exploration and wrenching tectonics – Michigan Basin
and environs. *In:* The Trenton Group (Upper Ordovician Series) of
Eastern North America. B.D. Keith (ed.). American Association of
Petroleum Geologists, Studies in Geology No. 29, p. 207-236.

Qing, H., Mountjoy, E., 1994. Formation of coarsely crystalline, hydrothermal dolomite reservoirs in the Presqu'ile Barrier, Western Canada Sedimentary Basin. AAPG Bulletin, v. 78, p. 55-77.

Warren, J., 2000. Dolomite: occurrence, evolution and economically important associations. Earth-Science Reviews, v. 52, p.1-81.

Wendte, J., Dravis, J., Stasiuk, L., Qing H., Moore, S., Ward, G., 1998. High-temperature saline (thermoflux) dolomitization of Devonian Swan Hills platform and bank carbonates, Wild River Area, west-central Alberta. Bulletin of Canadian Petroleum Geology, v. 46, p. 210-265.

White, D., 1957. Thermal waters of volcanic origin. Geological Society of America Bulletin, v. 68, p. 1637-1658.